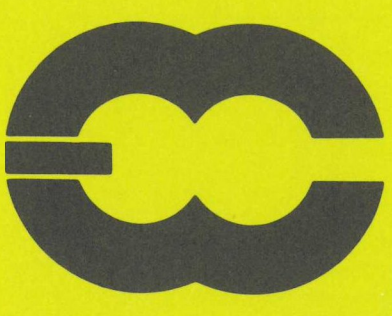

European Centre
for Medium Range
Weather Forecasts

A Comparative Study of Some Low Resolution Explicit and Semi-Implicit Spectral Integrations

Internal Report 17
Research Dept.

August 1978

Centre Européen pour les Prévisions Météorologiques
à Moyen Terme

Europäisches Zentrum für mittelfristige Wettervorhersage

A COMPARATIVE STUDY OF SOME LOW RESOLUTION EXPLICIT AND SEMI-IMPLICIT SPECTRAL INTEGRATIONS

by

A. W. Hansen and A. P. M. Baede

European Centre for Medium Range Weather Forecasts, Bracknell

Internal Report No. 17

RESEARCH DEPARTMENT

N O T E:

Introduction

Within the framework of a series of test integrations with several models at ECMWF (Arpe et al., 1976), it was decided to carry out a comparative study with a spectral model on real data. The purpose of the study is twofold: in the first place a comparison of explicit and semi-implicit integrations with an otherwise identical model, and in the second place an investigation of the forecasting abilities of spectral models compared with those of gridpoint models with an identical physical parameterisation scheme.

This preliminary report will concentrate mainly on the results of a comparison of explicit and semi-implicit integrations. Because available computer time prohibited the performance of a high-resolution explicit integration, the resolution used in this study is relatively low (triangular truncation, with highest wave number being 21 in zonal direction, further denoted as T21), but sufficient, as will be shown, to describe most of the important synoptic features.

The second part of our study, a comparison of the forecasting abilities of a spectral model, was carried out with a high-resolution (T40) spectral model and has been reported elsewhere (Baede and Hansen, 1977). In this report only little attention will be given to a comparison with other models.

Medium and long-range integrations with high-resolution primitive models are severely hampered by the necessity of very short timesteps due to the presence of high frequency gravity waves: therefore, for efficiency reasons, it would be of great importance if it could be shown that application of a semi-implicit time-stepping technique has no detrimental effect on the forecasting of the meteorological waves. If, however, the process

of geostrophic adjustment is of primary importance for a proper treatment of these waves, then theoretical studies by Janjic and Wiin-Nielsen (1977) and Wiin-Nielsen (1976) on linear homogeneous fluids in a cylinder and on a sphere may suggest that the semi-implicit scheme is inferior to an explicit scheme, such as the leapfrog scheme in case of unbalanced initial data. However, these studies were carried out in the absence of any forcing or dissipation terms. Therefore, in order to test the influence of the semi-implicit scheme on numerical medium-range weather forecasts, it was decided to carry out a number of 10-day integrations on real data with a T21 spectral model, both without any forcing and with a rather complete physical parameterisation scheme, but always such that the models are completely identical apart from the time-stepping scheme.

In Chapter I the adiabatic model is briefly described. The equations are presented in a continuous form, followed by a brief discussion of the finite difference approximations, the semi-implicit scheme in particular. The physical parameterisation scheme is summarised only in tabular form.

Chapter II presents the results of the comparison between the explicit and semi-implicit scheme. First the results of the adiabatic integrations are discussed. It was found that integrations from a data set which was by no means adjusted to our model, and which initially contained a significant amount of energy in high frequency modes, associated with initial imbalance, diverge rapidly. It could be shown, however, that the two schemes produce virtually identical integrations when high frequency oscillations are removed from the initial data. In the second part of Chapter II the non-adiabatic integrations are presented. Here it will he shown that without any

initialization, both time schemes produce almost identical results, even after 10 days. The conclusion can be that in these integrations, time truncation errors are negligible compared to other errors in the presence of forcing and dissipation.

In the final chapter the integrations with the non-adiabatic spectral model are briefly compared with those of other models with the same physical parameterisation scheme. It may be concluded that, although obviously the treatment of small scale features is inadequate due to the low spectral truncation, the overall performance is hardly inferior to that of other models. Some attention is given to features, peculiar to T21.

CHAPTER I - THE MODEL

The U.K. Universities Modelling group of Reading University has provided ECMWF with an adiabatic, semi-implicit, global spectral model, including an advective equation for the mixing ratio (Hoskins and Simmons, 1975). This model has prognostic equations for vorticity, divergence, temperature, surface pressure and, as mentioned above, mixing ratio. Horizontally a triangular truncation was chosen. In the vertical a finite difference formulation is used. For this study the σ-levels are those of the 9-level GFDL gridpoint model, used in previous studies at ECMWF (Miyakoda, 1973 and Arpe et al., 1976). The vertical scheme is energy conserving with respect to adiabatic vertical advection. Moreover, the form of the conversion term, in combination with the integration of the hydrostatic equation, ensures exact cancellation of transformations between kinetic and total potential energy. This implies that total energy is conserved, apart from the effect of time truncation. In addition to the semi-implicit time-stepping scheme, an explicit leap-frog scheme was implemented.

Apart from horizontal diffusion, the physical parameterisation scheme is that provided by GFDL and used in other ECMWF studies. A linear ∇^4 horizontal diffusion on σ-surfaces scheme is used.

The adiabatic part of the model has been described in detail by Hoskins and Simmons (1975), whereas the physical parameterisation scheme was documented in several publications of the GFDL-group and ECMWF (see for example Miyakoda (1973), GARP-report No. 14 (1974), and Arpe et al. (1976)). In this report we present the model equations in a continuous form. In a separate section we shall pay some attention to the semi-implicit scheme in view of its importance for the present study. The physical parameterisation scheme is presented briefly in tabular form.

I.1 The model equations in continuous form

The spectral model, used in this study is a baroclinic primitive equation model on the sphere with independent coordinates:

t = time

$\mu = \cos\phi$, ϕ being the latitude

λ = longitude

$\sigma = \frac{p}{p^*}$, p^* being the surface pressure

The prognostic variables of the model are

ζ absolute vorticity

D divergence

T temperature

q mixing ratio

$\ell n p^*$, p^* being the surface pressure

Beside the 5 prognostic equations, the hydrostatic equation provides a diagnostic equation.

All variables are non-dimensionalised, using:

length scale: $a = 6371000$ m. (radius of the earth)

time scale: $\Omega^{-1} = 13714$ sec. (inverse angular velocity of the earth)

temperature scale: $\frac{a^2\Omega^2}{R} = 752.015$ K

pressure scale: $p_o = 1000$ mb

The mixing ratio is expressed in kg/kg.

The continuous model equation can then be written as follows:

$$\frac{\partial \zeta}{\partial t} = \frac{1}{1-\mu^2}\frac{\partial F_v}{\partial \lambda} - \frac{\partial F_u}{\partial \mu} - K.\nabla^4\zeta \qquad (1)$$

$$\frac{\partial D}{\partial t} = \frac{1}{1-\mu^2}\frac{\partial F_u}{\partial \lambda} + \frac{\partial F_v}{\partial \mu} - \nabla^2\left(\frac{U^2+V^2}{2(1-\mu^2)} + \phi + T_o.\ell np_*\right) - K.\nabla^4 D \qquad (2)$$

$$\frac{\partial T'}{\partial t} = -\frac{1}{1-\mu^2}\frac{\partial UT'}{\partial \lambda} - \frac{\partial VT'}{\partial u} + DT' - \dot{\sigma}\frac{\partial T}{\partial \sigma} + K\frac{\omega T}{p} - K\nabla^4 T + P_T \qquad (3)$$

$$\frac{\partial q}{\partial t} = \frac{1}{1-\mu^2}\frac{\partial Uq}{\partial \lambda} - \frac{\partial Vq}{\partial \mu} + D.q - \dot{\sigma}\frac{\partial q}{\partial \sigma} - K.\nabla^4 q + P_q \qquad (4)$$

$$\frac{\partial \ell np*}{\partial t} = -\frac{U}{1-\mu^2}\frac{\partial \ell np*}{\partial \lambda} - V\frac{\partial \ell np*}{\partial \mu} - D - \frac{\partial \dot{\sigma}}{\partial \sigma} \qquad (5)$$

$$\frac{\partial \phi}{\partial \ell n\sigma} = -T \qquad (6)$$

with

$$F_u = V.\zeta - \dot{\sigma}\frac{\partial U}{\partial \sigma} - T'\frac{\partial \ell np*}{\partial \lambda} + P_u$$

$$F_v = -U.\zeta - \dot{\sigma}\frac{\partial V}{\partial \sigma} - (1-\mu^2)T'\frac{\partial \ell np*}{\partial \mu} + P_v$$

In these equations the following notation is used:

$$V = v.\cos\phi$$

$$U = u.\cos\phi$$

$$\omega = \frac{dp}{dt}$$

$$\dot{\sigma} = \frac{d\sigma}{dt}$$

$$T'(\lambda,\mu,\sigma) = T(\lambda,\mu,\sigma) - T_o(\sigma)$$

$T_o(\sigma)$ is a standard temperature profile, which we will comment upon in I.3. In this study $T_o(\sigma)$ was chosen for the initial σ-level mean of the temperature:

$$T_o(\sigma) = \frac{1}{4\pi} \int_0^{2\pi} \int_{-1}^{+1} T(t=o,\lambda,\mu,\sigma)d\mu d\lambda$$

From (5) a diagnostic equation for $\dot{\sigma}$ can be derived

$$\dot{\sigma} = \sigma \int_0^1 (\frac{U}{1-\mu^2} \cdot \frac{\partial \ell np*}{\partial \lambda} + V \frac{\partial \ell np*}{\partial \mu} + D)d\sigma$$

$$- \int_0^\sigma (\frac{U}{1-\mu^2} \frac{\partial \ell np*}{\partial \lambda} + V \frac{\partial \ell np*}{\partial \mu} + D)d\sigma \qquad (7)$$

and finally an expression is found for $\frac{\omega}{p}$

$$\frac{\omega}{p} = \frac{\dot{\sigma}}{\sigma} - \frac{\partial \dot{\sigma}}{\partial \sigma} - \frac{\partial \dot{\sigma}}{\partial \sigma} - D \qquad (8)$$

The forcing terms P_T, P_q, P_u and P_v, computed in GFDL's physical parameterisation scheme have the following form

$$P_T = \frac{\dot{Q}_r}{C_p} + CONV + SHFX \qquad (9)$$

$$P_q = \frac{\partial}{\partial \sigma}(K \frac{\partial q}{\partial \sigma}) + CND \qquad (10)$$

$$P_u = \frac{\partial}{\partial \sigma}(K \frac{\partial u}{\partial \sigma}) \qquad (11)$$

$$P_v = \frac{\partial}{\partial \sigma}(K \frac{\partial v}{\partial \sigma}) \qquad (12)$$

here $\dot{Q}_r$ is the heating rate due to radiation

CONV is the heating due to moist and dry adiabatic adjustment

SHFX is the heating due to the heat flux from the surface

CND is the humidity change due to condensation processes and the other terms are vertical diffusion terms, applied to the lowest four layers. A survey of the physical parameterisation scheme is presented in Table I.

The horizontal diffusion of ζ,D,T and q is a ∇^4 type linear diffusion chosen for its easy implementation in spectral models and its scale selectivity. The diffusion constant K was selected such that, rather arbitrarily, the e-folding time for the shortest waves due to horizontal diffusion alone was 36 hours for all four quantities. The components $\zeta_{0,1}$ and $D_{0,1}$, connected with a solid body rotation, are not diffused. No attempt was made to optimise the value of K. The same e-folding time was used in the high-resolution study (Baede and Hansen, 1977).

The question whether the results of this comparative study of explicit and semi-implicit integrations are influenced by our choice of the parameterisation scheme and horizontal diffusion cannot easily be answered. Their main purpose, however, is to provide reasonably realistic sources and sinks. It seems to us that there is no reason to believe that the conclusions would be highly different if another formulation had been chosen.

I.2 The spectral and finite difference approximations

All prognostic variables $x(\lambda,\mu,\sigma,t)$ are represented by a finite sum of the following form

$$x(\lambda,\mu,\sigma,t) = \sum_{M=-M}^{+M} \sum_{n=|m|}^{M} X_{m,n}(\sigma,t) P_{m,n}(\mu)\, e^{im\lambda} \qquad (13)$$

in which $x_{m,n}(\sigma,t)$ are complex spectral coefficients and $P_{m,n}(\mu)$ are associated Legendre polynomials. The type of truncation used in (13) is called a triangular truncation and for M=21 it is denoted T21.

In the vertical a finite difference representation is used. The 9 vertical levels are those of the GFDL model (see

Miyakoda, 1973). Boundary conditions are $\dot{\sigma}=0$ at the top and the bottom of the atmosphere. It should be stressed here, however, that the integration of the hydrostatic equation in this model (eq. 6) is different from the scheme applied in other models tested at ECMWF, in particular the 9-layer GFDL-model. In our model the integration proceeds from full level to level, assuming an isothermal lowest half layer. In the GFDL-model the integration proceeds from half-level to half-level, followed by a linear interpolation of the geopotential to the full levels. This requires a special assumption at the top of the atmosphere, rather than near the ground. Both the GFDL and our scheme are energy conserving with respect to adiabatic vertical advection.

The differences between the models compared in the second half of this report, apart from the horizontal representation are limited to the hydrostatic equation and the horizontal diffusion. Table II summarises the different horizontal diffusion schemes used in the models.

I.3 The semi-implicit time differencing scheme

Although the semi-implicit scheme has been described by Hoskins and Simmons, its application raises two problems, a brief discussion of which seems appropriate in this context.

First, the choice of the standard temperatures $T_o(\sigma_j)$, around which the gravity waves are linearised, is not entirely trivial, as was pointed out by Simmons et al. (1977). They showed that, if the local static stability differs significantly from the standard static stability, the semi-implicit scheme may become unconditionally unstable. This may easily happen by choosing the horizontal σ-surface mean temperatures. However, we did not encounter such problems. This might be due to the

relatively low vertical resolution, but might also be caused by a generally higher numerical stability of spectral models, in view of the fact that such stability problems actually were encountered in semi-implicit integrations with ECMWF's gridpoint model with the same vertical structure (Burridge, private communication). This point deserves further research.

The second problem concerns the selection of terms in the temperature equation, which are to be linearised and treated implicitly. After linearisation about $T_o(\sigma_j)$, both the vertical advection term $\dot{\sigma}\frac{\partial T}{\partial \sigma}$ and the conversion term $\kappa\frac{T\omega}{p}$ contribute linear components to the thermodynamic equation. However, as pointed out by Bourke et al. (1977), one might limit the linear terms, computed implicitly, to those originating from the conversion term alone. In fact, such a scheme was found by Bourke to be well behaved, and may have certain advantages, such as an evaluation of the vertical advection term consistent with all other vertical advection terms, and an increased numerical stability (Lepas, private communication). In the model, used in this study, however, terms from both the conversion term and the linear advection term were treated implicitly.

CHAPTER II - A COMPARISON OF EXPLICIT AND SEMI-IMPLICIT INTEGRATIONS

With the model described in the previous section a number of adiabatic and non-adiabatic integrations were performed on real data, in order to compare the explicit and semi-implicit scheme.

The initial data for these integrations is the data for 1 March 1965 00Z, produced by GFDL on σ-surfaces on a so-called modified Kurihara grid. This data, including the orography, was interpolated linearly to a Gaussian grid of 96 latitude lines and 256 points per latitude line. From this Gaussian data set a T63 spectral data set was produced which, for these experiments, was truncated to T21. The data for the high resolution experiments, reported in Baede and Hansen (1977) was obtained as well from this data set. All fields were truncated independently and no attempt was made to redefine the σ-surfaces on the basis of the truncated surface pressure field.

Clearly, this data set has not been tuned or initialised to our model. This, together with the imbalance already present in the original data set and the interpolation to Gaussian grid, makes it very probable that a disproportionate part of the initial energy is in the model's high frequency gravity wave modes. This is substantiated by a comparison of two short semi-implicit T21 integrations, one on this data set and the other on the same set after non-linear normal-mode initialisation (Machenhauer, 1977, Andersen, 1977) which effectively removes the energy present in the gravity wave modes. Fig. II.1, taken from Andersen, 1977, shows the forecast of the surface pressure and clearly indicates the presence of rapid oscillations in the surface pressure, related with gravity waves.

In the next sections we discuss the result of a series of explicit and implicit integrations on this data set, both adiabatic and in the presence of forcing and dissipation. In the adiabatic integration, no horizontal diffusion and time smoothing were applied. The time step lengths in all runs, together with the diffusion and time smoothing constants applied in the non-adiabatic integrations are summarised in Table III. It should be stressed that no attempt was made to optimise any of these constants.

II.1 Results of the adiabatic integrations

Three sets of adiabatic integration were performed. The first set was based on the data set, mentioned above, without any further initialisation. Due to the imbalances in the initial data large amplitude high frequency gravity waves were set up in the early stages of the forecast, causing the semi-implicit integration to diverge rapidly from the explicit one, particularly near the uppermost levels of the model and at the surface. This is clearly seen in Fig.II.2 which shows the 1000, 500 and 10 mb forecasts at day 1 for both schemes. By day 4 the results of both schemes were already very different. To make sure that these differences were associated with the time step schemes and not with the time step length, a semi-implicit integration was performed with Δt=10 min. This integration, however, showed the same large differences with the explicit run.

The second experiment used a GFDL N48 24 hr forecast as initial data, assuming that this data would be must better balanced due to the adjustment taking place during the model integration. In this case the agreement between both schemes was better, as can be seen from the day 4 forecasts shown in Fig.II.3.

The initial data for the third experiment was a 24hr T21

spectral forecast, produced by using the explicit scheme combined with a heavy timefilter (α=0.50), which effectively removed all high-frequency oscillations. The integrations from this "balanced" initial data set show a very good agreement between both schemes as can be observed from Fig.II.4.

Because we were not primarily interested in a comparison of adiabatic runs, no further attempt was made to investigate quantitatively the differences between both schemes. From a visual inspection of the results it may be concluded unambiguously that both schemes produce highly identical results, provided the initial data is reasonably well balanced.

II.2 Results of integrations with forcing and dissipation

With the model described in Chapter I, including the physical parameterisation scheme, the linear horizontal diffusion and the time smoothing, an explicit and a semi-implicit 10-day integration was made on the same data set. No attempt was made to initialise this data for the spectral model.

A visual inspection of the height maps reveals that the two integrations produce very similar results. This can be observed from Fig.II.5 which shows the 1000, 500 and 200 mb maps for day 10. To investigate the differences between the two runs we computed RMS-differences and correlation coefficients between the explicit version (EXP) and the semi-implicit version (IMP) and compared them to differences between EXP and GFDL's N48 models or NMC's analysis. For details we refer to Arpe et al. (1976) and to Baede and Hansen (1977). The results are shown in Fig.II.6-II.11.

Fig.II.6 is a display of the RMS-differences of the height-field averaged over the whole troposphere. Significantly lower values for IMP vs. EXP than for N48 vs. EXP and for

NMS vs. EXP are noticed. Even more interesting is the fact that the differences between IMP vs. EXP remain fairly constant throughout the forecasting period with a slight minimum around day 4, whereas the other differences steadily increase.

Fig.II.7 and II.8 suggest that the RMS height differences between the explicit and implicit integrations are caused mainly by random external gravity waves, "random" in the sense that the height differences have no clear preference for certain latitudes. Had the differences been associated with meteorological modes we would have expected RMS-charts more like the kind observed for N48 vs. EXP. This will also be the case, if two randomly selected atmospheric height-fields are compared, simply because the largest differences are located where the largest amplitudes are found. That means we expect two integration models to differ mostly near the jetstream.

The above mentioned features are seen again in Fig.II.9. The correlation coefficient of height anomalies in EXP and IMP are near 100% for the whole period. Only wave-numbers 10-20 show a smaller correlation.

Fig.II.10 and II.11 clearly demonstrate that EXP and IMP are closer together than EXP compared to N48 or NMC. Only near the surface by the end of the integration we see a growing tendency to smaller and smaller correlations. This is in accordance with the RMS-fields, and also EXP vs. N48 and EXP vs. NMC show the same evolution at the surface.

Charts of 500mb and 1000mb (not displayed in this report except for day 10) confirm the above objective comparison. There are only very small differences between EXP and IMP in these synoptic maps. For example the development of a low near the British Isles during day 2-3 is almost

identical in both integrations, but very different from N48.

To summarise the results of this paragraph: it was found that the two versions of the model produce very similar integrations, even on a data set in which initially a disproportionate part of the energy is present in gravity waves. It has not been established, however, whether the energy sources or sinks are really necessary or whether the horizontal diffusion alone may be sufficient or even essential to dissipate the gravity waves. This question is nevertheless important. The purpose of horizontal diffusion is to control the accumulation of unwanted noise at the short wave length end of the spectrum. In high resolution models this noise is accumulated at smaller scales and therefore such models may well be run with smaller diffusion constants. If it could be shown that diffusion is essential to keep both integrations together, the validity of the conclusions from this experiment may well be limited to low resolution models.

CHAPTER III - A COMPARISON WITH OTHER FORECASTING MODELS

In this chapter we compare the performance of the spectral model (T21) with that of two gridpoint forecasting models and with the observed state of the atmosphere. The two grid point models are an N24 version of ECMWF's grid point model (indicated by D24) and GFDL's N48 model. Both grid point models use an explicit leap-frog time-stepping scheme, but with different time smoothing. In D24 a simple timefilter is applied; in N48 this is combined with an occasional Euler-backward timestep.

In Chapter I we pointed already at the differences between the models, the performances of which are compared here. These differences are found in the horizontal diffusion and in the integration of the hydrostatic equation. For details we refer to Table II, to Baede and Hansen (1977) and to Internal Reports 6 and 9.

As in all integrations at ECMWF, the NMC analysis is supposed to represent the true state of the atmosphere.

In the study of the high-resolution run extensive comparisons were made with other models, including T21. Therefore we will present here only a limited discussion, mainly touching upon those features which are peculiar to T21, for the rest referring to Baede and Hansen (1977). We shall omit, for example, a synoptic description of the ten-day period and we shall not present any forecast maps.

In the first paragraph we present a very brief description of the differences in the initial data for the different models. Next we compare the models on the basis of RMS-errors and correlation coefficients, being aware of the difficulties due to the differences of the variances of the forecasts. In the following two paragraphs we discuss

two topics, which received little or no attention in the report of Baede and Hansen (1977). First we show some time averaged anomaly maps and conclude that the T21 forecast does not bear much resemblance with reality in the second half of the forecasting period. An important problem is the loss of kinetic energy, particularly in the zonal part, associated with a gradual breakdown of the subtropical jetstream. This is discussed in more detail in paragraph 4. Finally in the last two paragraphs we highlight two features in which T21 differs significantly from the other models. This is clearly related to the low resolution of T21 but we are not in a position to offer a detailed explanation. These two features are: the shape of the precipitation areas and the energy balance of the atmosphere.

The discussion is not, and is not meant to be, very comprehensive. It was felt from the very start that the horizontal resolution of T21 is too low to be useful for medium-range forecasting and therefore in this respect the emphasis should be put on a T40 integration. Indeed, from the results presented in Baede and Hansen (1977) it is clear that the resolution is insufficient to describe in detail meteorologically important small scale features, but nevertheless it is difficult in many cases to give objective arguments for one model's superiority above the other.

III.1 The initial data set of the different models

As described in Chapter II, the initial data for the integrations is taken from the 1 March 1965 00Z data set produced by GFDL on σ-surfaces on an N48 modified Kurihara grid. The GFDL set in its turn was derived from the NMC data, among other sources. This set was interpolated linearly to a Gaussian grid of 96 latitude lines and 256 points per line, from which a T63 spectral data set was

computed; this set was truncated to T21. Linear interpolation was also used to compute the data on the regular grid of ECMWF's D24 grid point model.

As can be seen from the maps in Fig.III.1 and III.2, some energy in the shortest waves was lost by the interpolation procedures, particularly in the low resolution models. This is confirmed by Fig.III.3 which shows the kinetic energy of the forecast as a function of time. The initial data of T21 and D24 have less kinetic energy than N48, which again has less energy than the NMC analysis, in all wave number groups.

III.2 Verification by means of RMS-errors and anomaly-correlations

Following other reports on numerical integrations at ECMWF we shall now present root-mean-square errors and correlations between anomalies. The latter is normalized by the variance of each field. To emphasize certain parts of the spectrum a spectral analysis is applied. At ECMWF the following grouping of wavenumbers is used: wavenumbers 1-3, 4-9 and 10-20 are combined together.

For a more formal presentation of the verification method we refer to Arpe et al. (1976).

Two curves are added to the RMS-error plots: one labelled "persistence" and one "normal". (Baede and Hansen, 1977). Whenever a curve for RMS-errors crosses either persistence or the normal we shall say that the prediction ceases to be useful. It will be shown later that this happens after different time lengths (from 2 days and up to 9-10 days) depending on spatial scale and pressure level.

RMS-errors should be interpreted with some care, if predicted and observed fields have a different spatial variance. This problem can be pronounced in T21 due to its relatively low resolution.

Let us now look at Fig. III.4. Here we see the error in the height field for the layer 1000-200 mb, averaged over most of the Northern Hemisphere. The distribution of errors in wavenumber groups clearly shows, that the smallest scales have the lowest RMS-errors. This is of course due to the fact that the energy in wavenumbers 10-20 is much smaller than in the rest of the spectrum. Already after 1-2 days it is better to use climatology, and this goes for all models. This is a general feature throughout the RMS-plots. However we cannot conclude from this that the short waves may be omitted. Their presence may be important for a proper simulation of interactions and transport processes in the integration.

The largest contribution to the total error comes from waves 1-3, but compared to the variance in these ultra long waves it is only a small error. We therefore find that the prediction here is relatively better than for the rest of the spectrum. We observe an error considerably lower than the normal. It is noteworthy that N48 does better than T21 and D24 after 5-6 days, although only by a small amount.

Obviously the prediction of the zonal part is difficult. Initially a relatively high RMS-error is found in D24. All models reach the normal very soon. It is also interesting to note that in the zonal part all asymptotic levels, including that of persistence, are close to NORM. This may indicate that the zonal NORM is not representative for this particular ten day period.

In the important wavenumber domain, 4-9, T21 apparently does best, but only after NORM has been reached. With the aid of the anomaly correlations shown in Fig. III.9 we can conclude once more that T21 has a low RMS-error due to low variance. That is, for most of the spectrum the different behaviour of the models after some days is

associated with the different smoothing effects in the models.

Comparing Figs. III.5 and III.6 we observe that near the surface the models approach their asymptotic level faster than they do in the middle of the troposphere. Fig. III.7 however shows that the absolute errors near the surface are small compared with those in the free atmosphere: the largest absolute error growth occurs near the tropopause. In latitudinal direction we observe the largest growth in middle latitudes. In both plots we see a close resemblance between the models. We have now compared errors, defined as the difference between a predicted field and NMC. Let us recall Fig. II.6. There we presented RMS-differences between models. We observed that the differences between N48 and EXP were of the same order of magnitude as that between NMC and EXP.

Correlation coefficients are especially sensitive to errors in displacements of waves. A clear indication of this is found in Figs. III.9, 10 and 11, which correspond to Fig. III.4, 7 and 8. The middle panel of Fig. III.9 clearly demonstrates that information in wavenumbers 10-20 is lost very early in the integrations. Almost the same can be said about wavenumber group 4-9. There is no need to distinguish between the models. Wavenumbers 1-3 are predicted most accurately also with respect to this correlation plot. We see that all models are clearly better than persistence, indicating that at least for one week we can trust the displacements of those very long waves. T21 and N48 produce better correlations than D24. The persistence level for the zonal part is rather high, so changes in the zonal field are minor, but those which are there are not predicted with better skill than persistence can achieve.

We may conclude that no strong preference can be given to any model on the basis of the traditional RMS and

correlation scores along. D24 tends to score lower, particularly in the second half of the forecasting period, but all models have then reached the NORM RMS error level. Other skill scores or verification measures should be used in order to come to a meaningful quality distinction between the models.

III.3 Time averaged anomaly maps

In Baede and Hansen (1977) we presented a synoptic comparison on the basis of day by day maps of the different forecasts during the ten day period. In this report we attempt to present the models' general performance by comparison of time averaged anomaly maps (500mb) for T21, N48 and NMC.

These maps are constructed by first defining 5 days means centred around day 2.5 and day 7.5. From these fields the mean state of 500mb for March is subtracted. In this way we easily recognize areas with above average cyclogenesis or anticyclogenesis. For the first period these are: North-Pacific, North-Atlantic plus Western Europe, Central U.K. plus Central Atlantic, the Northern part of the American continent and finally the Central parts of Asia. Figure III.12a, c,d, show the major cyclone areas are predicted very well in both T21 and N48, with respect to absolute values, locations and shapes. The highs, however, are not predicted with the same quality in T21. The values observed for both areas are too low. We believe that this is due to the smoothing effect of the low resolution of T21. The explanation is also valid for negative-anomaly areas. The relatively good agreement over Western Europe is not due to a good simulation of individual events, taking place in this area. The trough at 500mb, moving eastward over Europe, has a structure in T21 quite different from that in NMC. T21 predicts generally lower 500mb heights for the whole polar region, which is further amplified by

this trough. In reality more intense but more locally defined disturbances travelled through this area. The areas with positive anomaly, however, have less activity, whereby the truncation of T21 is visualized better. We must conclude that T21 can predict areas with cyclogenesis with reasonable accuracy but conclusions should not be made on mean charts alone, but also on the evolution of individual events. In other words, we will expect T21 to produce lows and highs in the climatologically right areas, but the resemblance to reality will often be poor.

If we proceed to Fig. III.12b,e,f, we observe only a crude resemblance of T21's anomaly chart to NMC's. In particular the quadrant between 60°W and 30°E is predicted poorly. The positive anomaly over North America is to some extent predicted well in T21 and N48. N48 also underestimates the intensity of the highs. One feature is interesting: the slow eastward displacement of the negative anomaly over U.S. is simulated properly in T21 but not in N48. We must, however conclude that the general impression is that only the first 5 days have any meaning in a synoptic comparison of T21 with reality. Beyond that point the model behaves climatologically correctly, but we can no longer draw conclusions about single lows or highs because they differ from reality with the same amount as two arbitrarily chosen situations.

III.4 Zonal means of temperature and zonal wind speed

One of the most characteristic features in the integrations performed at ECMWF, and indeed a common feature of many forecasting models, is the loss of kinetic energy. Fig. III.3 shows that this is the case for both the long and the baroclinic waves, but moreover the low resolution models suffer from a substantial decrease of zonal kinetic energy.

We can associate that with a gradual breakdown of the subtropical jetstream, in the models much more so than in reality. This is shown particularly well in Fig.III.13, which shows the latitude-time distribution of kinetic energy, averaged over the troposphere. Figure III.14, 15 and 16 show the time evolution of zonal mean of zonal wind in three steps: mean of day 1-4, day 4.5-7 and day 7.5-10. Fig. 14 in the series shows an initial clear underestimation of the strength of the jet. T21 especially has a low maximum of the wind 35m/s vs. 45m/s in NMC. We can attribute this to the relatively severe truncation in T21, combined with the use of interpolation procedures to obtain a gaussian gridpoint field. Horizontal variations are smaller in the forecast models, the polar jet especially is shown as less pronounced. We know from the synoptic evolution that the polar jet is lost in the first five days of integrations. This can be confirmed by looking at Fig.III.15 where we notice a complete lack of the local maximum of windspeed near 70^{o}N in 300mb. Again T21 stands out with the lowest value of the subtropical jet. It should be noted that NMC also shows a marked breakdown of the polar jet in the later stages (Figure III.16).

It is also interesting to observe the vertical slopes of the jet axis as time goes on. The two gridpoint models, D24 and N48, develop an almost vertical axis in the lower troposphere, whereas NMC has a vertical axis in the upper parts. In T21 we find an intermediate evolution with a linear profile.

Another way of looking at the gradual breakdown of the subtropical jet stream is presented in Fig.III.17 where $\frac{\partial T}{\partial y}$ at 500mb is shown as a function of latitude, zonally averaged. The frontal zones are of course represented by regions with high negative values and we see that these regions weaken with time. We observe moreover the breakdown of the polar front, both in reality and in the models.

In this section we have seen that the low resolution models suffer from a decrease of zonal kinetic energy, apparently due to a breakdown of the sub tropical front. That the vertical resolution also plays a role is suggested by the observation that also N48 is unable to keep the front at its right intensity.

III.5 Precipitation

In this and the following paragraph we discuss two phenomena, both related to precipitation, in which T21 behaves differently from the other models. In this paragraph we discuss the synoptic rain patterns produced by the models. The effect of the rain through latent heat release is discussed in the next section within the framework of a general discussion of the heat balance of the atmosphere.

Figs.III.18a-c show rainfall patterns in the three forecast models, D24-data were not available but instead data from a similar run with non-linear diffusion are used. Also our T40-version is presented. The plots show accumulated rainfall over 24 hours, ending at day 1, day 5 and day 10, respectively. No distinction is made between what is called large scale rainfall and small scale rainfall. Unfortunately, no observations were available for comparison.

The patterns in the northern hemisphere for the first day are almost the same in all models. We know that the global amount of rainfall differs from model to model. It is due to rainfall outside the region shown in Fig.III.18.

Fig.III.19 shows the latitude-dependence of 12 hours accumulated rainfall for the periods 1-12h, 24-36h and 48-60h (units are W/m^2 instead of kg water/m^2). It is obvious from these two plots that both models develop an intense rainfall in the tropics, and the intensity continues to grow after $2\frac{1}{2}$ days. The middle latitude-rainfall belt, however, levels

off at almost the same precipitation rate in the two models. Note the very high values of rainfall in the gridpoint model near the Equator. The increasing rainfall in the tropics represents an enormous surplus of energy input in the atmosphere after a couple of days (see Fig.III.20), after an initial deficit.

Fig.III.18a-c emphasize the resolution-problem in T21. The circular rainfall patterns indicate that T21 is too low a resolution at middle latitudes to resolve real synoptic disturbances. T40 is obviously much better in that respect. Another unsuccessful feature of T21, not displayed in a plot, is a constant and heavy rainfall over East China. This may be due to the fact that horizontal diffusion takes place on σ-surfaces rather than p-surfaces which might cause a spurious transport of humidity upwards against the steep south-easterly slope of the Himalayas. This would also explain the resolution dependence of this phenomenon.

The overall impression is that rainfall occurs where it is expected, i.e. at middle latitudes in extra-tropical disturbances and in the tropics. We have no way of verifying the intensity of the different regions, but the global mean approaches the climatological mean (Fig.III.18).

III.6 The energy balance of the atmosphere

In this paragraph we shall draw attention to a few aspects of the energy balance of the atmosphere, which are peculiar to either spectral models in general, or to T21 in particular.

Fig.III.20, to which we referred earlier, shows the energy gain of the atmosphere due to latent heat release by rainfall. Snow is omitted from this discussion. It does not exhibit

any peculiarities and is fairly constant. Clearly during the first few days all models have an enormous deficit of rainfall. The gridpoint models and T40 produce a large surplus by day 3, to relax during the next few days to an asymptotical level of about 100W/m^2. Only T21 reacts much more gently and hardly shows any surplus peak. As we saw in Fig.III.18, the high rain intensity by day 3 is associated with heavy rainfall in the tropics and cannot be explained by mid-latitudinal synoptic features. We must conclude that T21 is too highly truncated to allow strong static instabilities to occur over large areas. The initial deficit is thought (Baede and Hansen, 1977) to be caused by a poor initial humidity analysis, together with an unrealistic divergence (and therefore vertical velocity field). The poor quality of the initial humidity analysis is also suggested by the observation that the model suffers from an enormous evaporation during the first few hours of the integration.

The asymptotic level of latent heat release to which all models tend (100W/m^2) corresponds to 3.5mm rain/day, which is generally accepted as the climatological mean. Something like that could of course be expected, when one keeps in mind that the physical parameterization scheme is taken from a general circulation model.

At first sight Fig.III.21 is surprising, because apparently the spectral models transfer heat to the earth, whereas the gridpoint models do the opposite. But we have reasons to believe that surface heat flux in our models on a global scale is a secondary process, in the sense that it is more or less determined by the atmospheric response to other processes such as radiation and precipitation. In Fig.III.21 we ought to add the initial values of surface heat flux, because these show that all models initially start up with positive values. Also radiation has almost the same level in the beginning of the integration.

Thereafter in the gridpoint models, however, the cooling from radiation increases compared to a weakening or constant radiation in the spectral models. Some sort of compensation is then observed in the surface heat flux. We would like to stress that the problem is not solved by the above argument. A more detailed analysis is necessary. There is at least no reason to believe that the spectral model with another physical scheme would behave in the same way.

Conclusions

Although the work presented in this report is by no means complete, some useful conclusions may be drawn.

If high frequency gravity waves are removed from the initial data, the time stepping scheme makes no difference to the result of the forecast. If forcing and dissipation terms are included, the difference between an explicit and a semi-implicit integration is very small, at least compared to the differences with reality or any other model, even if high frequency modes are present in the initial data set. It has, however, not yet been established whether this is brought about solely by the horizontal diffusion or also by the physical forcing. If the former is true, this conclusion may well be valid only for the rather low resolution used in this system. Further work on this problem is in progress.

With respect to the comparison with other models, it was found to be impossible to judge the forecasting capabilities only on the basis of RMS-errors and correlation coefficients. Clearly small scale features are missing from the T21 integration, but major troughs and ridges, associated with areas of cyclogenesis and anti-cyclogenesis are predicted quite well for the first five days. All this is based, however, on one 1965 data set.

The influence on the precipitation of the low resolution is clearly demonstrated. To obtain precipitation areas with a more realistic shape, a higher resolution than T21 is required.

Physical Parameterization	Type and Comments
1. Radiation	Manabe and Strickler (1964) / Manabe and Wetherald (1967). Radiation calculation is dependent on: (i) Climatological distribution of absorbers (H_2O, CO_2, O_3) (ii) Climatological surface temperature for sea and sea ice points. (iii) Specified zonal mean cloudiness. (iv) Specified limits of sea ice extent. (v) Time dependent surface albedo influenced by snow, soil moisture, ice. (vi) Specified absorptivity, reflectivity and height of zonal mean clouds.
2. Vertical Diffusion	Mixing length hypothesis. ℓ= 0 at 2.5 km. No vertical diffusion of temperature.
3. Surface Fluxes	Bulk aerodynamic formulae. C_d = 0.002.
4. Convection (moist and dry)	Energy conserving convective adjustment type. Critical relative humidity for onset of moist adjustment = 0.8.
5. Hydrology	Account taken of rainfall, evaporation, snow accumulation, snow melt and run-off.

TABLE I : Summary of physical parameterization included in all models discussed in this report.

Symbol	Meaning	Horizontal Diffusion	Reference
T40	This integration	$K.\nabla^4 X, K=4.8\times10^{15} m^4 s^{-1}$	This report
T21	Low resolution spectral integration	$K.\nabla^4 X, K=6.0\times10^{16} m^4 s^{-1}$	Hansen and Baede, 1977
T48	GFDL N48 9-layer model	Non-linear diffusion (Smagorinsky)	Arpe et al, 1976, Miyakoda, 1973.
D24	ECMWF grid-point model 9-layer N24 version	$K.\nabla^2 X, K=2.5\times10^{5} m^2 s^{-1}$	Gauntlett et al, 1977
NL2	ECMWF grid-point model. 9-layer N24 version	Non-linear diffusion $K.\lvert\nabla^2 X\rvert.\nabla^2 X$ (K is variable-dependent)	Gauntlett et al, 1977
D48	ECMWF grid-point model. 9-layer N48 version	Non-linear diffusion $K.\lvert\nabla^2 X\rvert.\nabla^2 X$ (K is variable-dependent)	Gauntlett et al, unpubl
NMC	Set of NMC analyses of forecast period	-	Arpe et al, 1976.

TABLE II: The models referred to in this report

	Δ t (min)		α		K ($m^4 . S^{-1}$)
	EXPL.	IMPL.	EXPL.	IMPL.	EXPL. + IMPL.
T21	10	30	.015	.05	$6.0 * 10^{16}$
T40	-	20	-	.03	$4.8 * 10^{15}$

TABLE III Time step length, time smoothing constant and horizontal diffusion constant of the runs discussed in this report.

References

Andersen, J.H. (1977) "A Routine for Normal Mode Initialisation with Non-Linear Correction for a Multi-level Spectral Model with Triangular Truncation" ECMWF Internal Report No. 15

Arpe, K., Bengtsson, L., Hollingsworth, A. and Janjic, Z. (1976) "A case study of a ten-day prediction" ECMWF Technical Report No. 1

Baede, A.P.M. and Hansen, A.W. (1977) "A ten-day High-resolution Non-adiabatic Spectral Integration; a comparative study" ECMWF Technical Report No. 7

Bourke, W., McAveney, B., Puri, K. and Thurling, R. (1977) "Global Modelling of Atmospheric flow by spectral methods" "Methods in Computational Physics", Vol.17,Ed. J. Chang, Academic Press, 1977,pp.267-324.

Hoskins, B.J. and Simmons, A.J. (1975) "A Multi-layer spectral model and the semi-implicit method" Quart. J.R. Met. Soc., 101, pp.637-655.

Janjic, Z. and Wiin-Nielsen, A. (1977) "On Geostrophic Adjustment and Numerical Procedures in a Rotating Fluid" J. Atmos. Sci.,34, pp.297-310.

Machenhauer, B. (1977) "On the Dynamics of Gravity Oscillations in a Shallow Water Model, with Applications to Normal Mode Initialisation" Beitr.z.Phys.der Atmosphäre,50 pp.253-271.

References (contd.):

Miyakoda, K. (1973) "Cumulative results of testing a mathematical model. The description of the model" Proc. Roy. Irish Academy, 73A, pp.99-130.

Wiin-Nielsen, A. (1976) "On Geostrophic Adjustment on the Sphere" Beiträge zur Physik der Atmosphäre 49, pp.254-271.

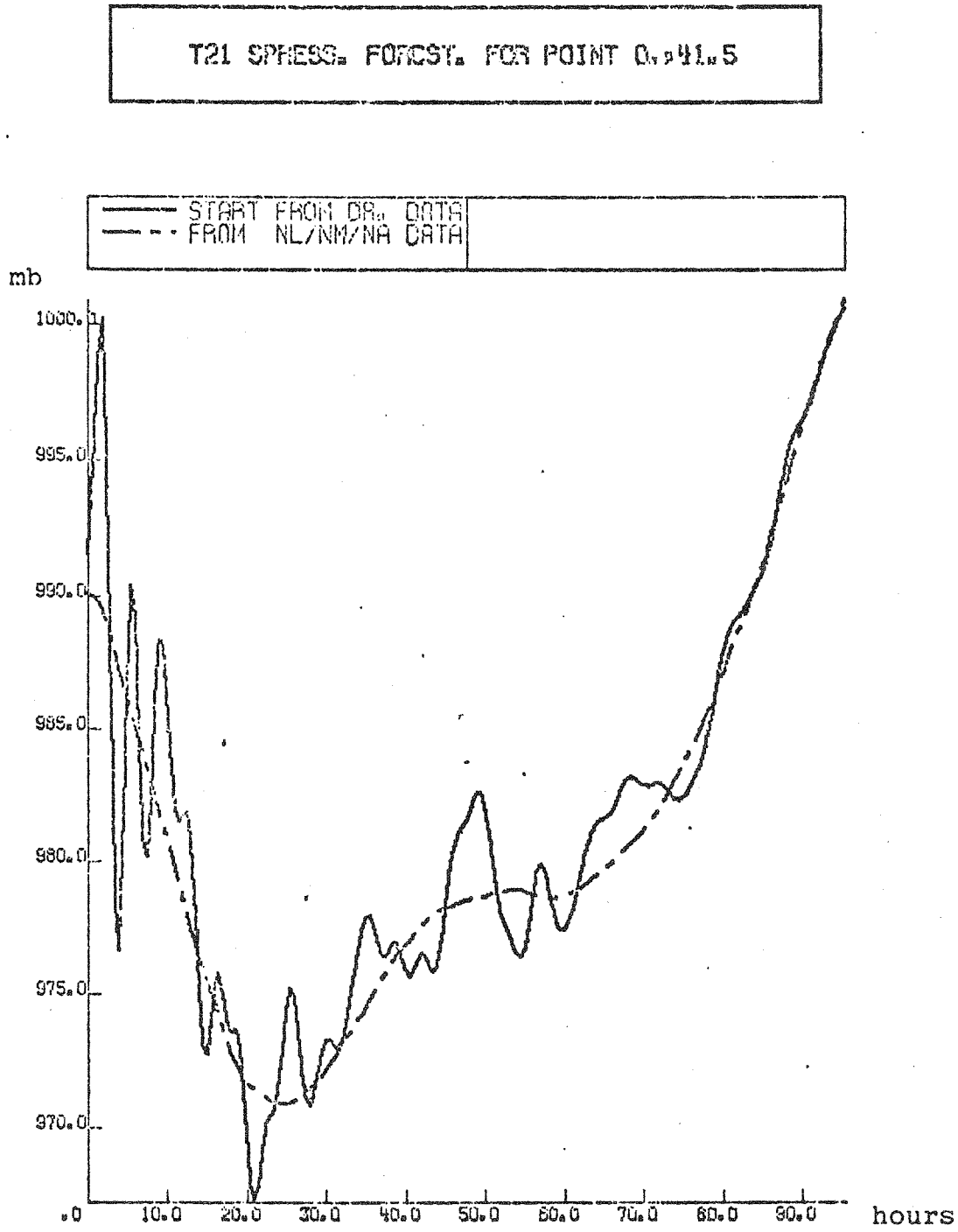

Fig.II.1.

The effect of initialization for the surface pressure forecast of a gridpoint located at $(\lambda,\phi) = 0^{o}.,41^{o}.5$

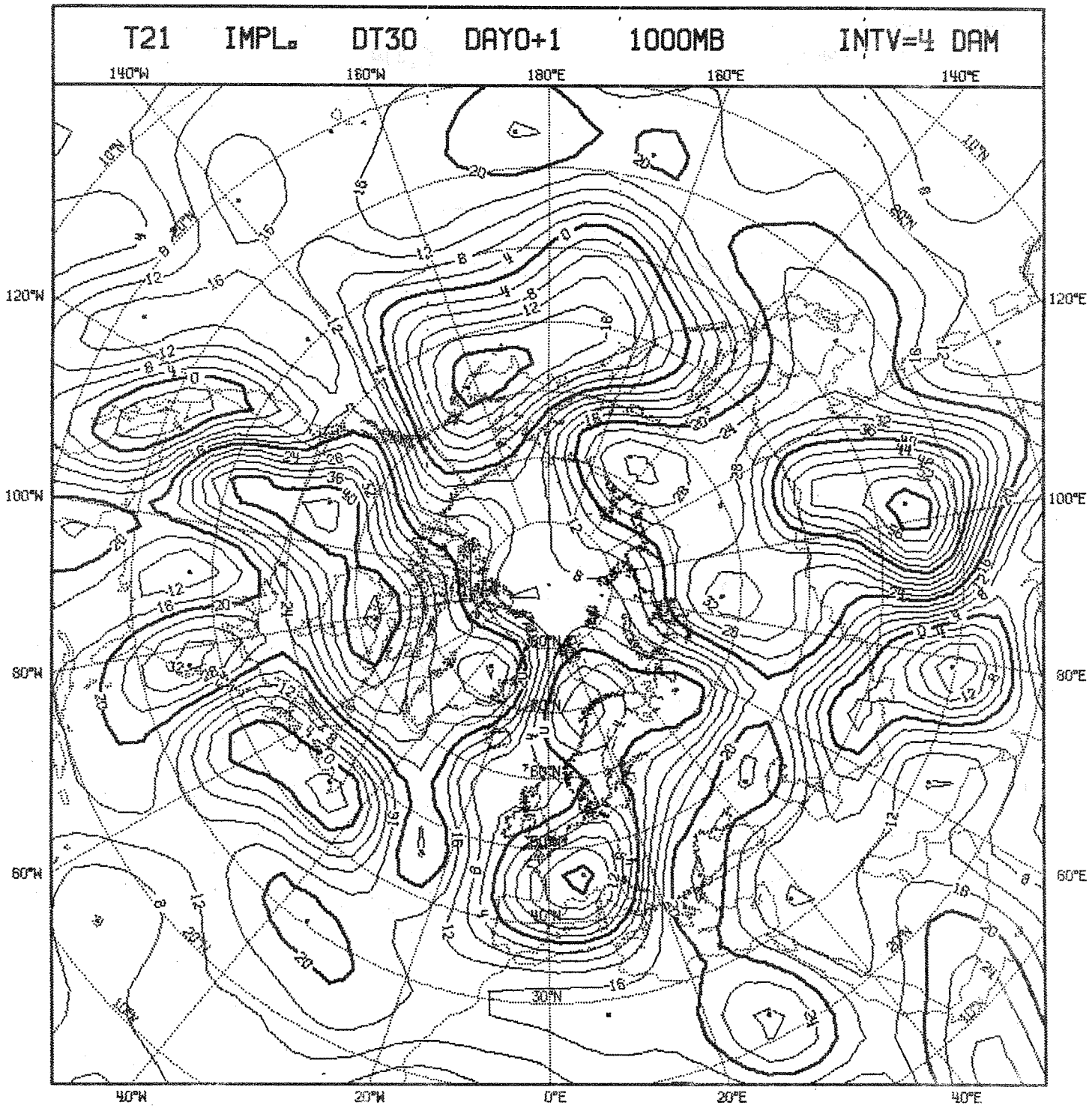
T21 IMPL. DT30 DAY0+1 1000MB INTV=4 DAM
140°W
180°W
180°E
140°E
120°W
120°E
100°W
100°E
80°W
80°E
60°W
60°E
40°W
20°W
0°E
20°E
40°E

Fig.II.2a.

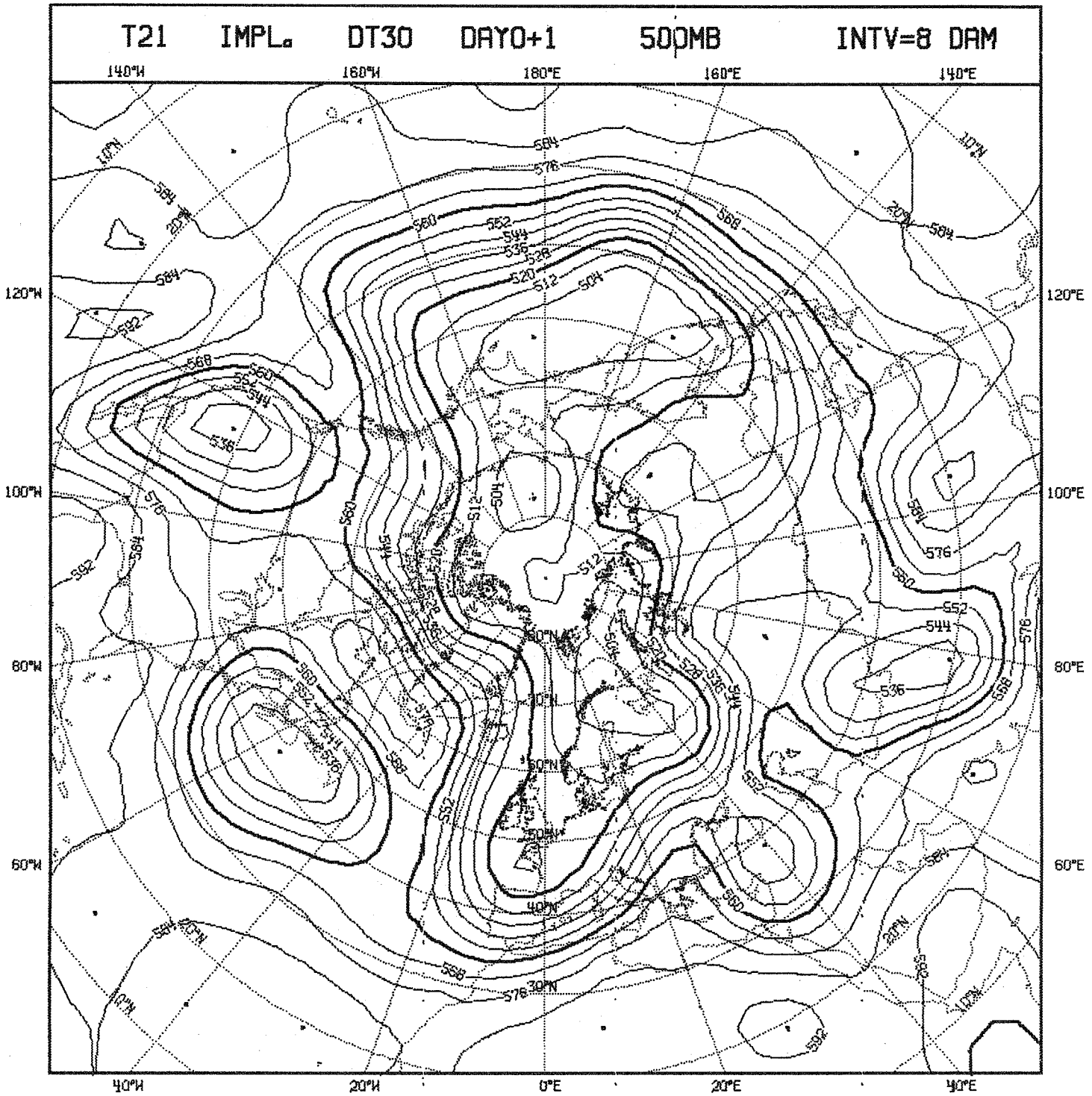
T21 IMPL. DT30 DAY0+1 500MB INTV=8 DAM
140°W
160°W
180°E
160°E
140°E
120°W
100°W
80°W
60°W
120°E
100°E
80°E
60°E
40°W
20°W
0°E
20°E
40°E
10°N
20°N
30°N
40°N
50°N
60°N
584
576
568
560
552
544
536
528
520
512
504
592

Fig.II.2b.

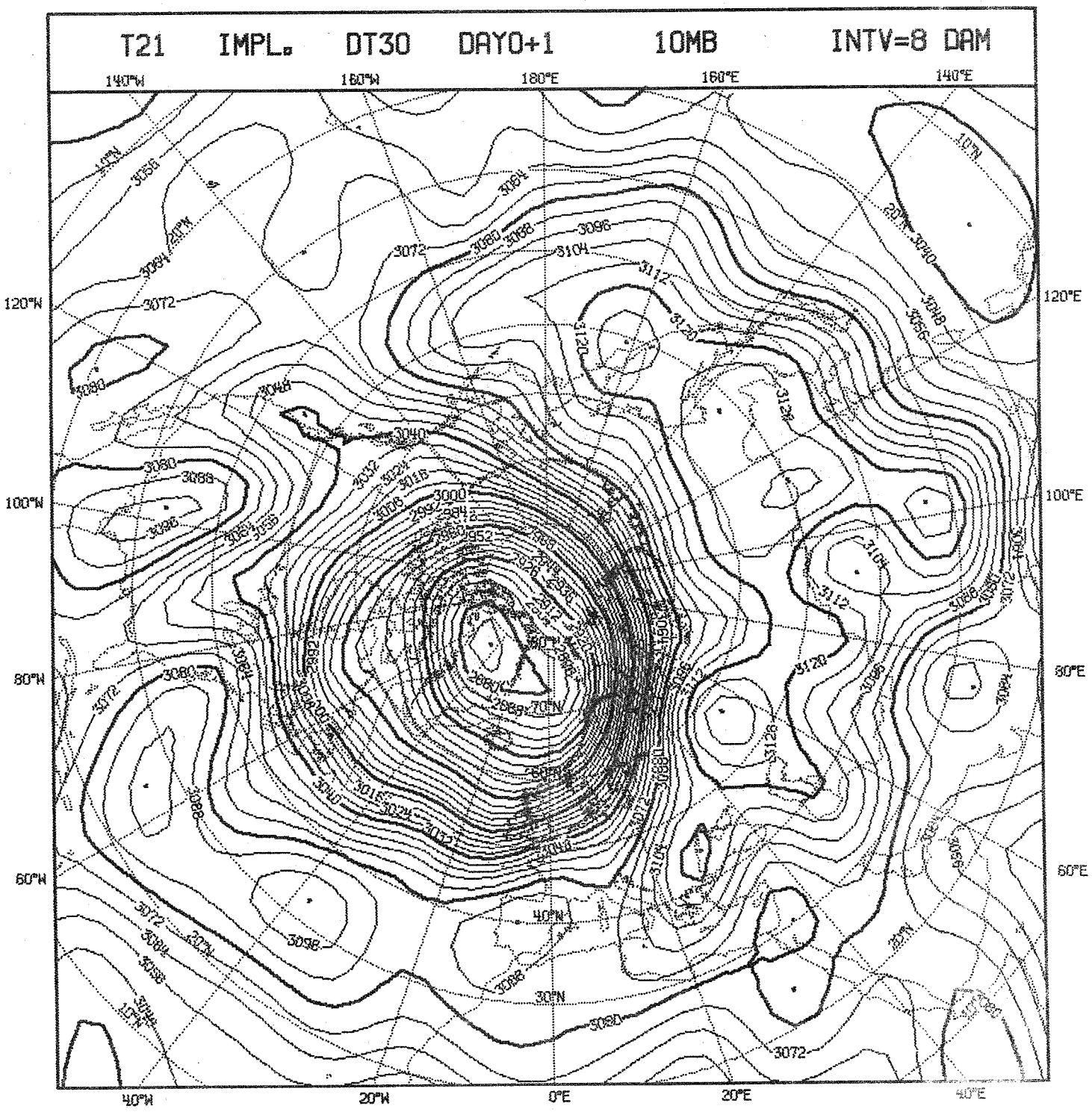
T21 IMPL. DT30 DAY0+1 10MB INTV=8 DAM
140°W
160°W
180°E
160°E
140°E
120°W
120°E
100°W
100°E
80°W
80°E
60°W
60°E
40°W
20°W
0°E
20°E
40°E
70°N
40°N
30°N

Fig.II.2c.

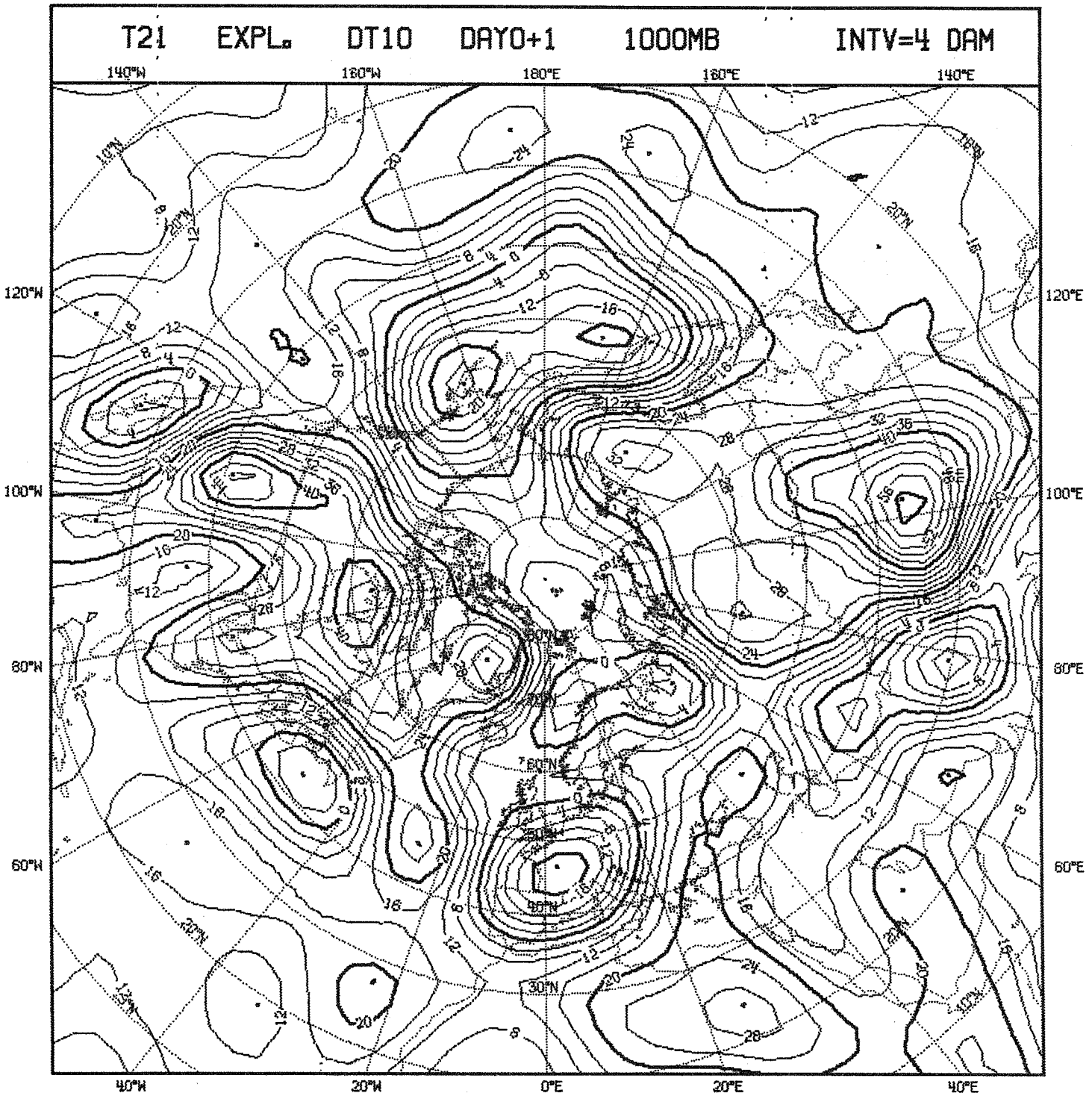
T21 EXPL. DT10 DAY0+1 1000MB INTV=4 DAM
140°W
160°W
180°E
160°E
140°E
120°W
100°W
80°W
60°W
120°E
100°E
80°E
60°E
40°W
20°W
0°E
20°E
40°E
60°N
30°N

Fig.II.2d.

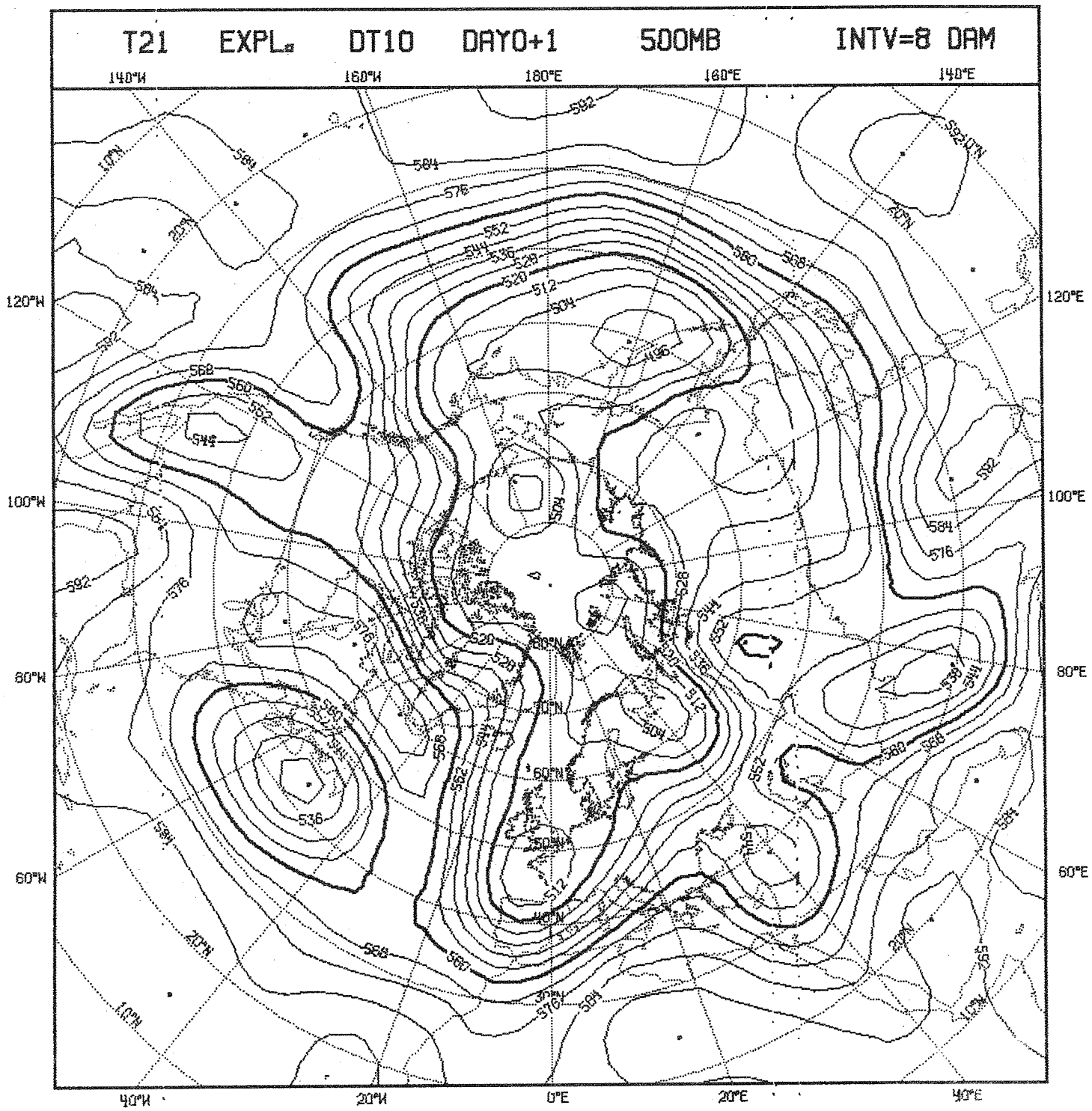
T21 EXPL. DT10 DAY0+1 500MB INTV=8 DAM
140°W
160°W
180°E
160°E
140°E
120°W
100°W
80°W
60°W
120°E
100°E
80°E
60°E
40°W
20°W
0°E
20°E
40°E

Fig.II.2e.

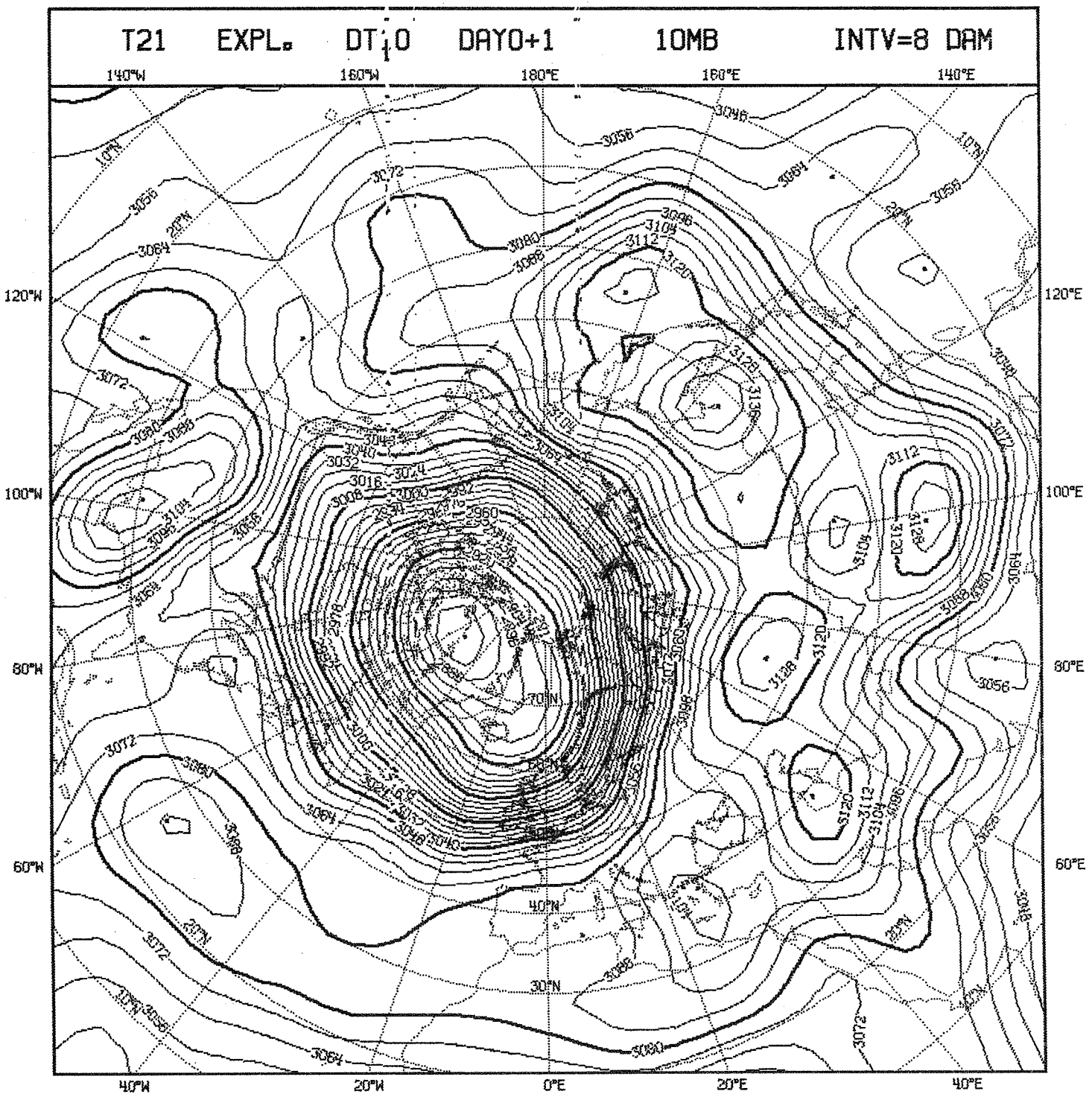
T21 EXPL. DT 0 DAY0+1 10MB INTV=8 DAM
140°W
160°W
180°E
160°E
140°E
120°W
100°W
80°W
60°W
120°E
100°E
80°E
60°E
40°W
20°W
0°E
20°E
40°E
70°N
60°N
50°N
40°N
30°N
20°N
10°N

Fig.II.2f.

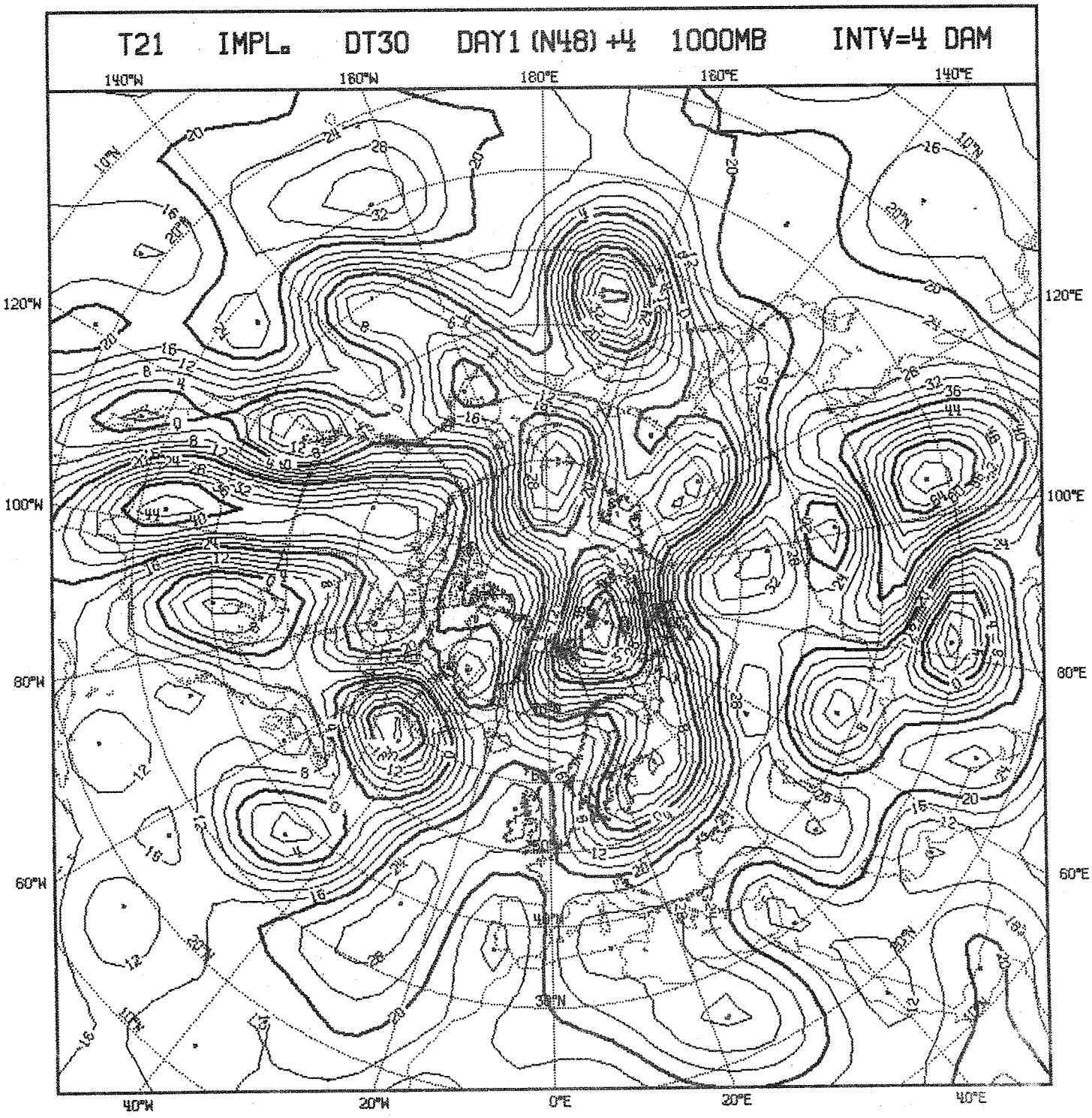
T21 IMPL. DT30 DAY1 (N48) +4 1000MB INTV=4 DAM
140°W
160°W
180°E
160°E
140°E
120°W
120°E
100°W
100°E
80°W
80°E
60°W
60°E
40°W
20°W
0°E
20°E
40°E

Fig.II.3a.

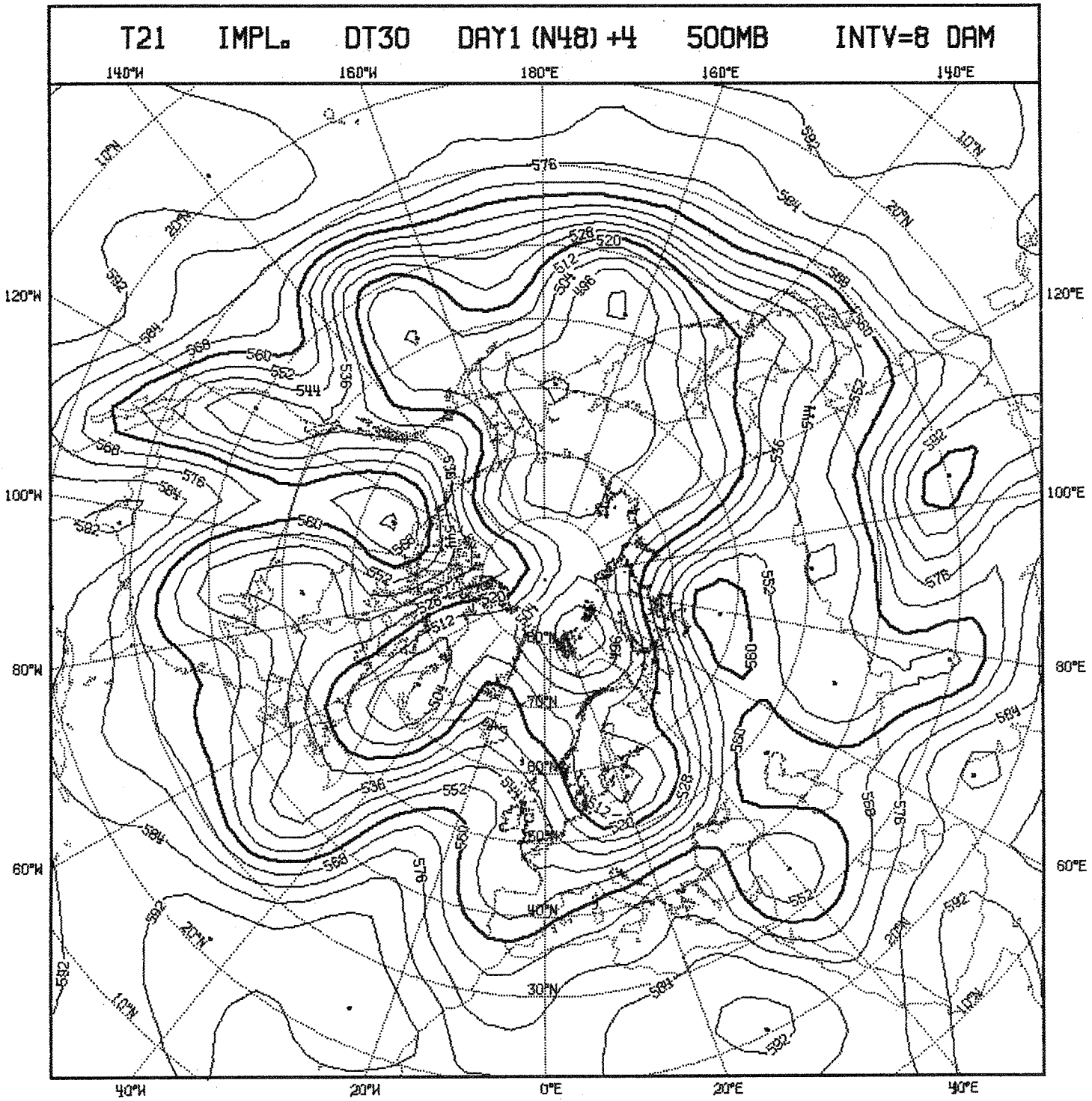
T21 IMPL. DT30 DAY1 (N48) +4 500MB INTV=8 DAM
140°W
160°W
180°E
160°E
140°E
120°W
100°W
80°W
60°W
120°E
100°E
80°E
60°E
40°W
20°W
0°E
20°E
40°E
10°N
20°N
30°N
40°N
50°N
60°N
70°N
80°N

Fig.II.3b.

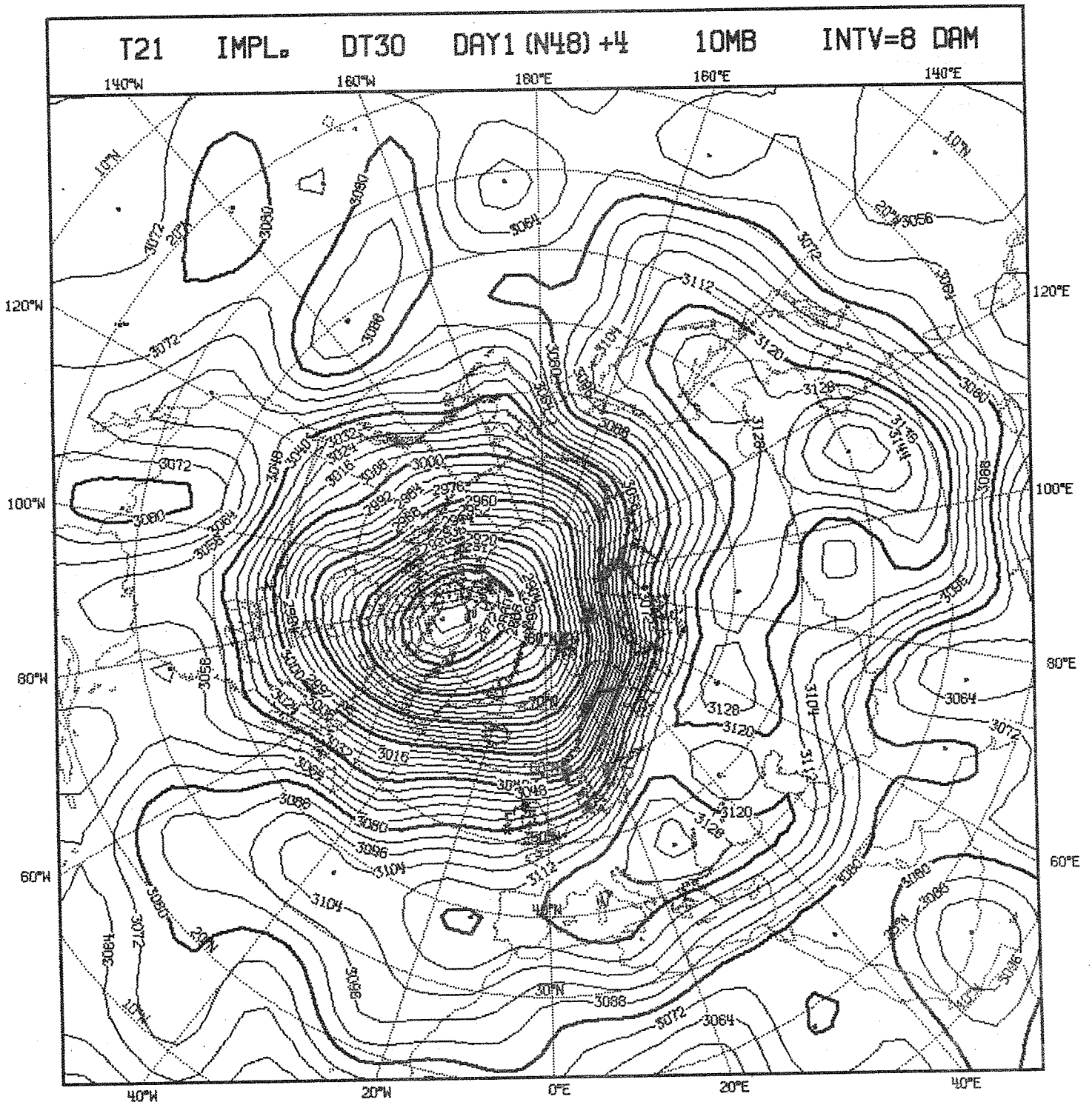
T21 IMPL. DT30 DAY1 (N48) +4 10MB INTV=8 DAM
140°W
160°W
180°E
160°E
140°E
120°W
100°W
80°W
60°W
120°E
100°E
80°E
60°E
40°W
20°W
0°E
20°E
40°E

Fig.II.3c.

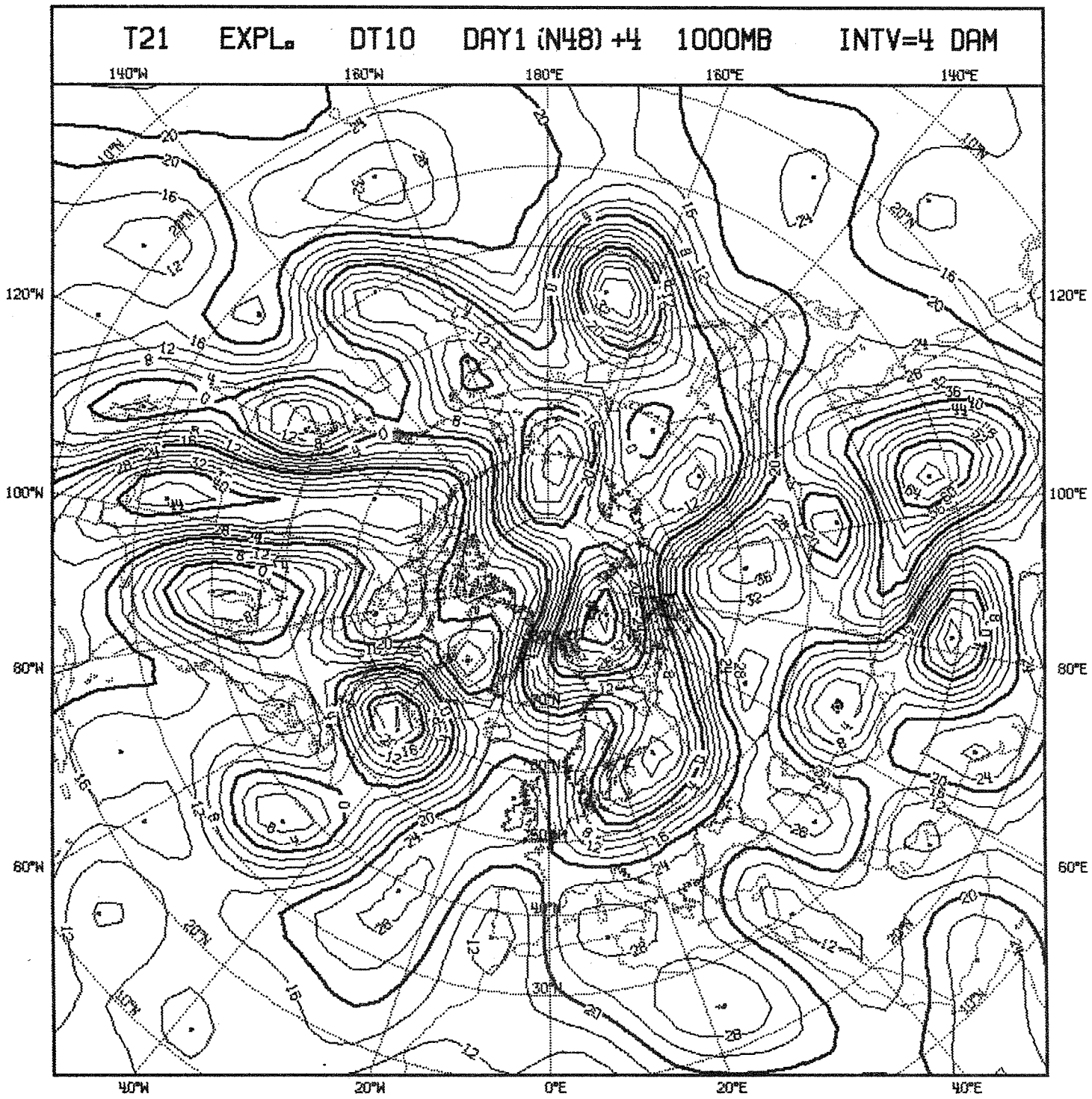
T21 EXPL. DT10 DAY1 (N48) +4 1000MB INTV=4 DAM
140°W
160°W
180°E
160°E
140°E
120°W
100°W
80°W
60°W
120°E
100°E
80°E
60°E
40°W
20°W
0°E
20°E
40°E

Fig.II.3d.

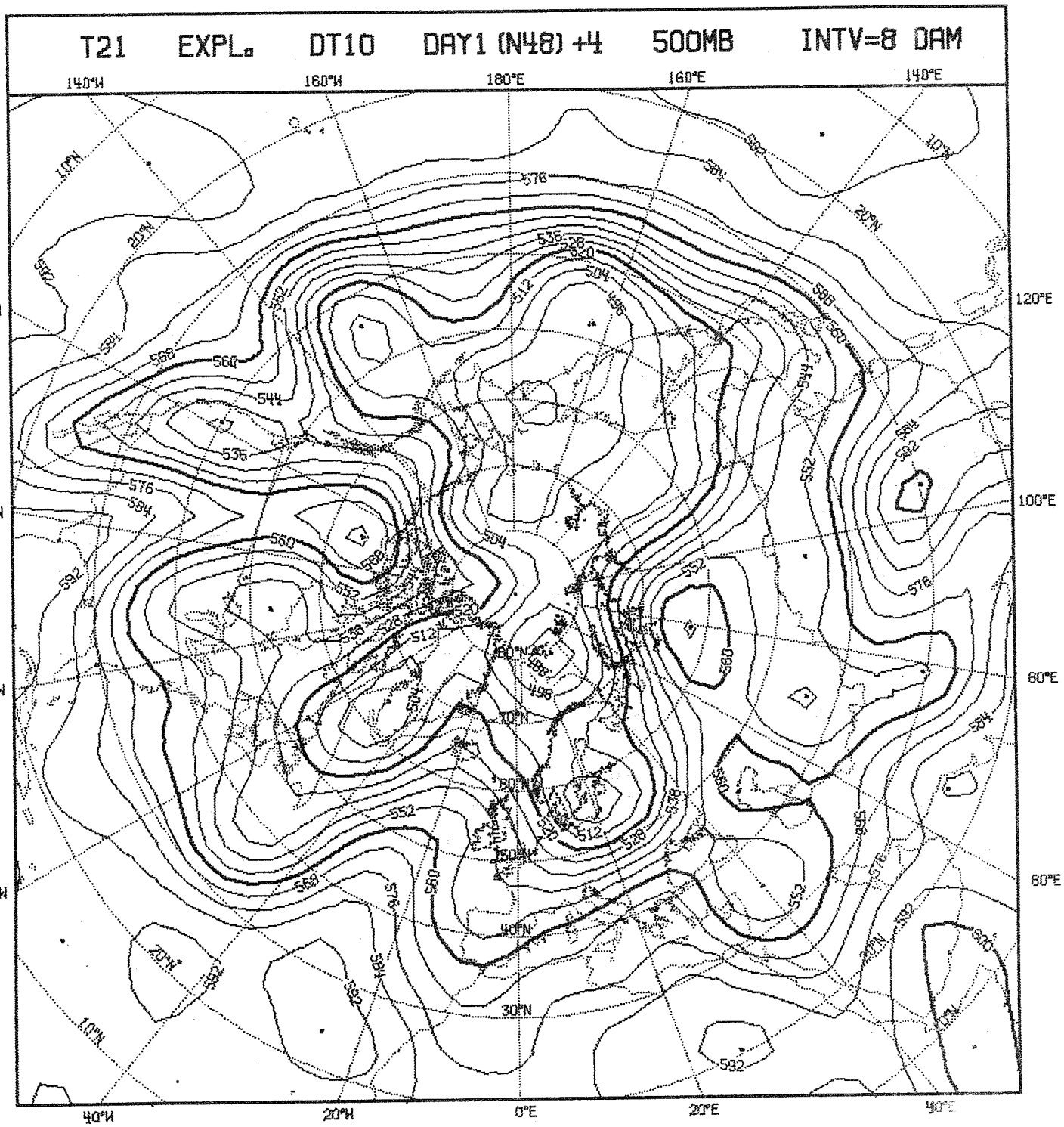
T21 EXPL. DT10 DAY1 (N48) +4 500MB INTV=8 DAM
140°W
160°W
180°E
160°E
140°E
120°W
100°W
80°W
60°W
120°E
100°E
80°E
60°E
40°W
20°W
0°E
20°E
40°E
10°N
20°N
30°N
40°N
576
536
528
520
504
496
512
544
560
552
568
584
592

Fig.II.3e.

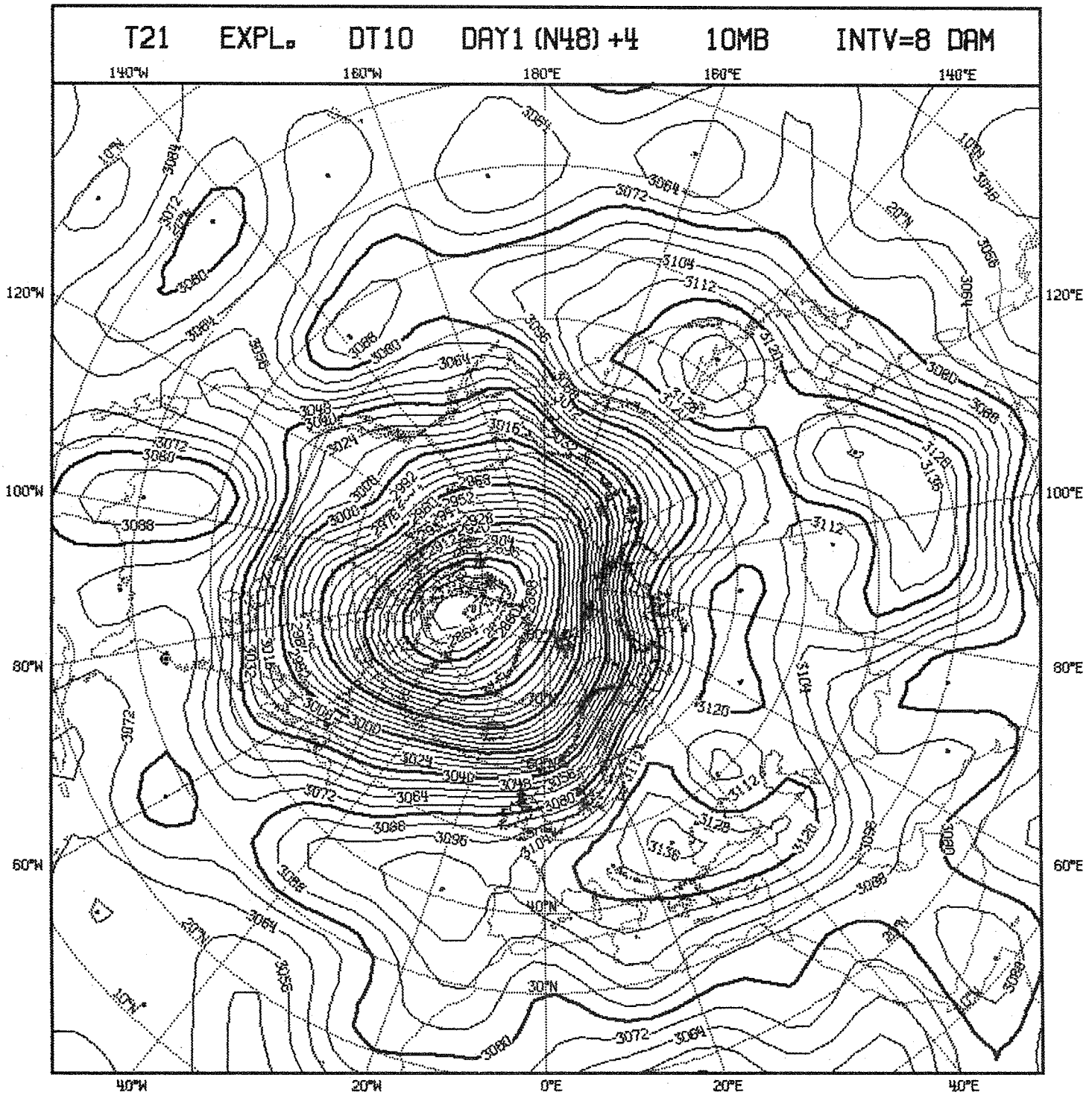
T21 EXPL. DT10 DAY1 (N48) +4 10MB INTV=8 DAM
140°W
160°W
180°E
160°E
140°E
120°W
100°W
80°W
60°W
120°E
100°E
80°E
60°E
40°W
20°W
0°E
20°E
40°E
40°N
30°N
20°N
10°N

Fig.II.3f.

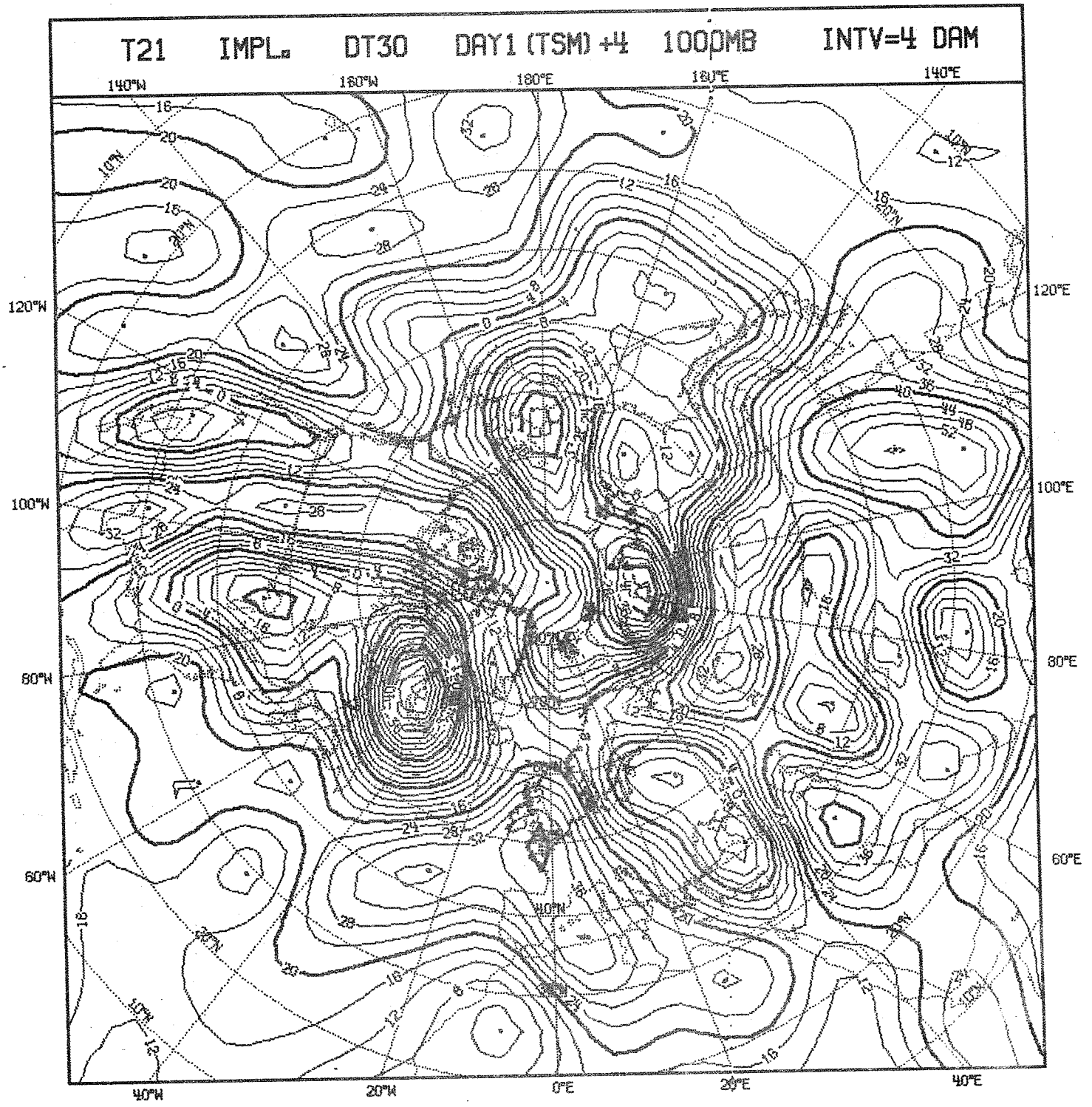
T21 IMPL. DT30 DAY1 (TSM) +4 100MB INTV=4 DAM
140°W
160°W
180°E
160°E
140°E
120°W
100°W
80°W
60°W
120°E
100°E
80°E
60°E
40°W
20°W
0°E
20°E
40°E

Fig.II.4a.

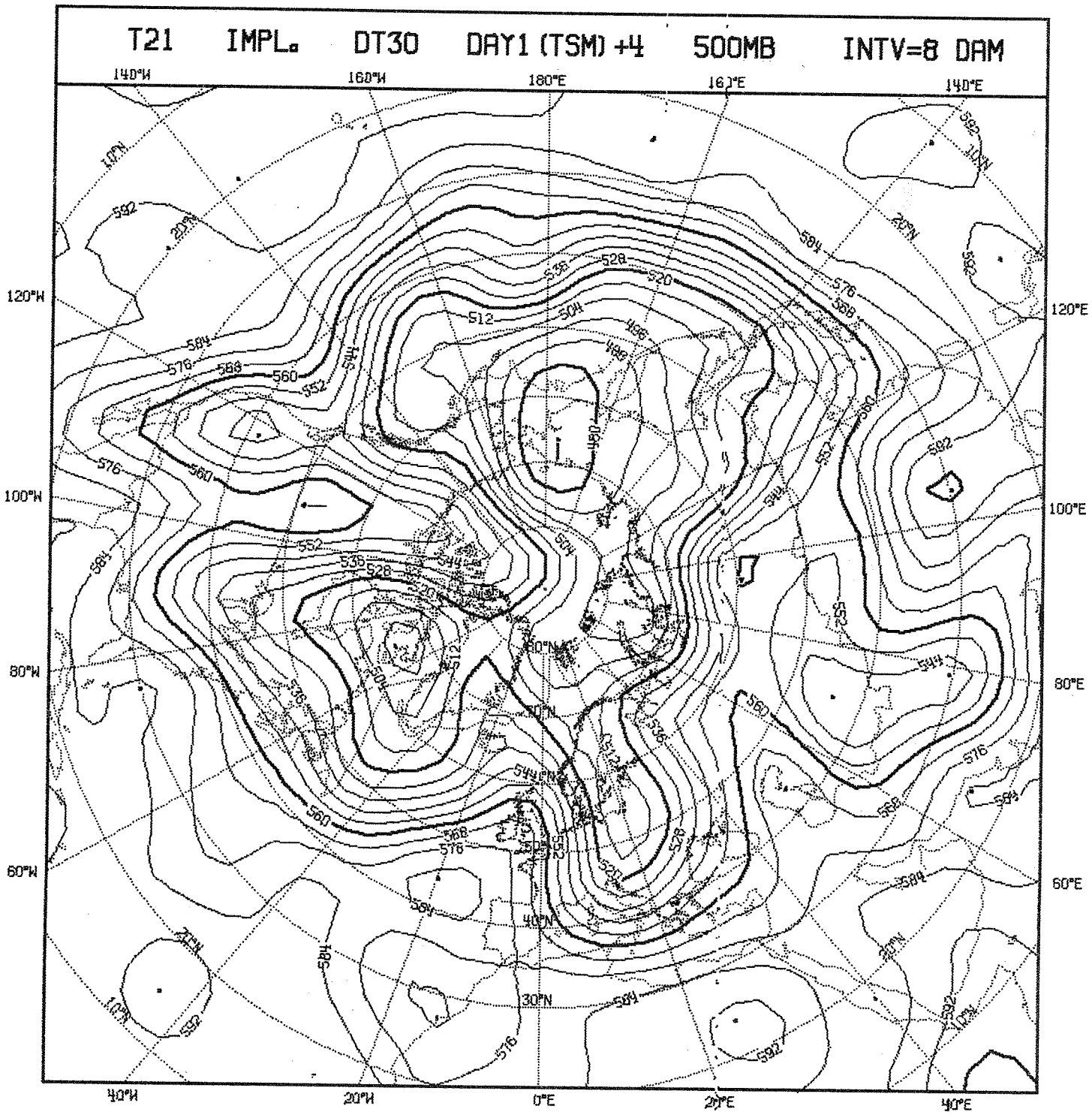
T21 IMPL. DT30 DAY1 (TSM) +4 500MB INTV=8 DAM
140°W
160°W
180°E
160°E
140°E
120°W
100°W
80°W
60°W
120°E
100°E
80°E
60°E
40°W
20°W
0°E
20°E
40°E
80°N
60°N
40°N
30°N
20°N
10°N
L

Fig.II.4b.

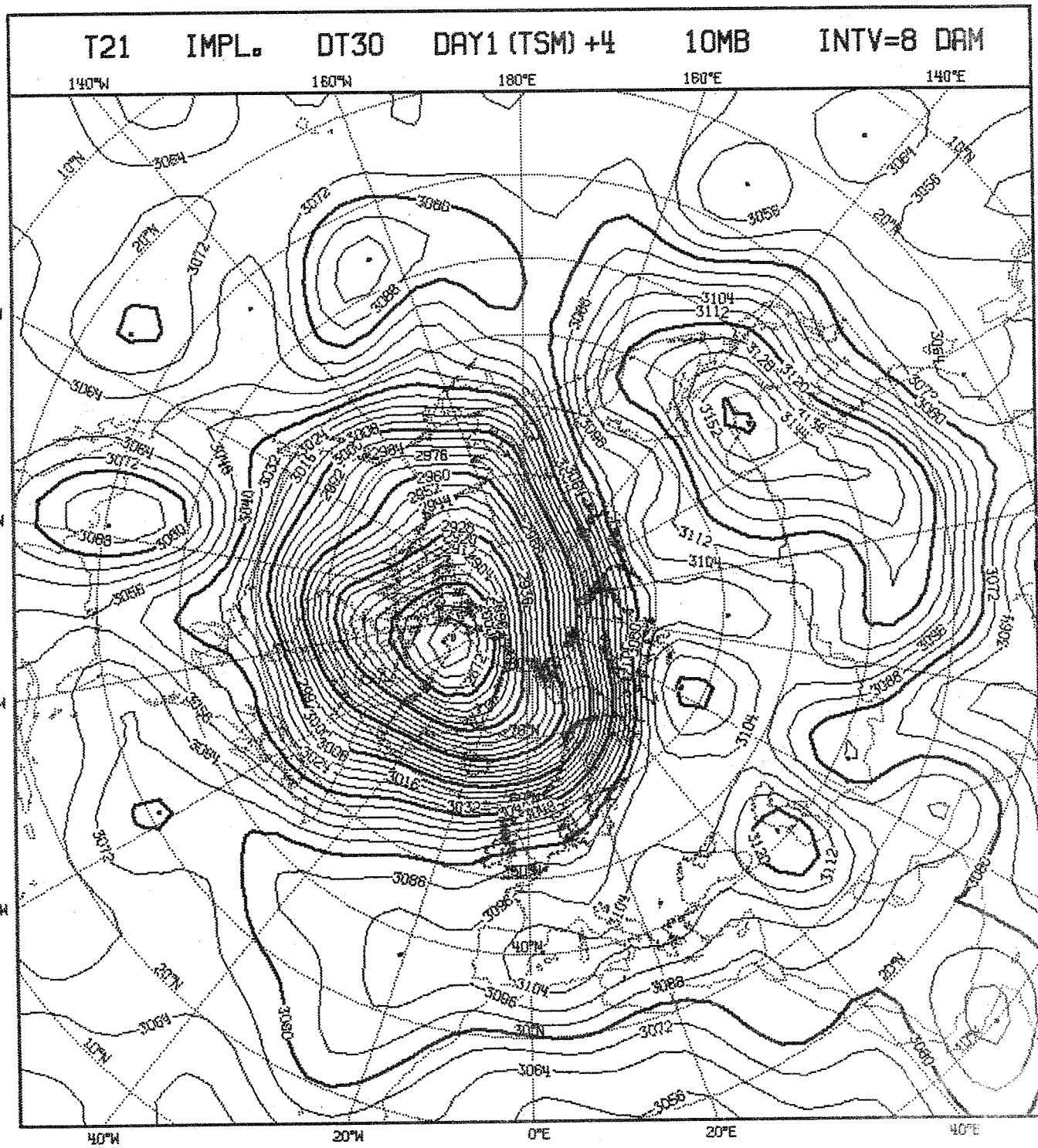
T21 IMPL. DT30 DAY1 (TSM) +4 10MB INTV=8 DAM
140°W
180°W
180°E
160°E
140°E
120°W
120°E
100°W
100°E
80°W
80°E
60°W
60°E
40°W
20°W
0°E
20°E
40°E

Fig.II.4c.

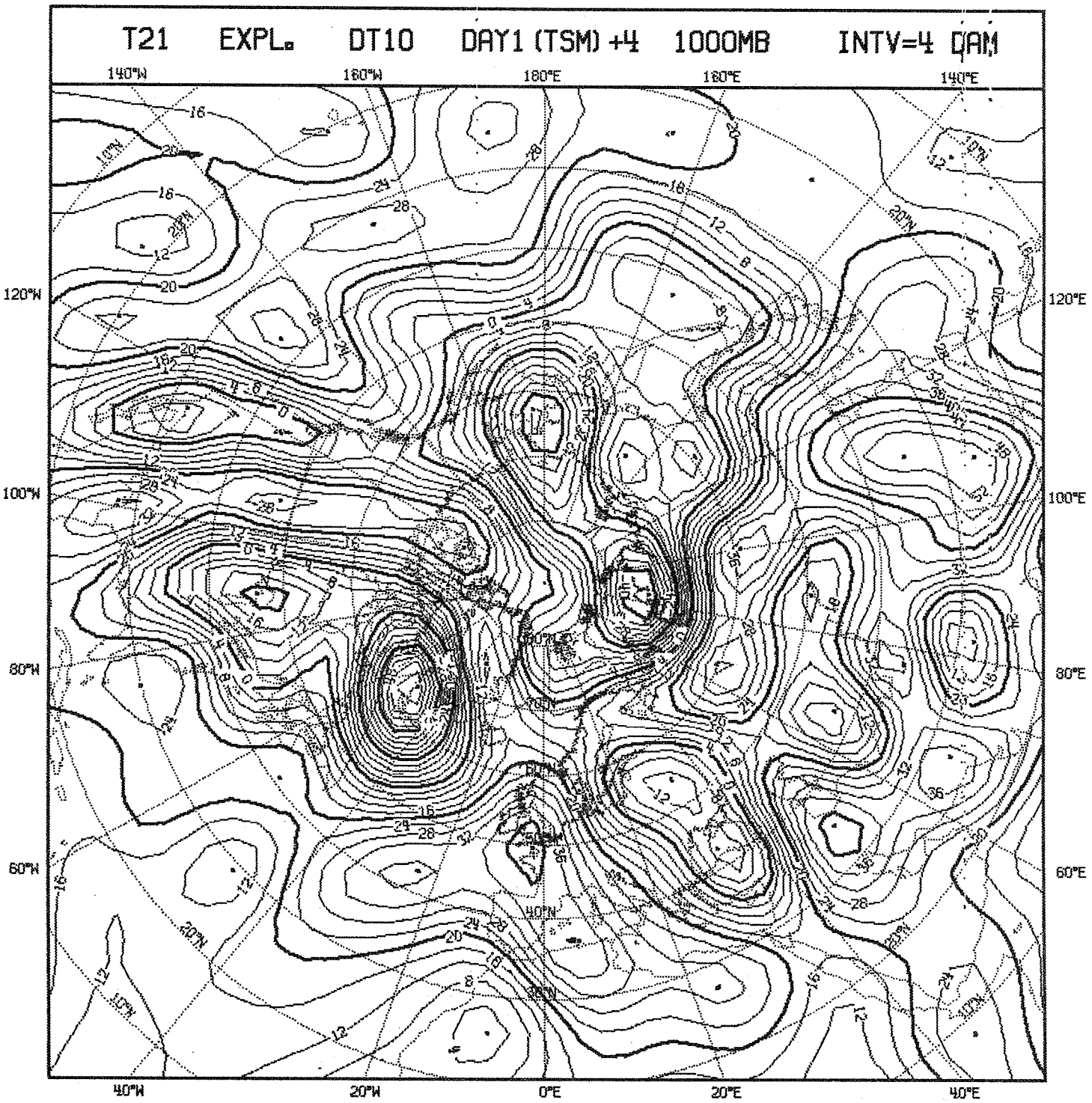
T21 EXPL. DT10 DAY1 (TSM) +4 1000MB INTV=4 DAM
140°W
160°W
180°E
160°E
140°E
120°W
120°E
100°W
100°E
80°W
80°E
60°W
60°E
40°W
20°W
0°E
20°E
40°E

Fig.II.4d.

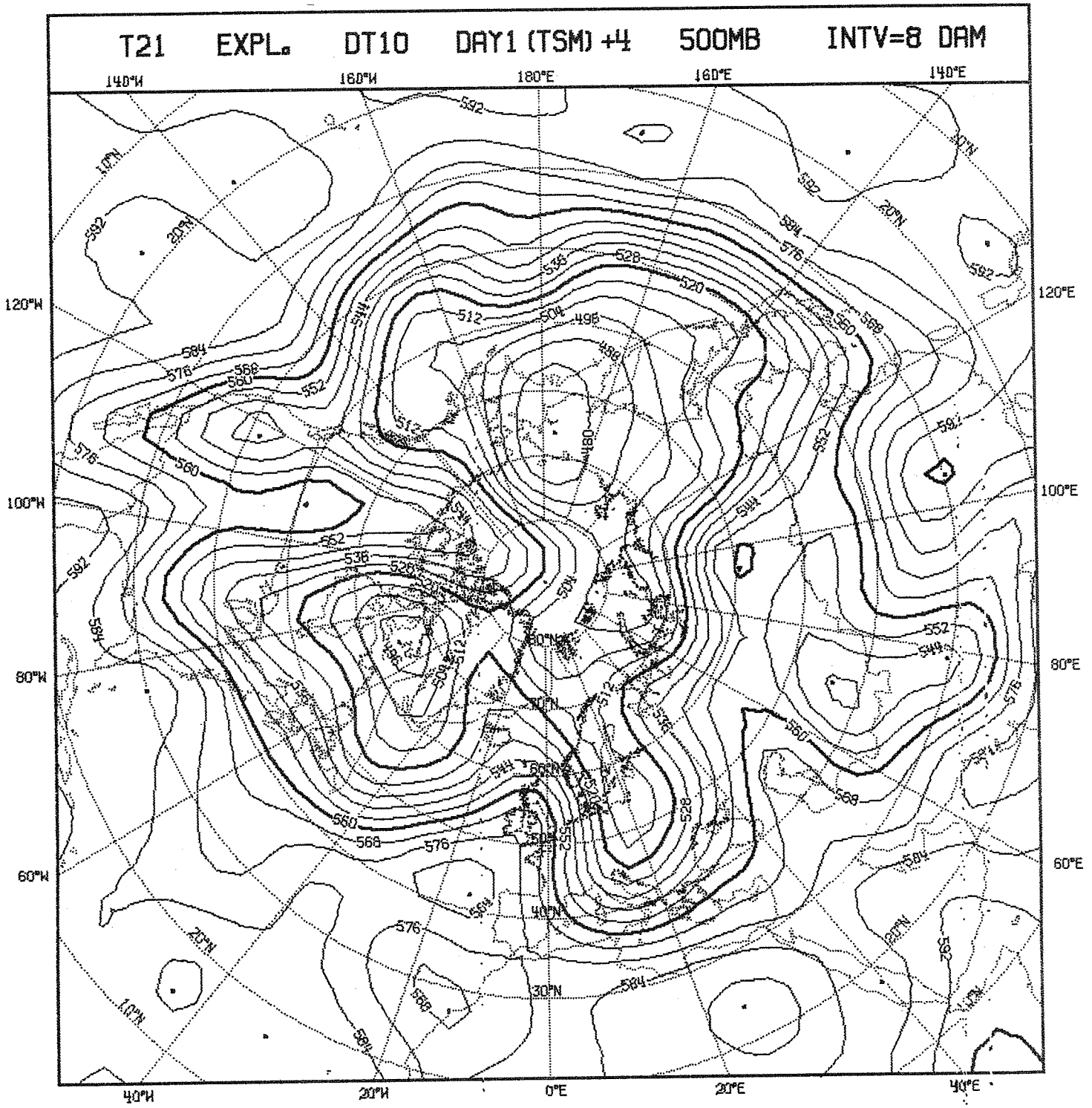

Fig.II.4e.

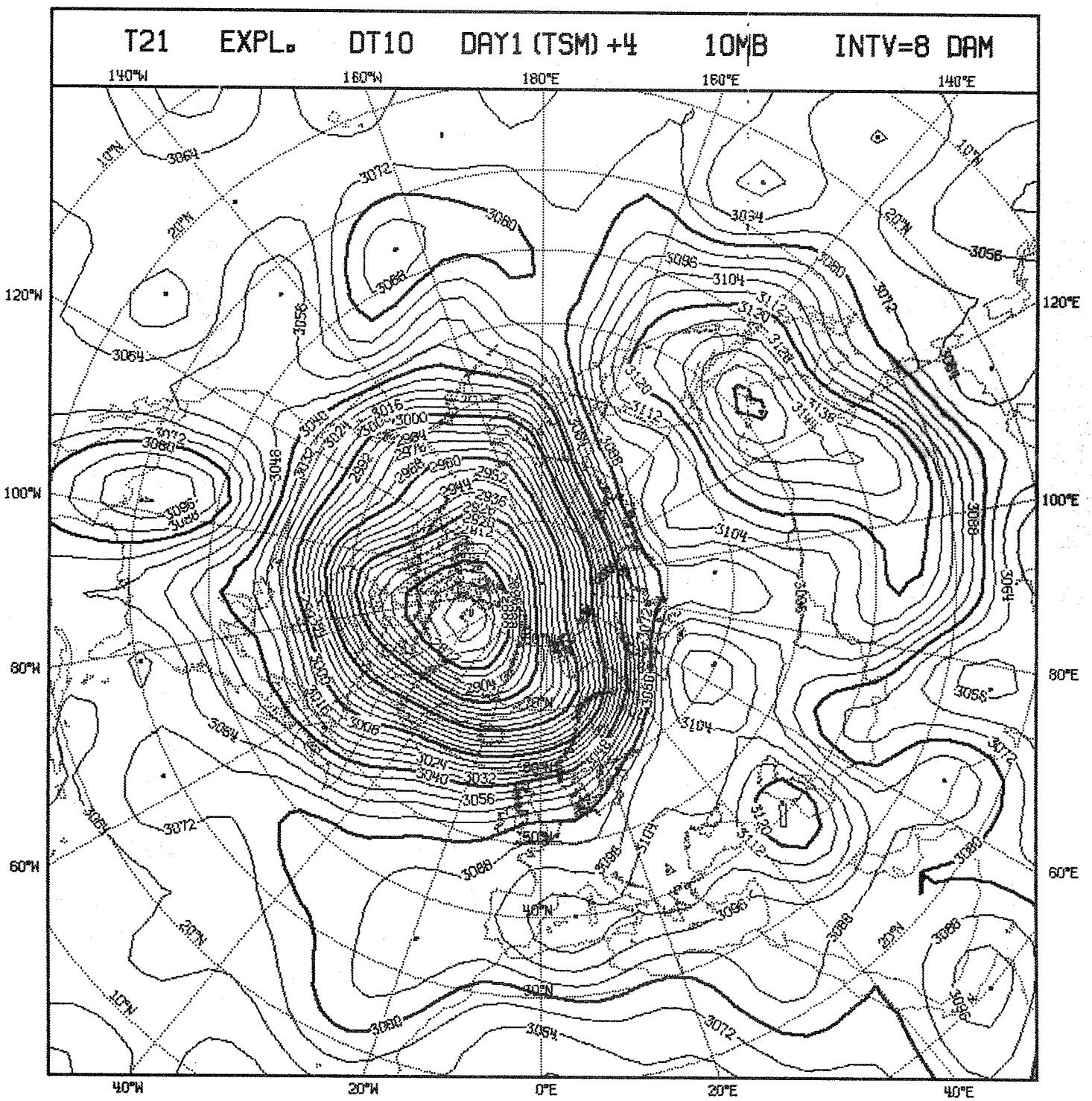
T21 EXPL. DT10 DAY1 (TSM) +4 10MB INTV=8 DAM
140°W
160°W
180°E
160°E
140°E
120°W
100°W
80°W
60°W
120°E
100°E
80°E
60°E
40°W
20°W
0°E
20°E
40°E

Fig.II.4f.

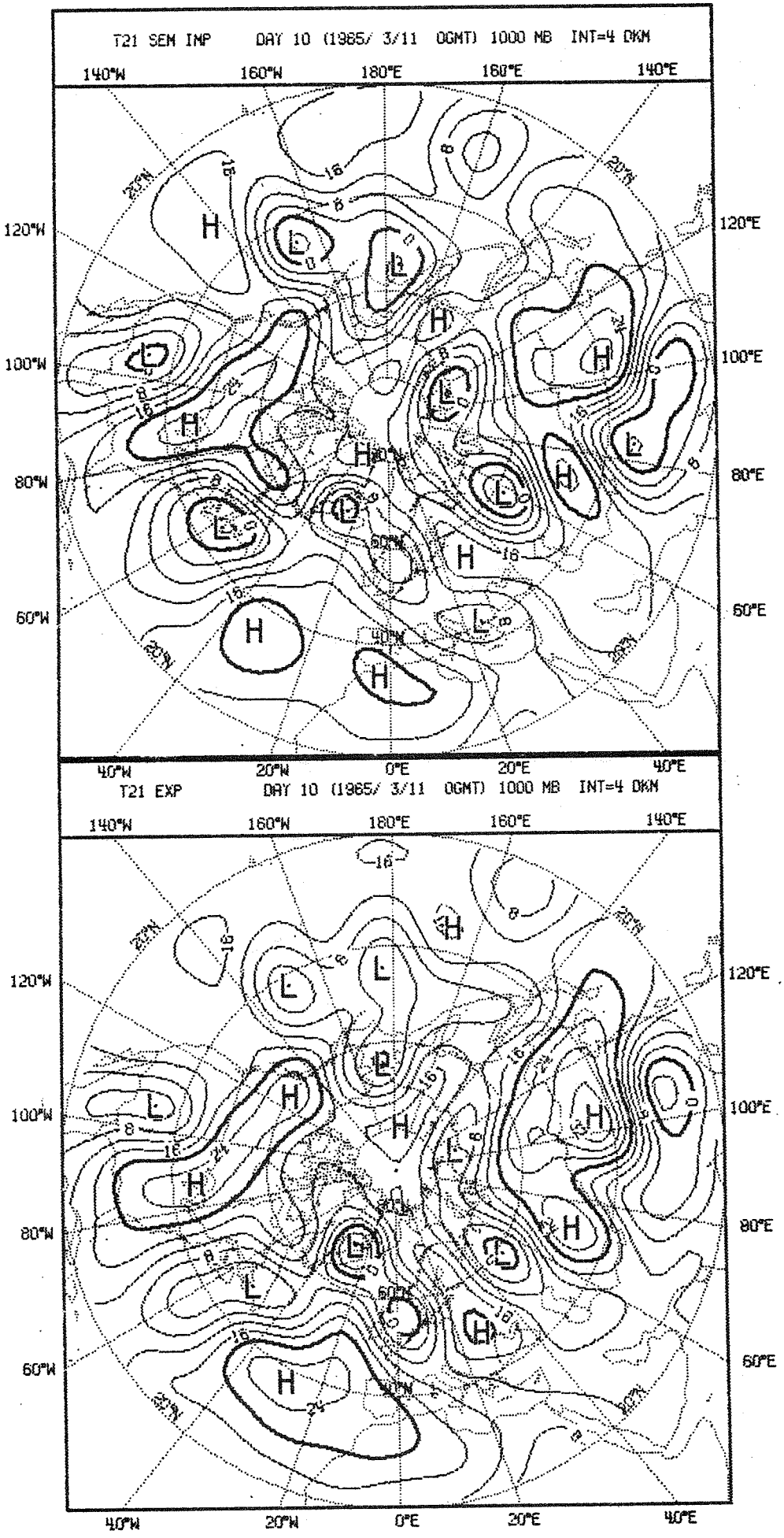
T21 SEM IMP DAY 10 (1985/ 3/11 0GMT) 1000 MB INT=4 DKM
140°W 160°W 180°E 160°E 140°E
120°W 120°E
100°W 100°E
80°W 80°E
60°W 60°E
40°W 20°W 0°E 20°E 40°E
T21 EXP DAY 10 (1985/ 3/11 0GMT) 1000 MB INT=4 DKM
140°W 160°W 180°E 160°E 140°E
120°W 120°E
100°W 100°E
80°W 80°E
60°W 60°E
40°W 20°W 0°E 20°E 40°E

Fig. II.5a.

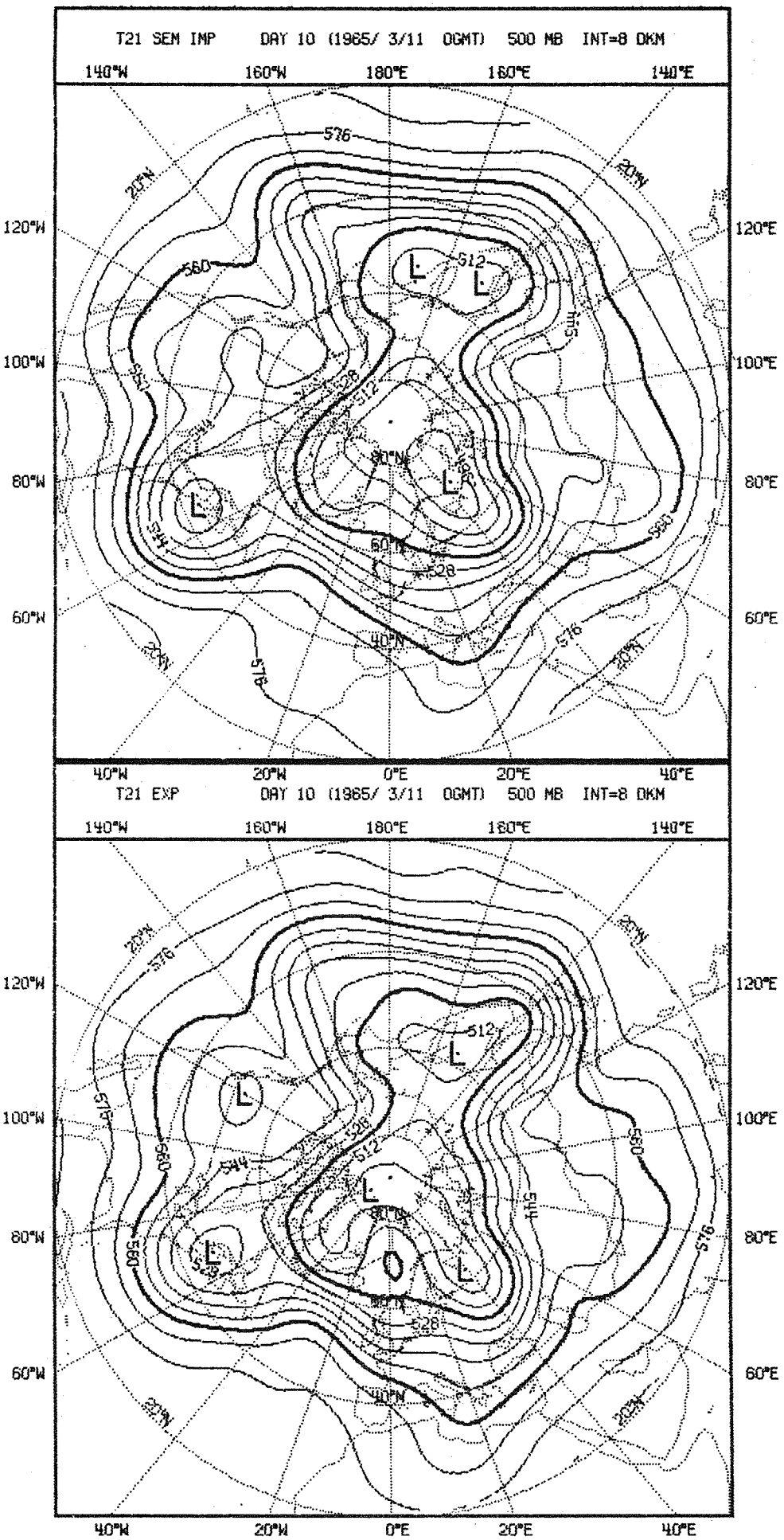
T21 SEM IMP DAY 10 (1985/ 3/11 0GMT) 500 MB INT=8 DKM
140°W 160°W 180°E 160°E 140°E
120°W 100°W 80°W 60°W
120°E 100°E 80°E 60°E
40°W 20°W 0°E 20°E 40°E
20°N 40°N 60°N 80°N
576 560 544 528 512
T21 EXP DAY 10 (1985/ 3/11 0GMT) 500 MB INT=8 DKM
140°W 160°W 180°E 160°E 140°E
120°W 100°W 80°W 60°W
120°E 100°E 80°E 60°E
40°W 20°W 0°E 20°E 40°E
20°N 40°N 60°N 80°N
576 560 544 528 512

Fig. II.5b.

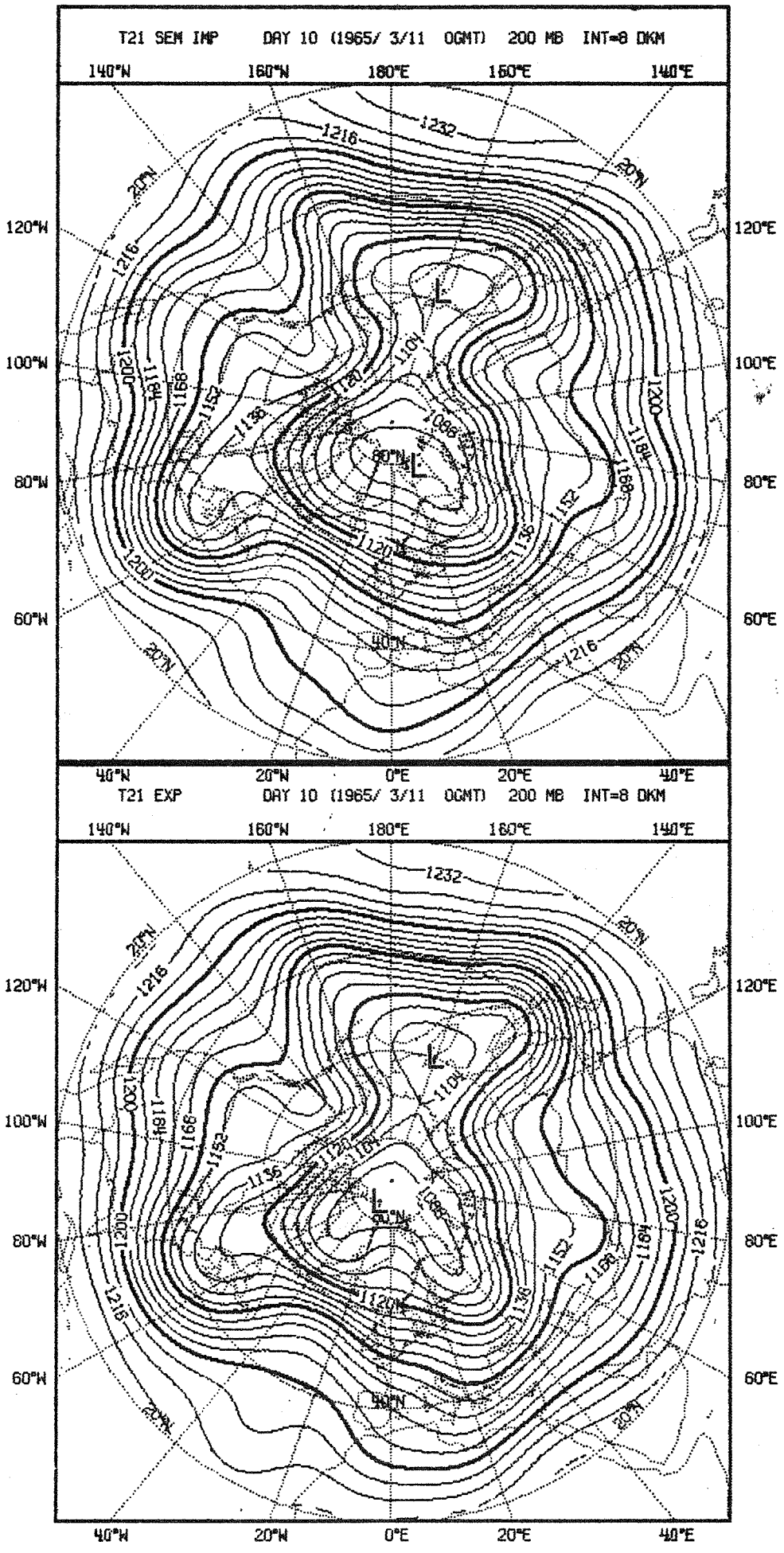
T21 SEM IMP DAY 10 (1965/ 3/11 0GMT) 200 MB INT=8 DKM
140°W 160°W 180°E 160°E 140°E
120°W 100°W 80°W 60°W
120°E 100°E 80°E 60°E
40°N 20°N 0°E 20°E 40°E
1232 1216 1200 1184 1168 1152 1136 1120 1104 1088
T21 EXP DAY 10 (1965/ 3/11 0GMT) 200 MB INT=8 DKM
140°W 160°W 180°E 160°E 140°E
120°W 100°W 80°W 60°W
120°E 100°E 80°E 60°E
40°N 20°N 0°E 20°E 40°E
1232 1216 1200 1184 1168 1152 1136 1120 1104 1088

Fig. II.5c.

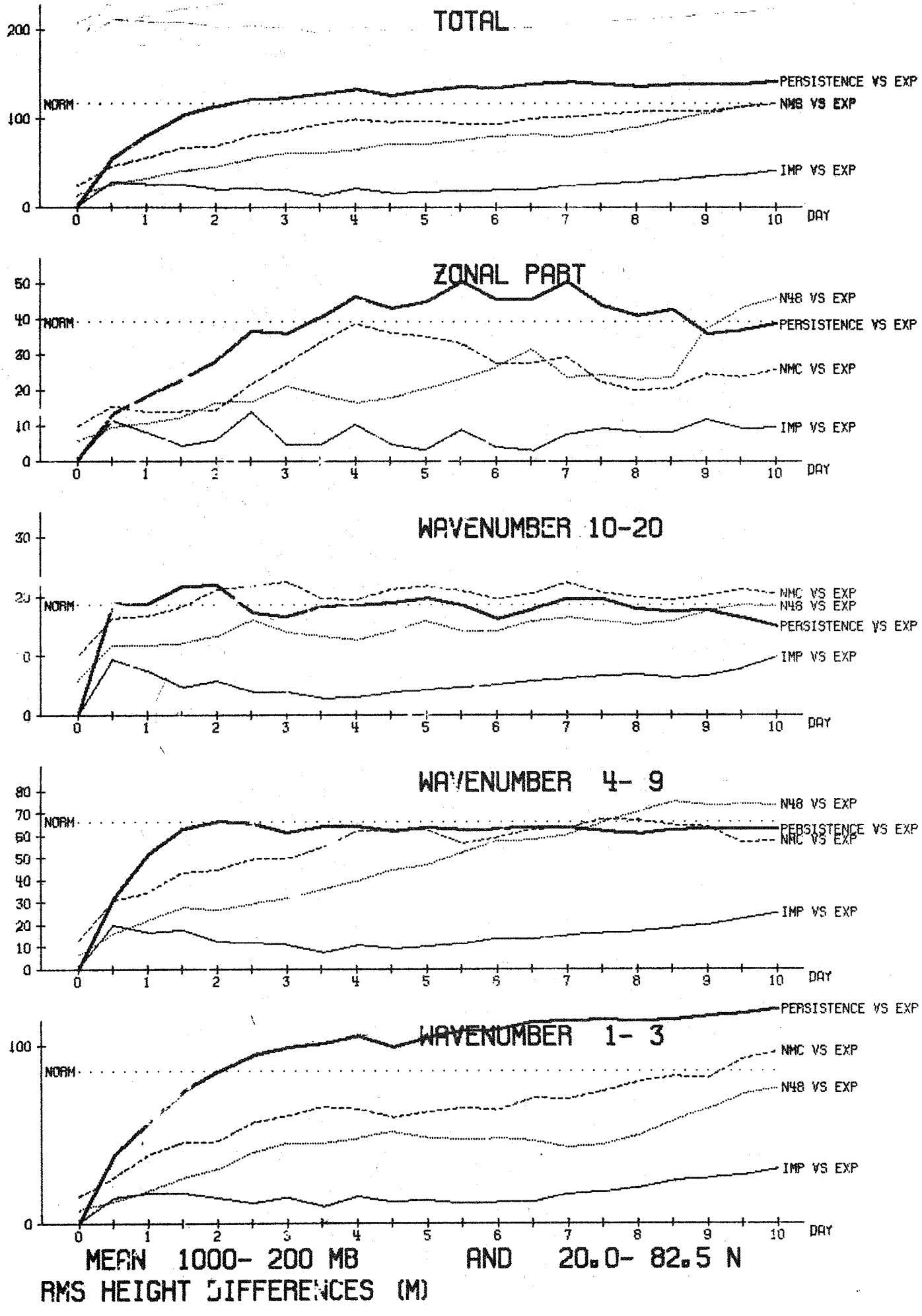
TOTAL
NORM
PERSISTENCE VS EXP
N48 VS EXP
IMP VS EXP
DAY
ZONAL PART
NORM
N48 VS EXP
PERSISTENCE VS EXP
NMC VS EXP
IMP VS EXP
DAY
WAVENUMBER 10-20
NORM
NMC VS EXP
N48 VS EXP
PERSISTENCE VS EXP
IMP VS EXP
DAY
WAVENUMBER 4- 9
NORM
N48 VS EXP
PERSISTENCE VS EXP
NMC VS EXP
IMP VS EXP
DAY
WAVENUMBER 1- 3
NORM
PERSISTENCE VS EXP
NMC VS EXP
N48 VS EXP
IMP VS EXP
DAY
MEAN 1000- 200 MB AND 20.0- 82.5 N
RMS HEIGHT DIFFERENCES (M)

Fig. II.6.

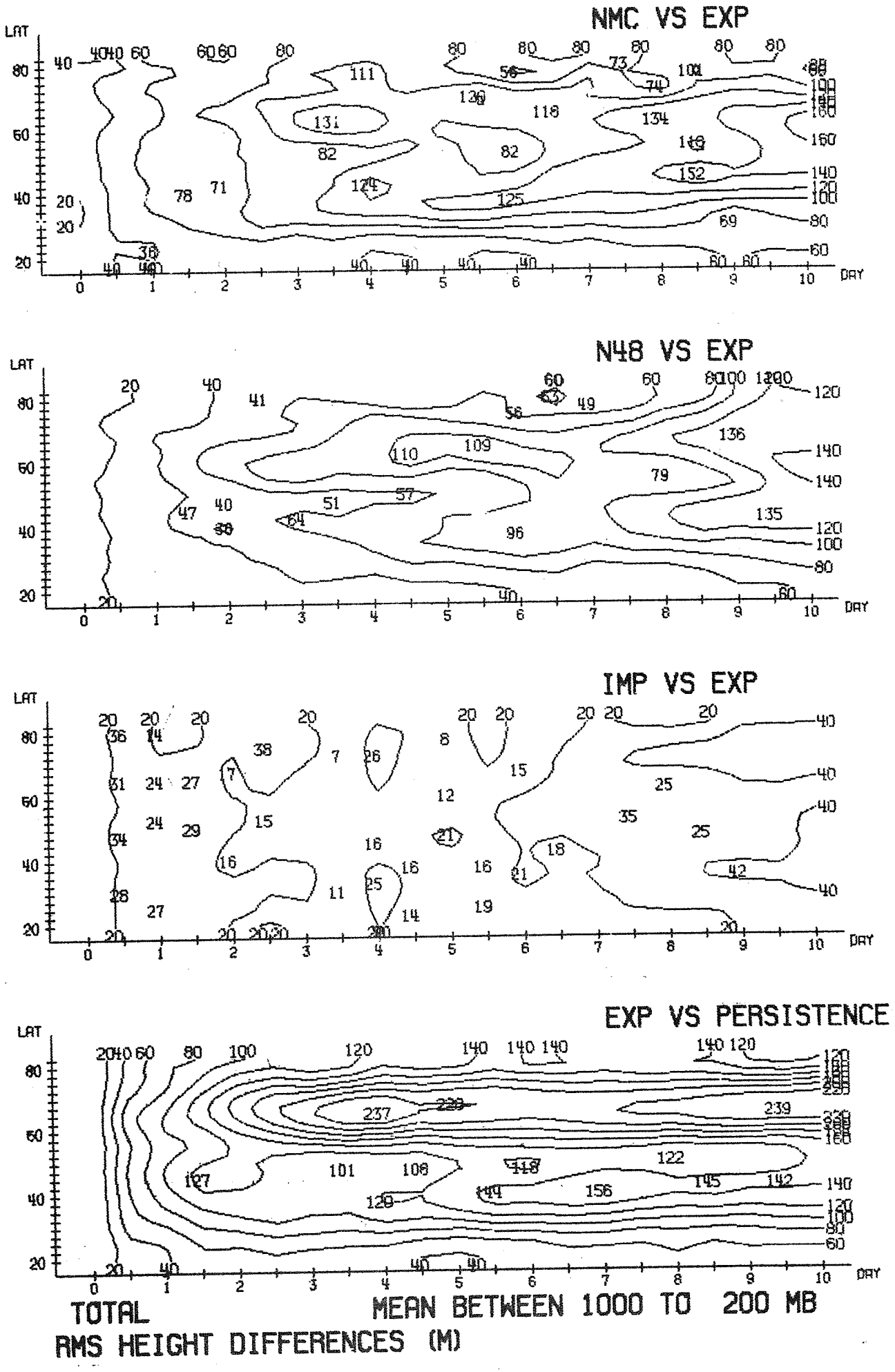
NMC VS EXP
N48 VS EXP
IMP VS EXP
EXP VS PERSISTENCE
LAT
DAY
TOTAL
MEAN BETWEEN 1000 TO 200 MB
RMS HEIGHT DIFFERENCES (M)

Fig. II.7.

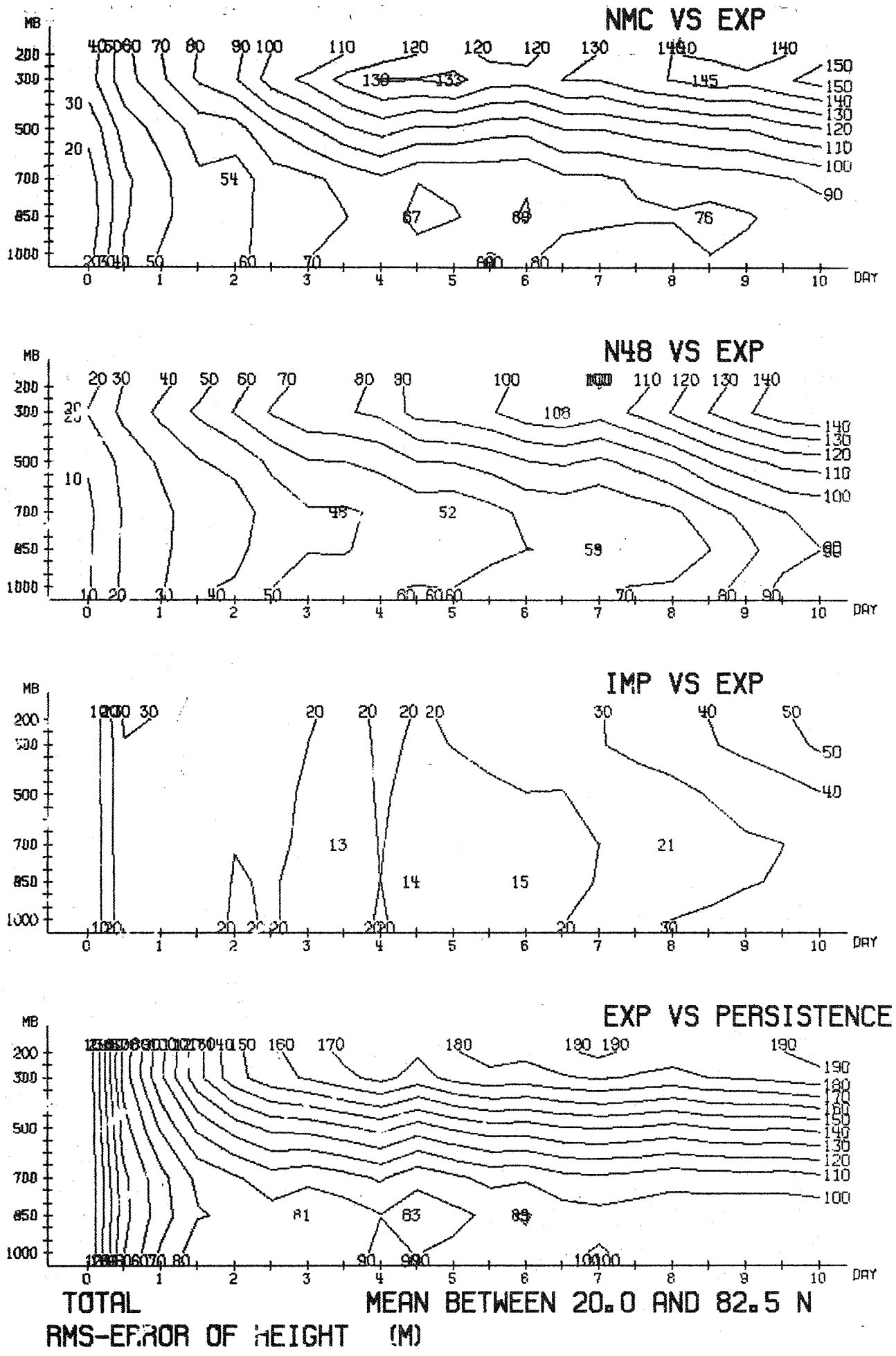
NMC VS EXP
N48 VS EXP
IMP VS EXP
EXP VS PERSISTENCE
MB
DAY
TOTAL
MEAN BETWEEN 20.0 AND 82.5 N
RMS-ERROR OF HEIGHT (M)

Fig. II.8.

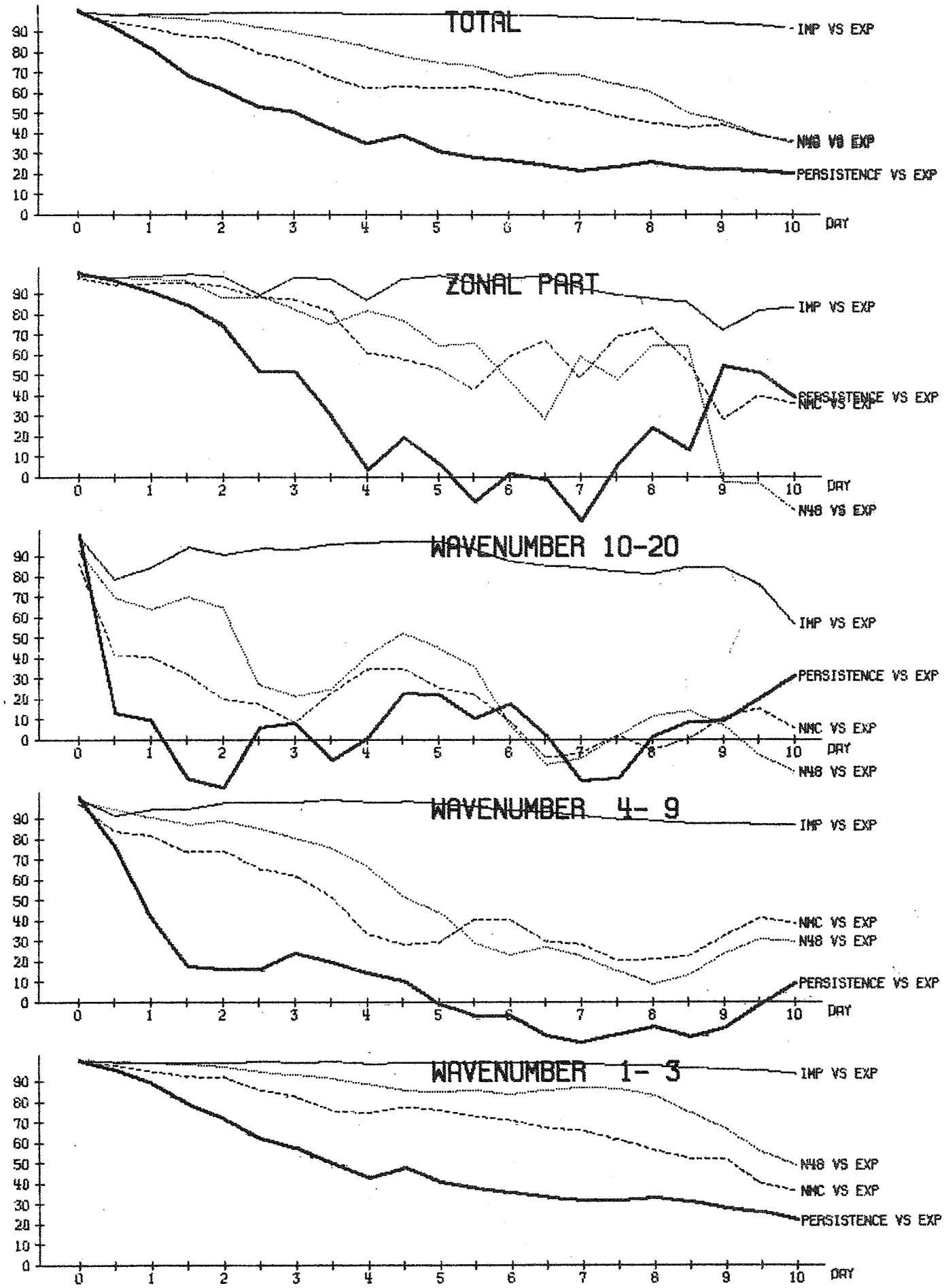
TOTAL
IMP VS EXP
NMB VS EXP
PERSISTENCE VS EXP
DAY
ZONAL PART
IMP VS EXP
PERSISTENCE VS EXP
NMC VS EXP
NMB VS EXP
DAY
WAVENUMBER 10-20
IMP VS EXP
PERSISTENCE VS EXP
NMC VS EXP
NMB VS EXP
DAY
WAVENUMBER 4- 9
IMP VS EXP
NMC VS EXP
NMB VS EXP
PERSISTENCE VS EXP
DAY
WAVENUMBER 1- 3
IMP VS EXP
NMB VS EXP
NMC VS EXP
PERSISTENCE VS EXP
DAY
MEAN 1000- 200 MB AND 20.0- 82.5 N
CORRELATION OF HEIGHT %

Fig. II.9.

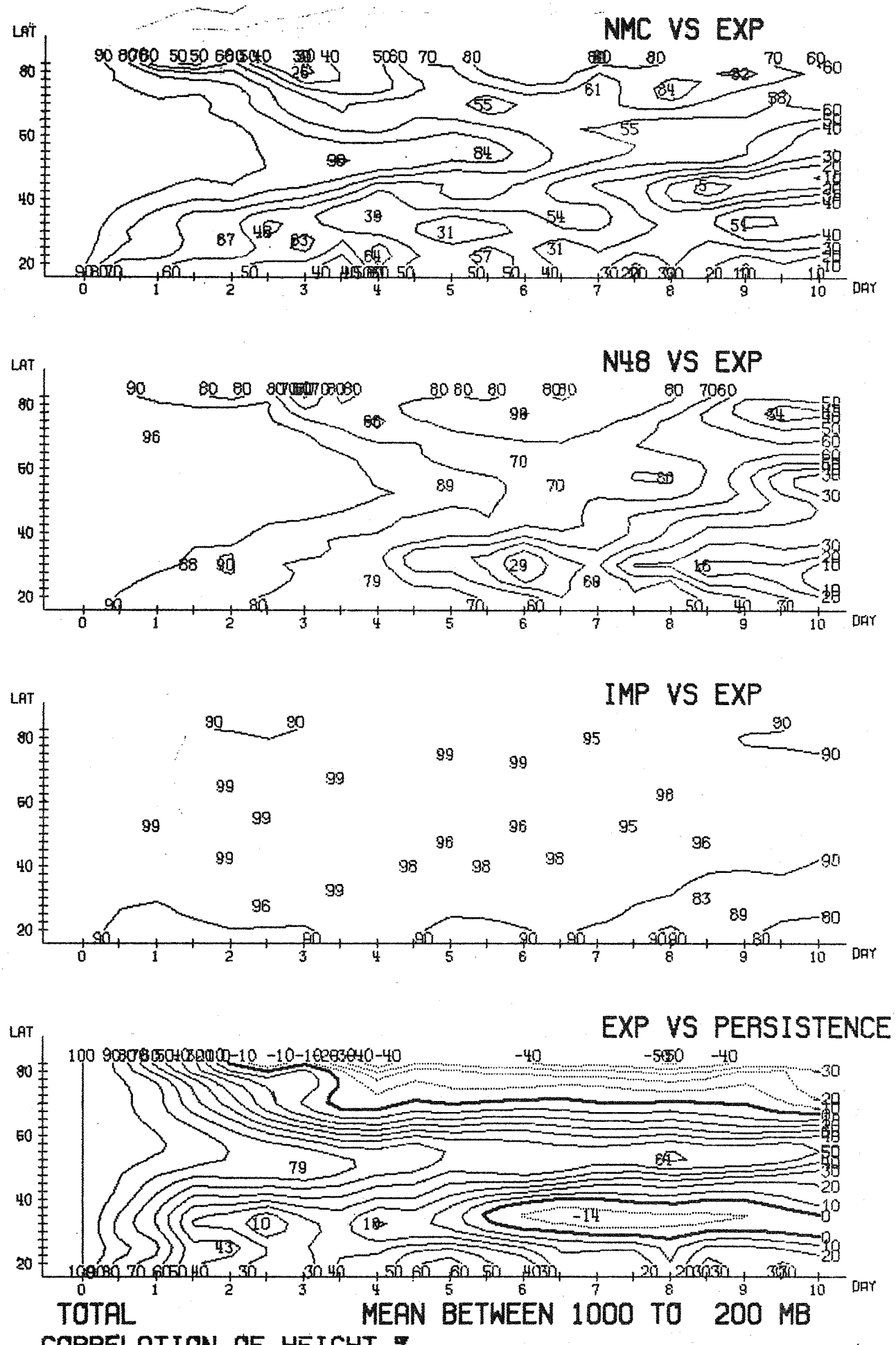
NMC VS EXP
N48 VS EXP
IMP VS EXP
EXP VS PERSISTENCE
LAT
DAY
TOTAL MEAN BETWEEN 1000 TO 200 MB
CORRELATION OF HEIGHT %

Fig. II.10.

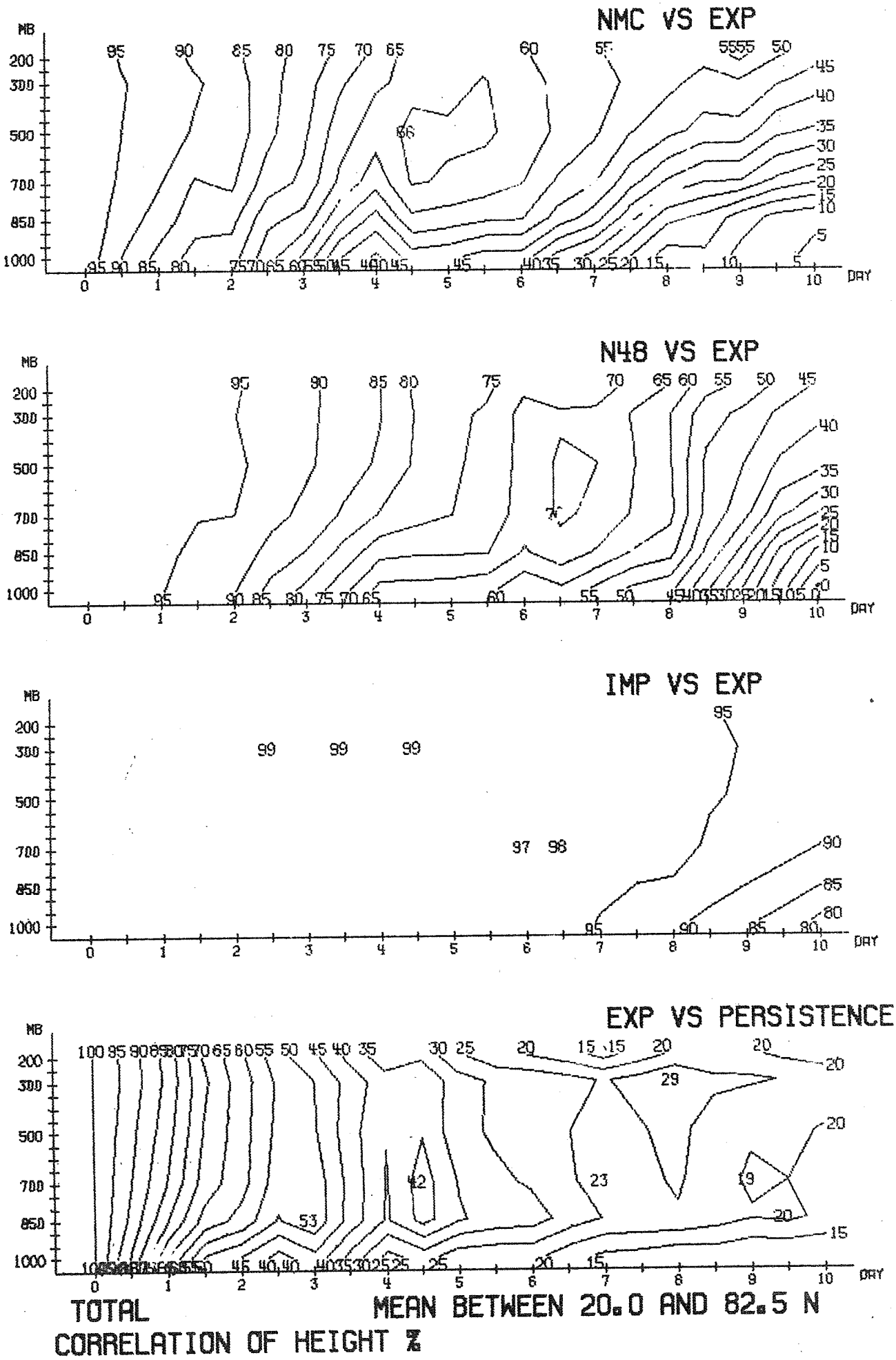
NMC VS EXP
N48 VS EXP
IMP VS EXP
EXP VS PERSISTENCE
MB
DAY
TOTAL
CORRELATION OF HEIGHT %
MEAN BETWEEN 20.0 AND 82.5 N

Fig. II.11.

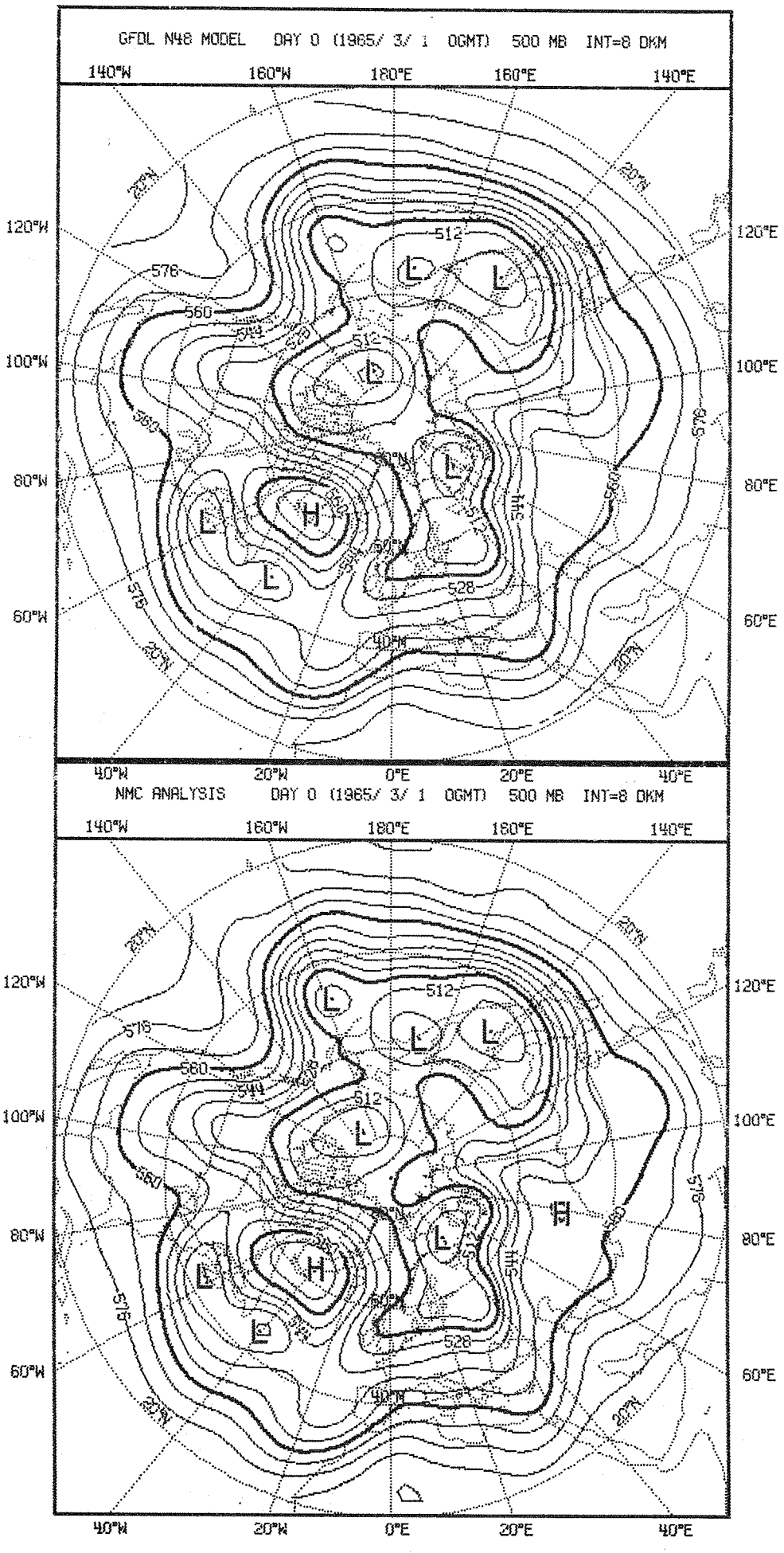
GFDL N48 MODEL DAY 0 (1985/ 3/ 1 0GMT) 500 MB INT=8 DKM
140°W
160°W
180°E
160°E
140°E
120°W
100°W
80°W
60°W
120°E
100°E
80°E
60°E
20°N
40°N
512
576
560
544
528
40°W
20°W
0°E
20°E
40°E
NMC ANALYSIS DAY 0 (1985/ 3/ 1 0GMT) 500 MB INT=8 DKM

Fig.III.1a.

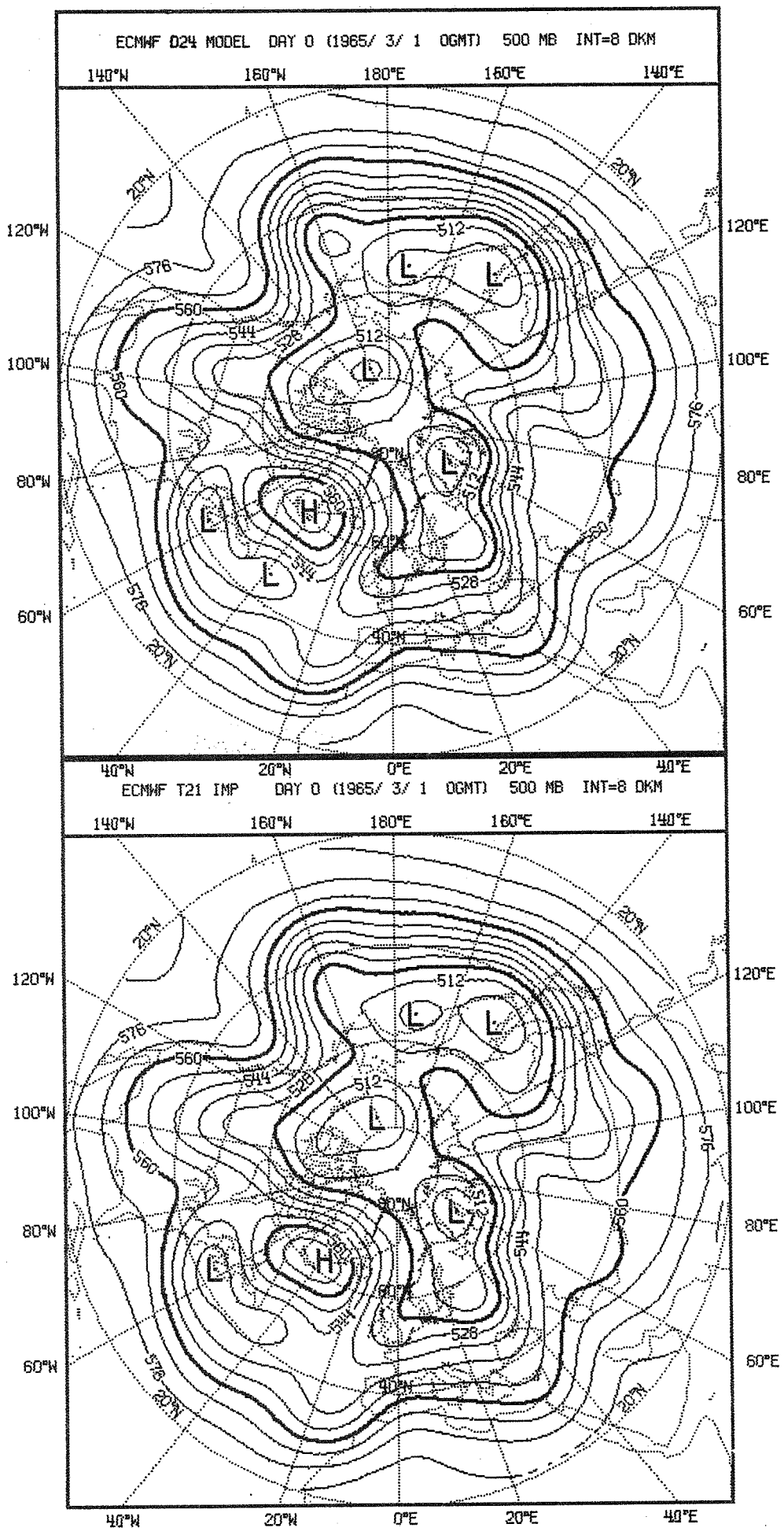
ECMWF D24 MODEL DAY 0 (1965/ 3/ 1 0GMT) 500 MB INT=8 DKM
140°W
160°W
180°E
160°E
140°E
120°W
120°E
100°W
100°E
80°W
80°E
60°W
60°E
40°W
20°W
0°E
20°E
40°E
20°N
40°N
512
544
560
576
528
H
L
ECMWF T21 IMP DAY 0 (1965/ 3/ 1 0GMT) 500 MB INT=8 DKM

Fig.III.1b.

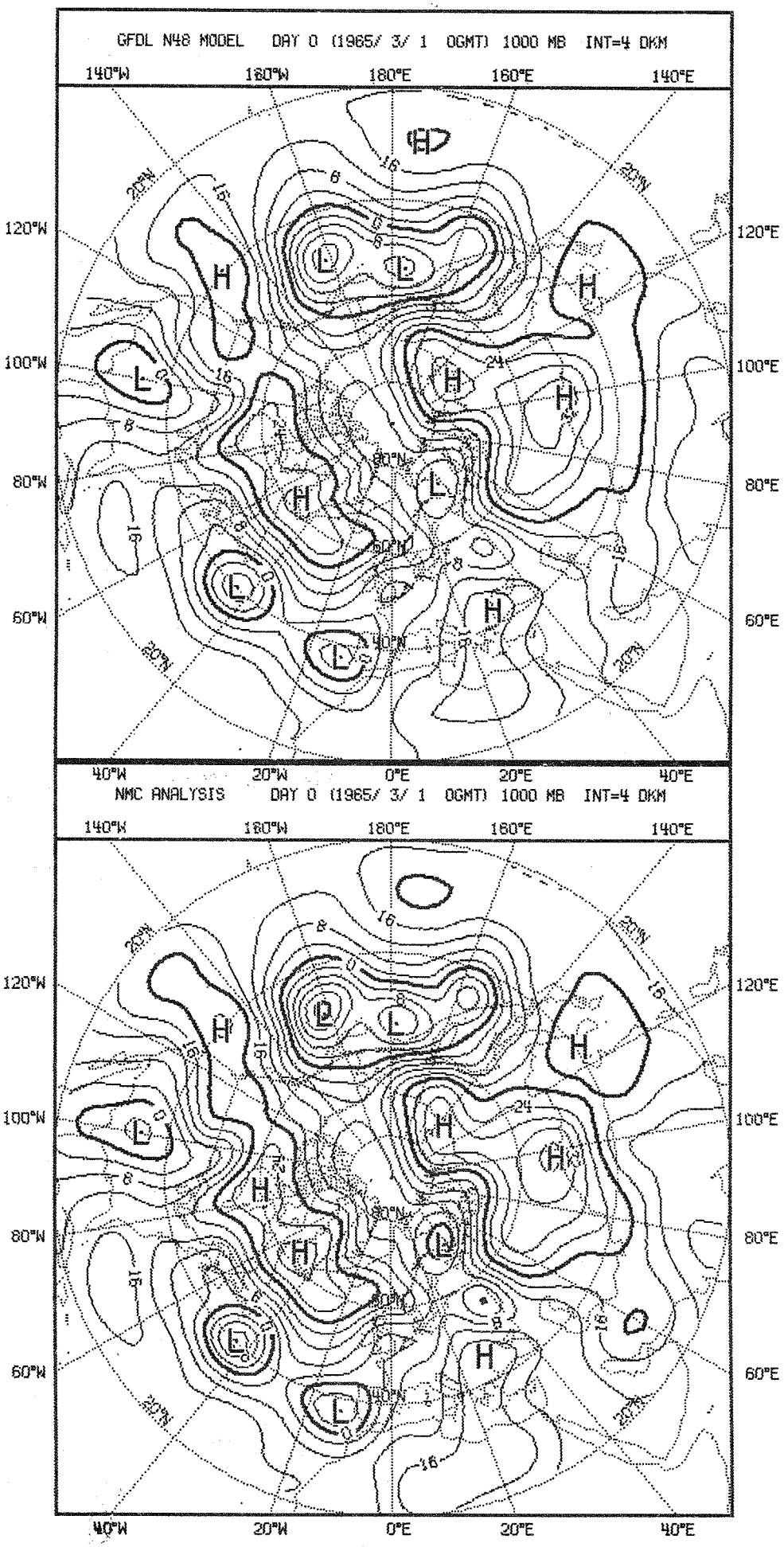
GFDL N48 MODEL DAY 0 (1965/ 3/ 1 0GMT) 1000 MB INT=4 DKM
140°W
160°W
180°E
160°E
140°E
120°W
100°W
80°W
60°W
120°E
100°E
80°E
60°E
40°W
20°W
0°E
20°E
40°E
NMC ANALYSIS DAY 0 (1965/ 3/ 1 0GMT) 1000 MB INT=4 DKM

Fig.III.2a.

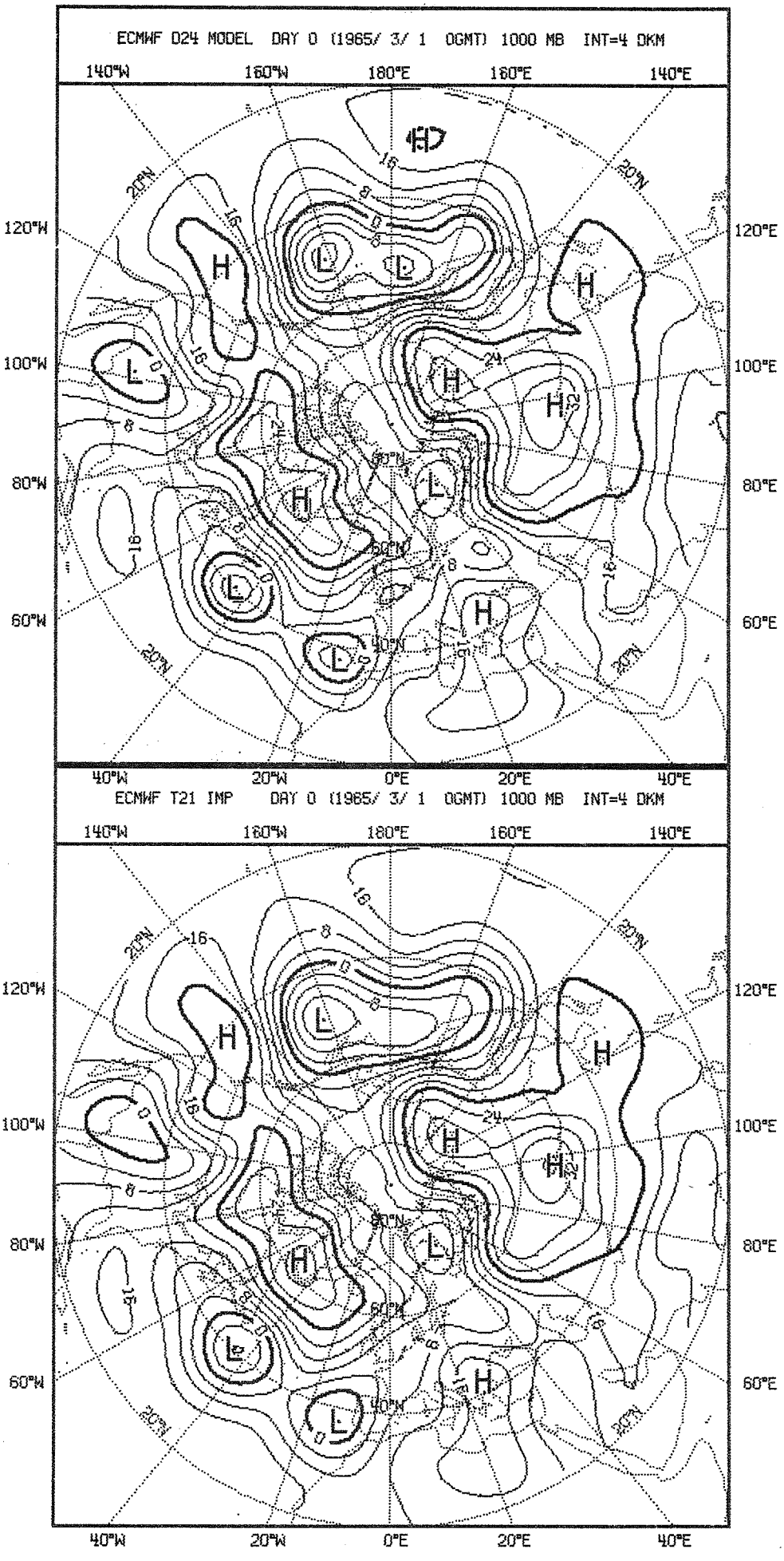
ECMWF D24 MODEL DAY 0 (1985/ 3/ 1 0GMT) 1000 MB INT=4 DKM
140°W
160°W
180°E
160°E
140°E
120°W
100°W
80°W
60°W
120°E
100°E
80°E
60°E
20°N
40°N
60°N
80°N
40°W
20°W
0°E
20°E
40°E
ECMWF T21 IMP DAY 0 (1985/ 3/ 1 0GMT) 1000 MB INT=4 DKM

Fig.III.2b.

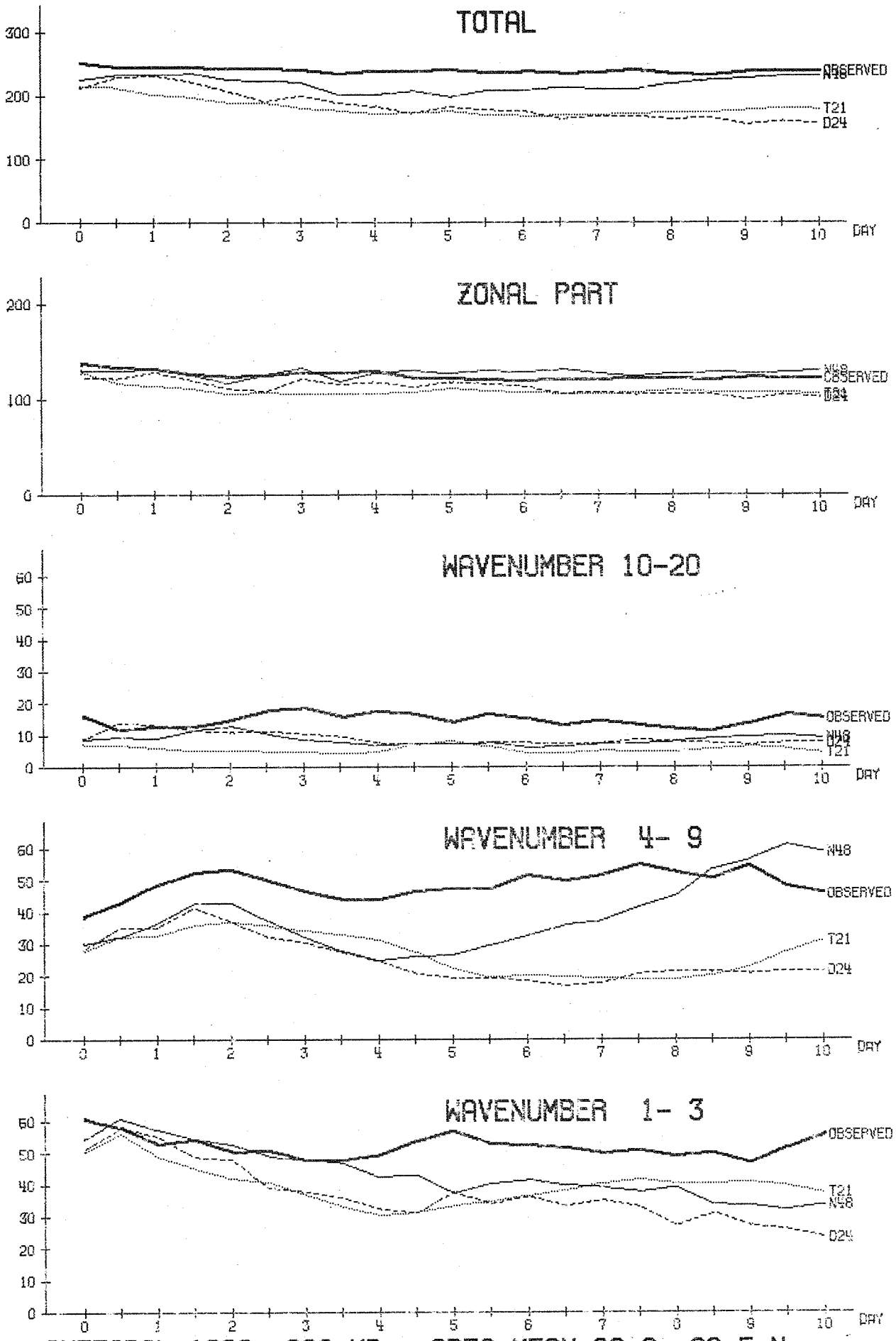
TOTAL
OBSERVED
T21
D24
DAY
ZONAL PART
OBSERVED
DAY
WAVENUMBER 10-20
OBSERVED
T21
DAY
WAVENUMBER 4- 9
N48
OBSERVED
T21
D24
DAY
WAVENUMBER 1- 3
OBSERVED
T21
D24
DAY
INTEGRAL 1000- 200 MB AREA MEAN 20.0- 82.5 N
KE (10 KJ/M2)

Fig.III.3.

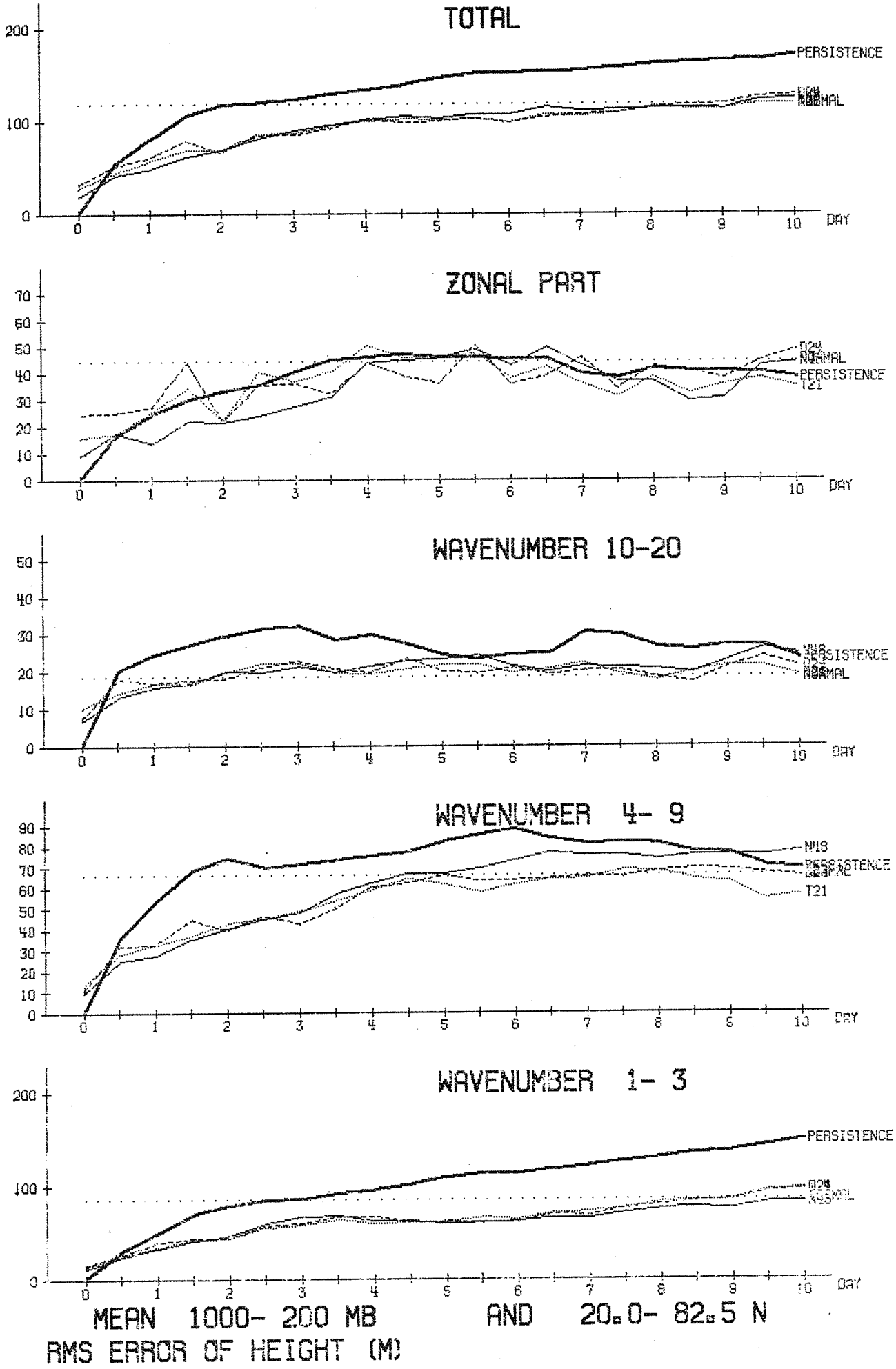
TOTAL
PERSISTENCE
DAY
ZONAL PART
PERSISTENCE
T21
DAY
WAVENUMBER 10-20
PERSISTENCE
DAY
WAVENUMBER 4- 9
T21
DAY
WAVENUMBER 1- 3
PERSISTENCE
DAY
MEAN 1000- 200 MB AND 20.0- 82.5 N
RMS ERROR OF HEIGHT (M)

Fig.III.4.

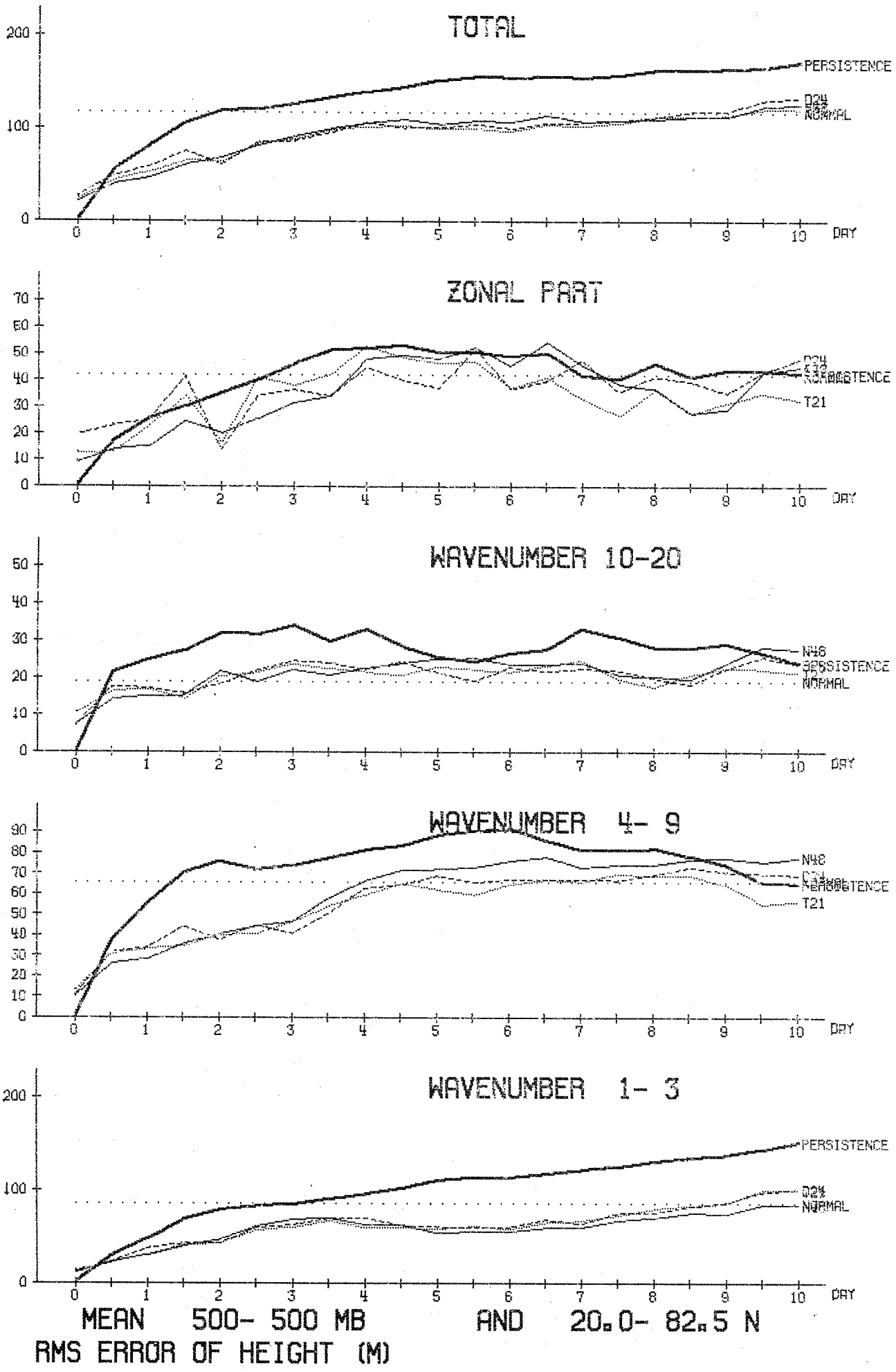
TOTAL
PERSISTENCE
D24
NORMAL
DAY
ZONAL PART
T21
DAY
WAVENUMBER 10-20
N48
PERSISTENCE
NORMAL
DAY
WAVENUMBER 4- 9
N48
T21
DAY
WAVENUMBER 1- 3
PERSISTENCE
D24
NORMAL
DAY
MEAN 500- 500 MB AND 20.0- 82.5 N
RMS ERROR OF HEIGHT (M)

Fig.III.5.

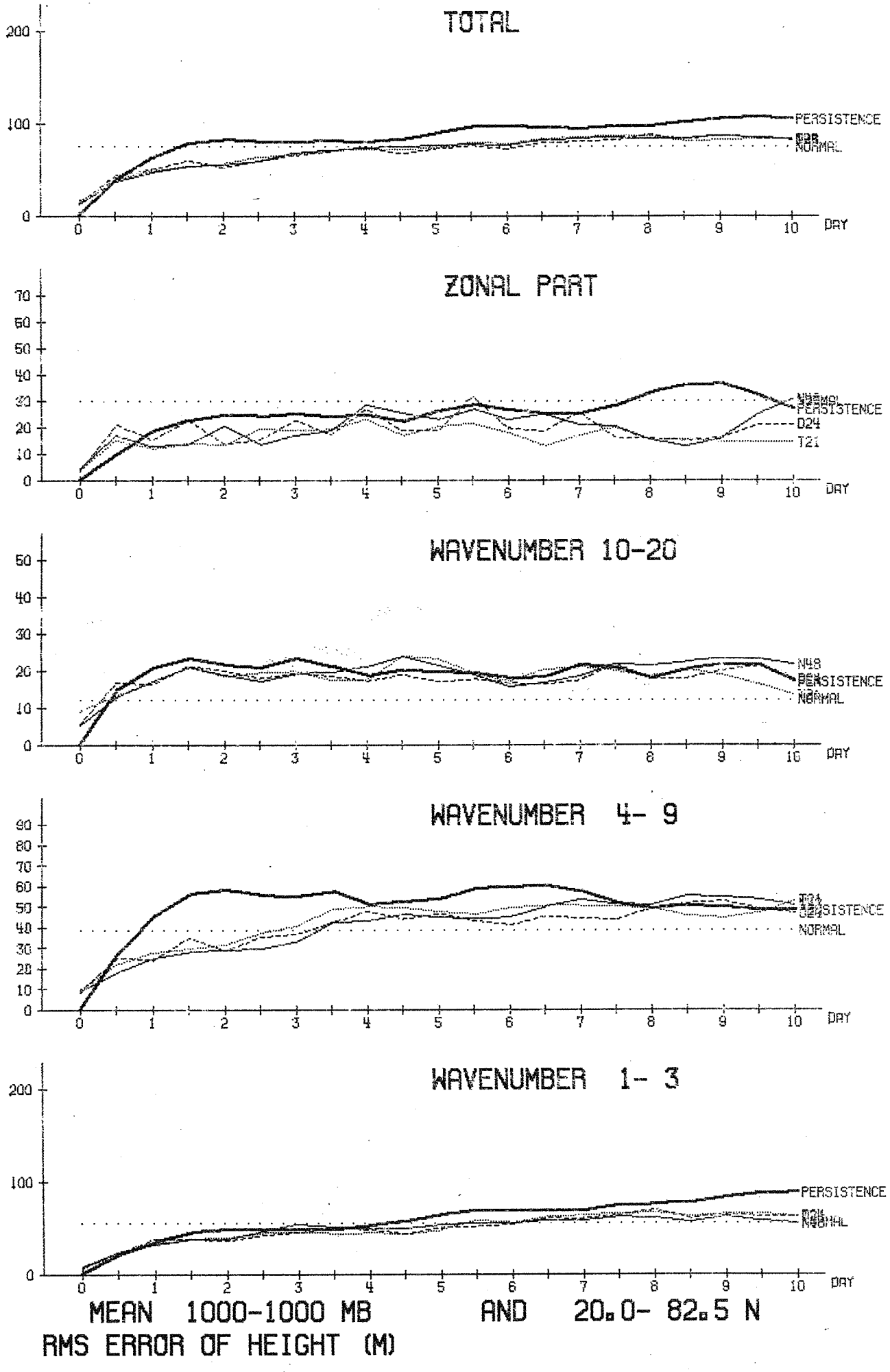
TOTAL
PERSISTENCE
NORMAL
DAY
ZONAL PART
PERSISTENCE
D24
T21
DAY
WAVENUMBER 10-20
PERSISTENCE
NORMAL
DAY
WAVENUMBER 4- 9
NORMAL
DAY
WAVENUMBER 1- 3
PERSISTENCE
DAY
MEAN 1000-1000 MB AND 20.0- 82.5 N
RMS ERROR OF HEIGHT (M)

Fig.III.6.

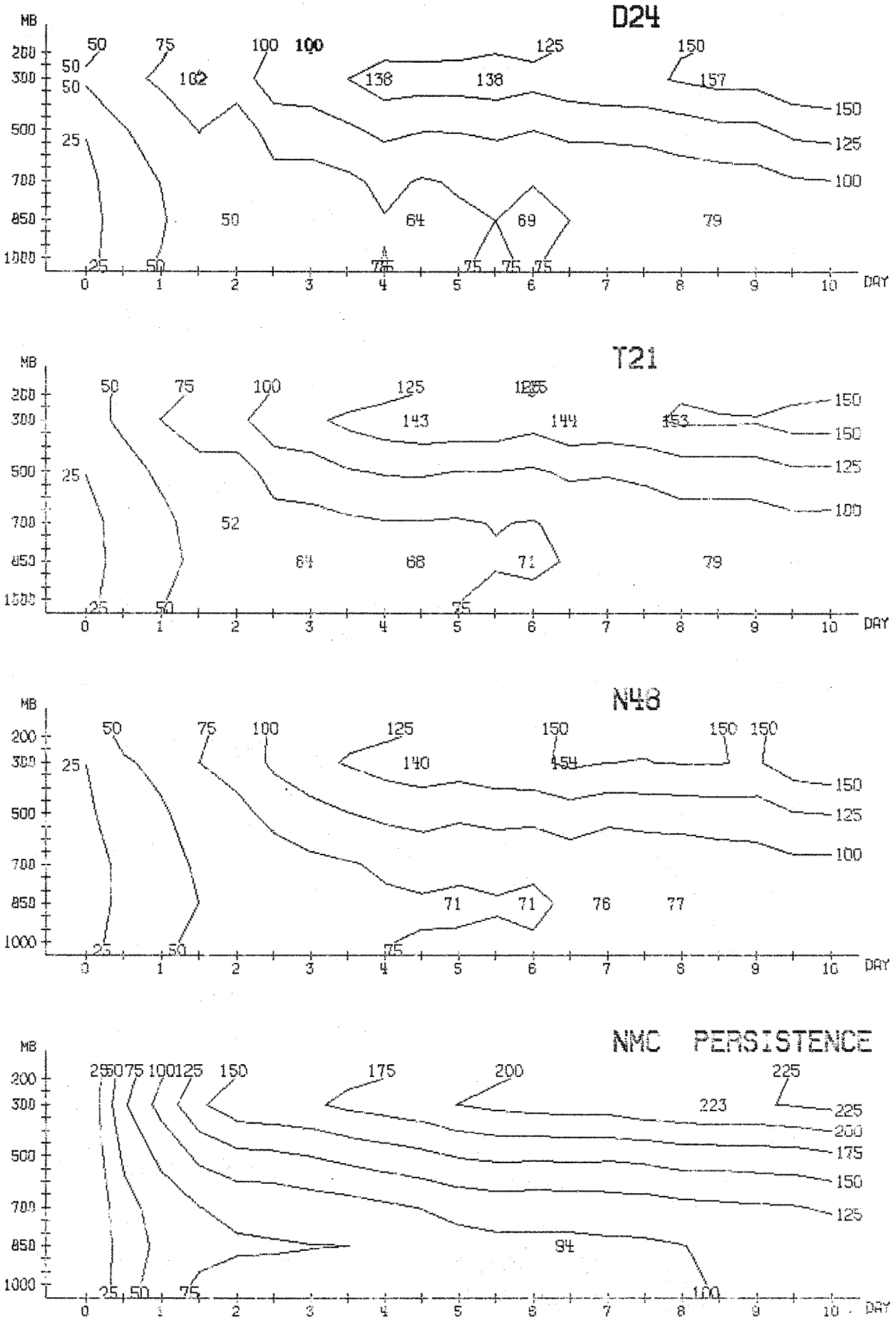
D24
T21
N48
NMC PERSISTENCE
MB
DAY
TOTAL RMS-ERROR OF HEIGHT (M)
MEAN BETWEEN 20.0 AND 82.5 N

Fig.III.7.

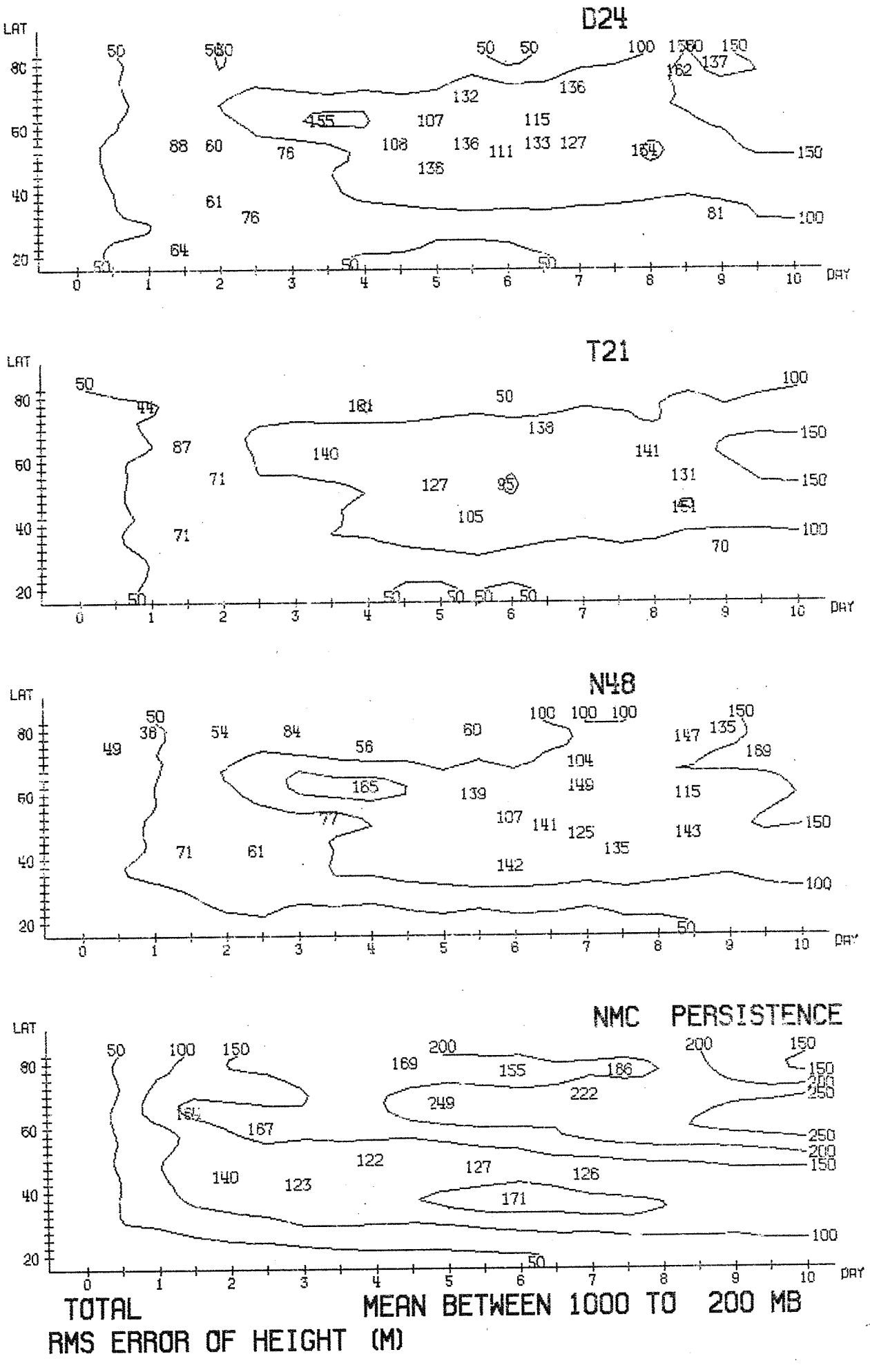
D24
T21
N48
NMC PERSISTENCE
LAT
DAY
TOTAL RMS ERROR OF HEIGHT (M)
MEAN BETWEEN 1000 TO 200 MB

Fig.III.8.

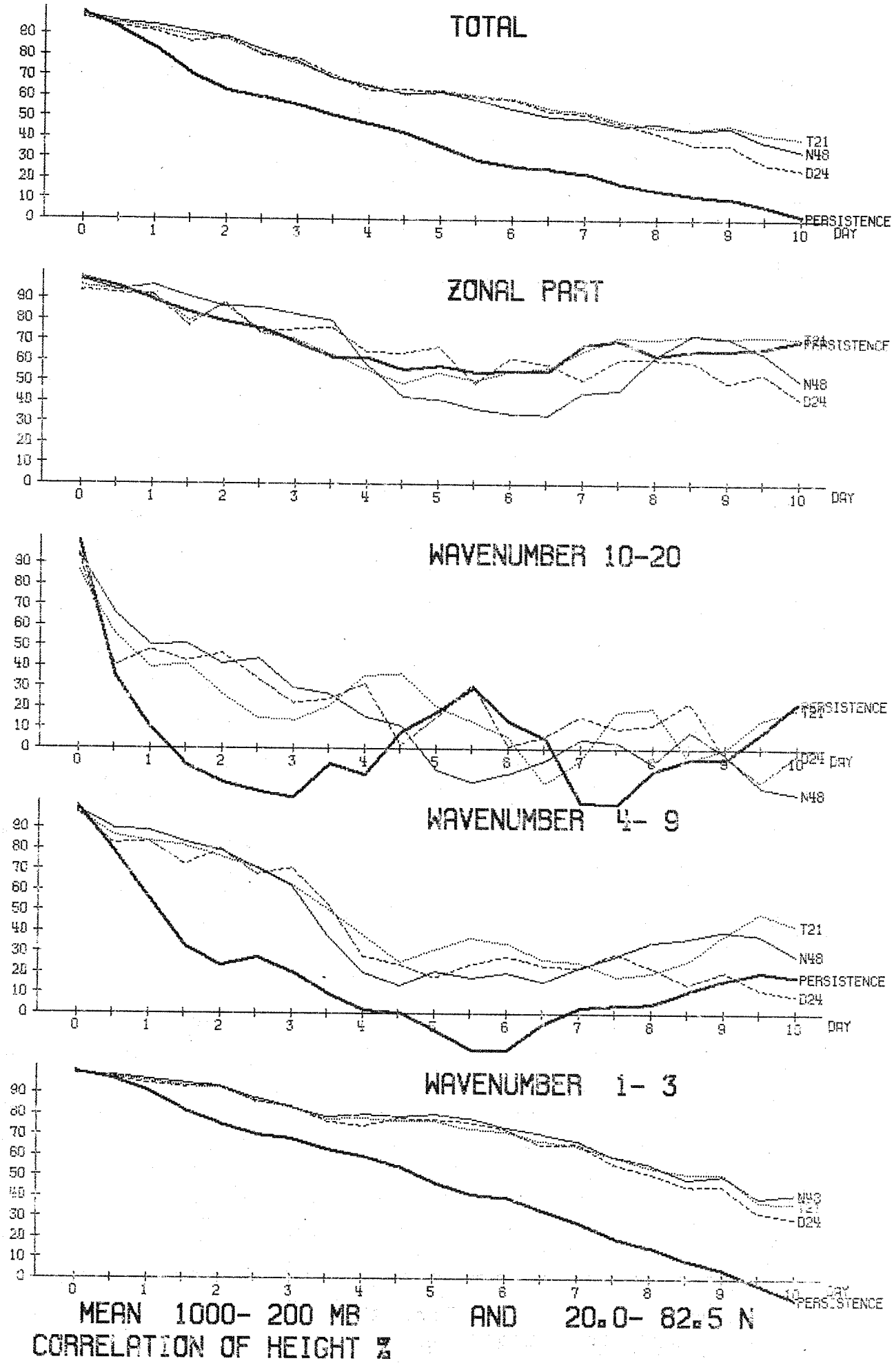
TOTAL
T21
N48
D24
PERSISTENCE
DAY
ZONAL PART
PERSISTENCE
N48
D24
DAY
WAVENUMBER 10-20
PERSISTENCE
T21
D24
DAY
N48
WAVENUMBER 4- 9
T21
N48
PERSISTENCE
D24
DAY
WAVENUMBER 1- 3
N48
T21
D24
PERSISTENCE
MEAN 1000- 200 MB AND 20.0- 82.5 N
CORRELATION OF HEIGHT %

Fig.III.9.

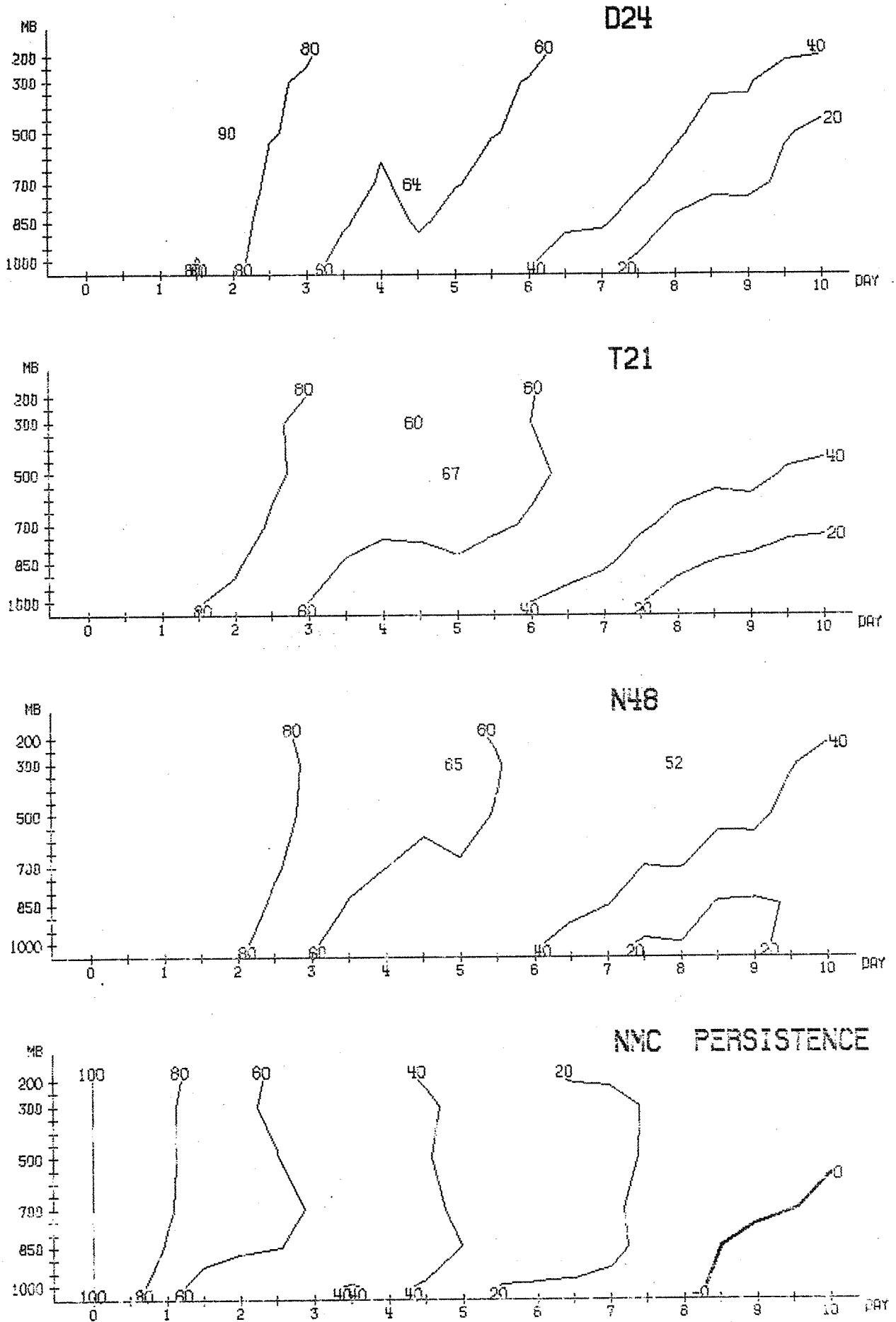
D24
MB
200
300
500
700
850
1000
80
90
64
60
40
20
DAY
T21
67
N48
65
52
NMC PERSISTENCE
100
0
TOTAL
CORRELATION OF HEIGHT %
MEAN BETWEEN 20.0 AND 82.5 N

Fig.III.10.

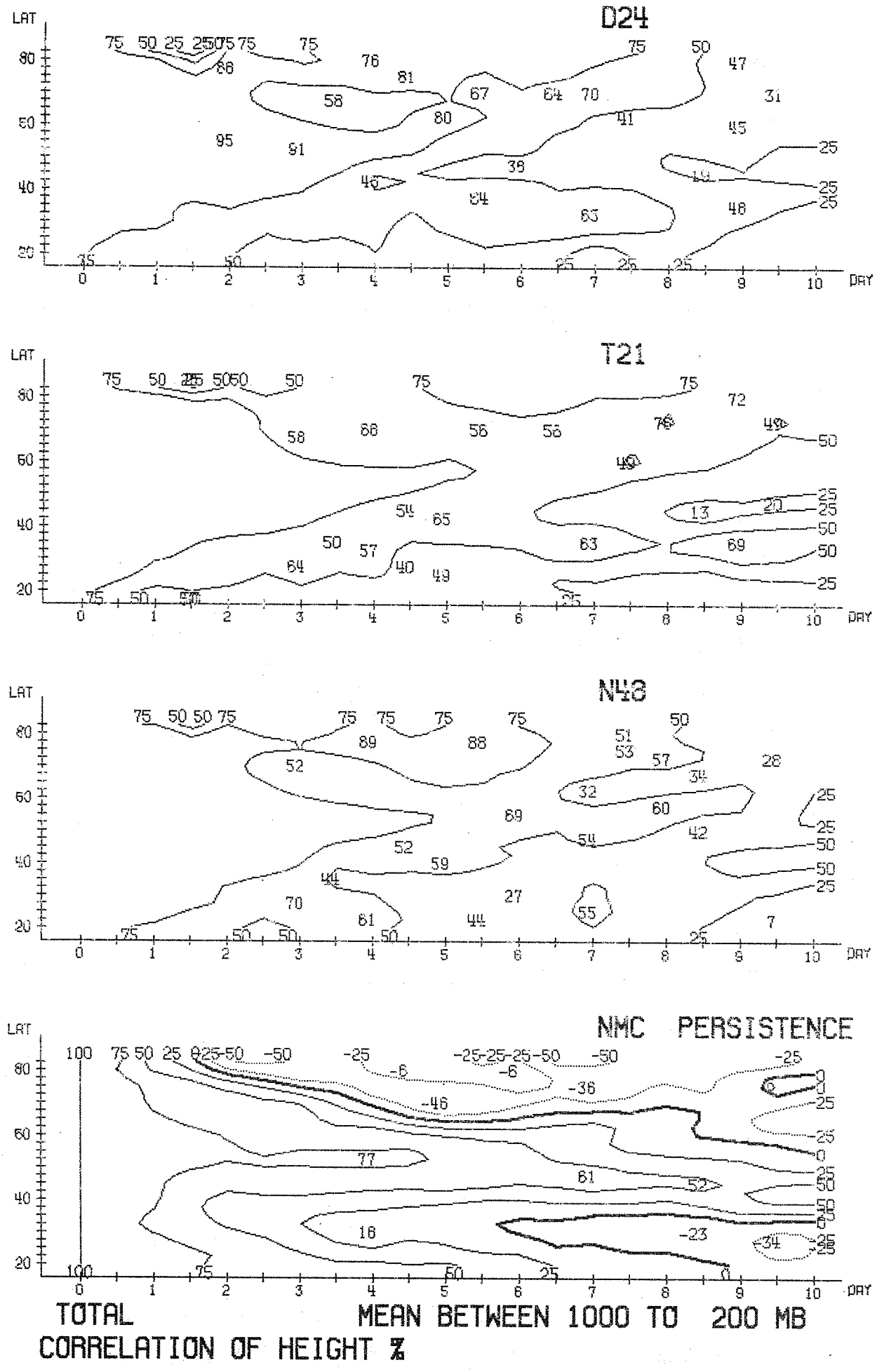
D24
T21
N48
NMC PERSISTENCE
LAT
DAY
TOTAL
MEAN BETWEEN 1000 TO 200 MB
CORRELATION OF HEIGHT %

Fig.III.11.

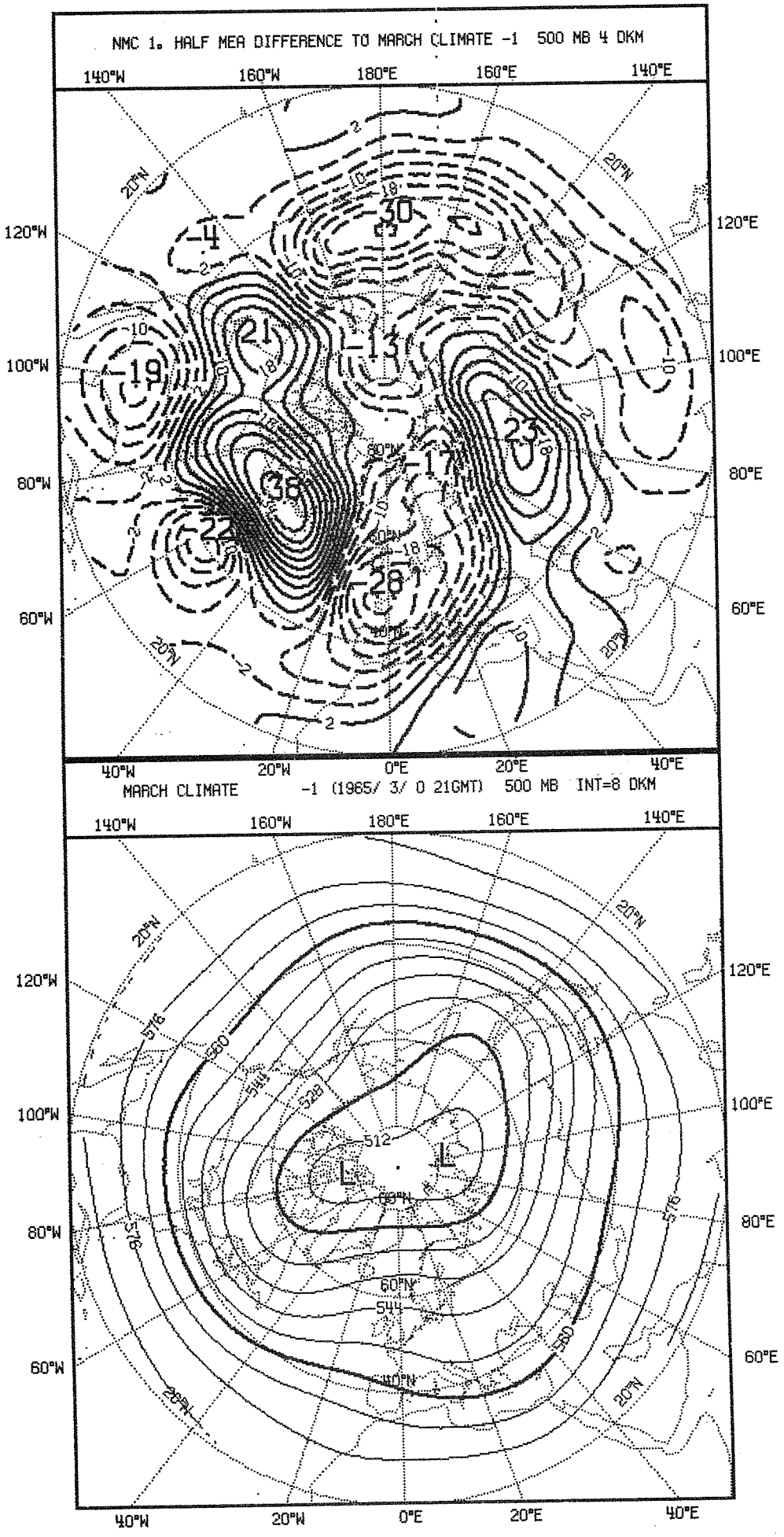
NMC 1. HALF MEA DIFFERENCE TO MARCH CLIMATE -1 500 MB 4 DKM
140°W
160°W
180°E
160°E
140°E
120°W
120°E
100°W
100°E
80°W
80°E
60°W
60°E
20°N
40°W
20°W
0°E
20°E
40°E
MARCH CLIMATE -1 (1965/ 3/ 0 21GMT) 500 MB INT=8 DKM
60°N
576
560
544
528
512
L

Fig.III.12a.

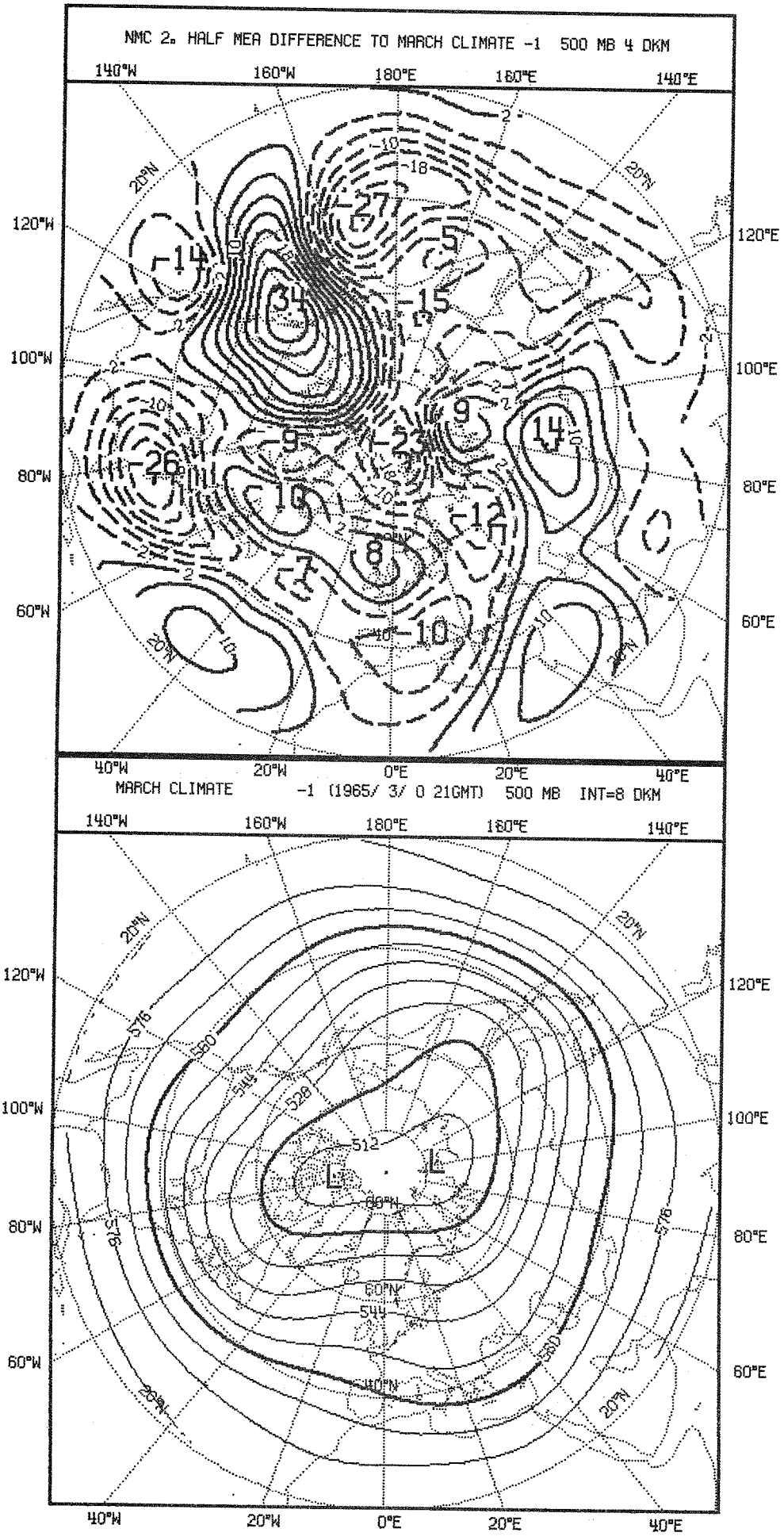
NMC 2. HALF MEA DIFFERENCE TO MARCH CLIMATE -1 500 MB 4 DKM
140°W
160°W
180°E
160°E
140°E
120°W
120°E
100°W
100°E
80°W
80°E
60°W
60°E
20°N
40°W
20°W
0°E
20°E
40°E
MARCH CLIMATE -1 (1965/ 3/ 0 21GMT) 500 MB INT=8 DKM
576
560
544
528
512
L
80°N
60°N
40°N

Fig.III.12b.

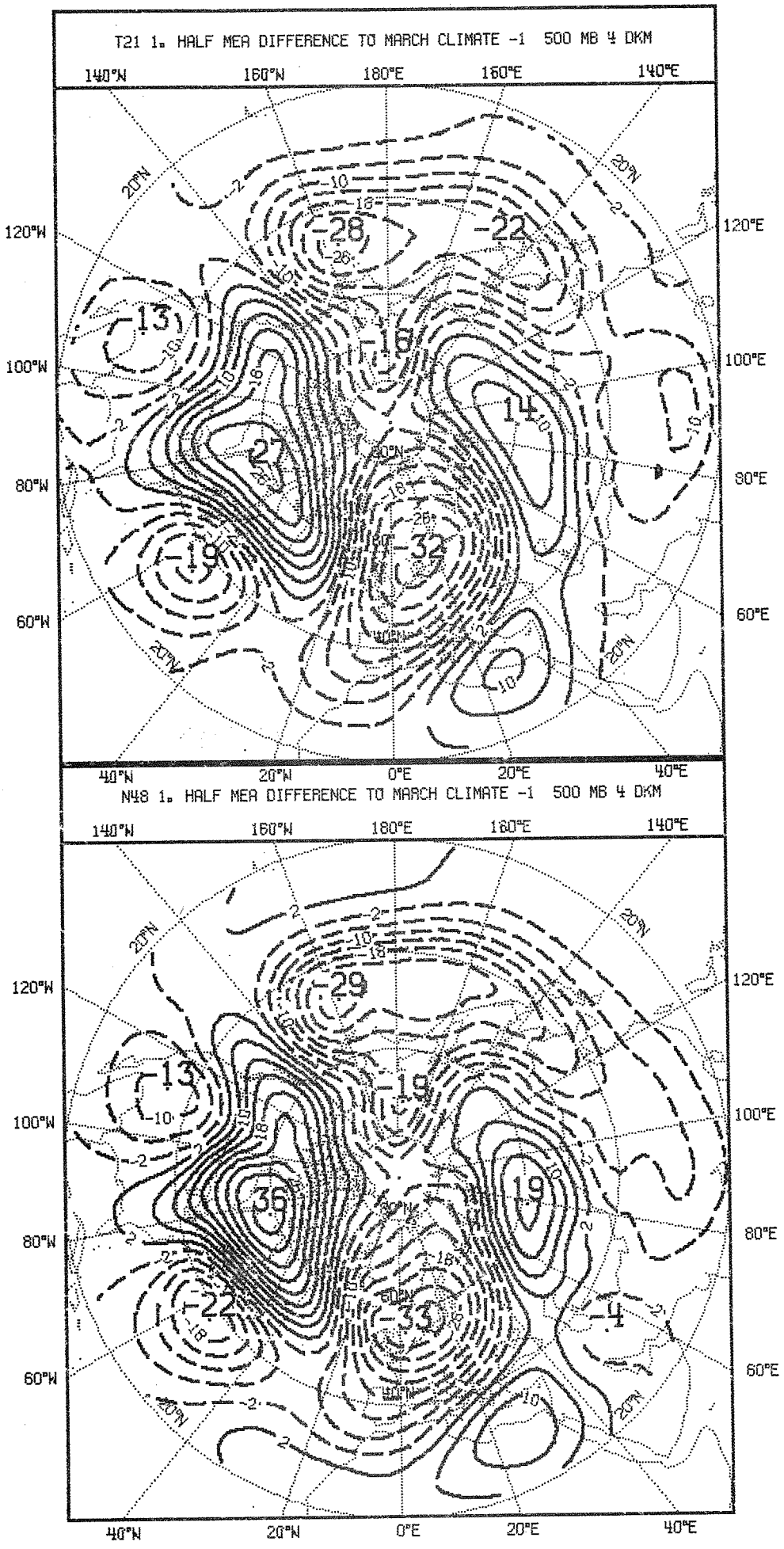
T21 1. HALF MEA DIFFERENCE TO MARCH CLIMATE -1 500 MB 4 DKM
140°W
160°W
180°E
160°E
140°E
120°W
120°E
100°W
100°E
80°W
80°E
60°W
60°E
40°N
20°N
0°E
20°E
40°E
-28
-22
-13
-16
14
27
-19
-32
N48 1. HALF MEA DIFFERENCE TO MARCH CLIMATE -1 500 MB 4 DKM
-29
-13
-19
36
19
-22
-33
-4

Fig.III.12c/d.

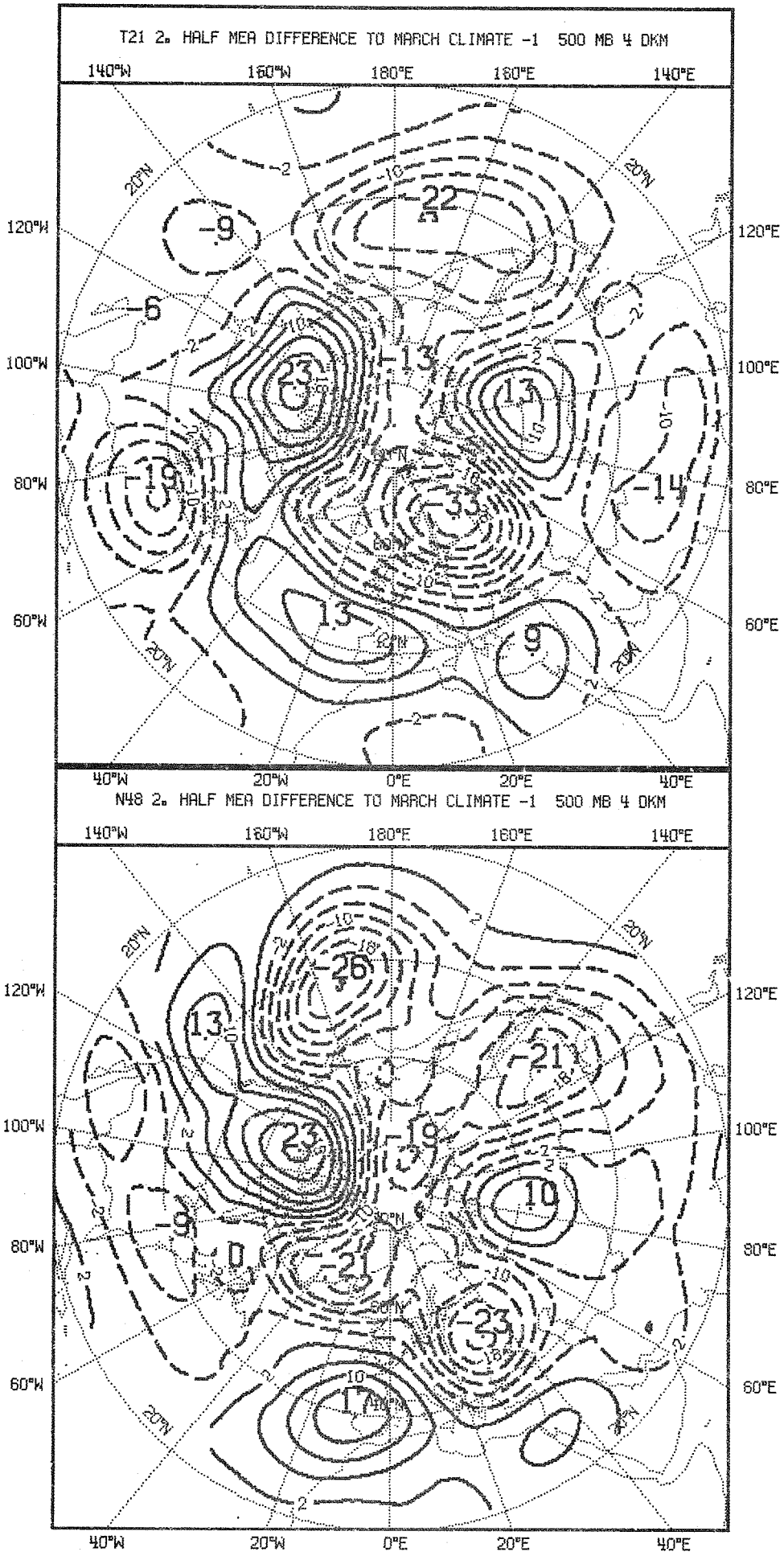
T21 2. HALF MEA DIFFERENCE TO MARCH CLIMATE -1 500 MB 4 DKM
140°W
160°W
180°E
160°E
140°E
120°W
120°E
100°W
100°E
80°W
80°E
60°W
60°E
20°N
40°W
20°W
0°E
20°E
40°E
N48 2. HALF MEA DIFFERENCE TO MARCH CLIMATE -1 500 MB 4 DKM

Fig.III.12e/f

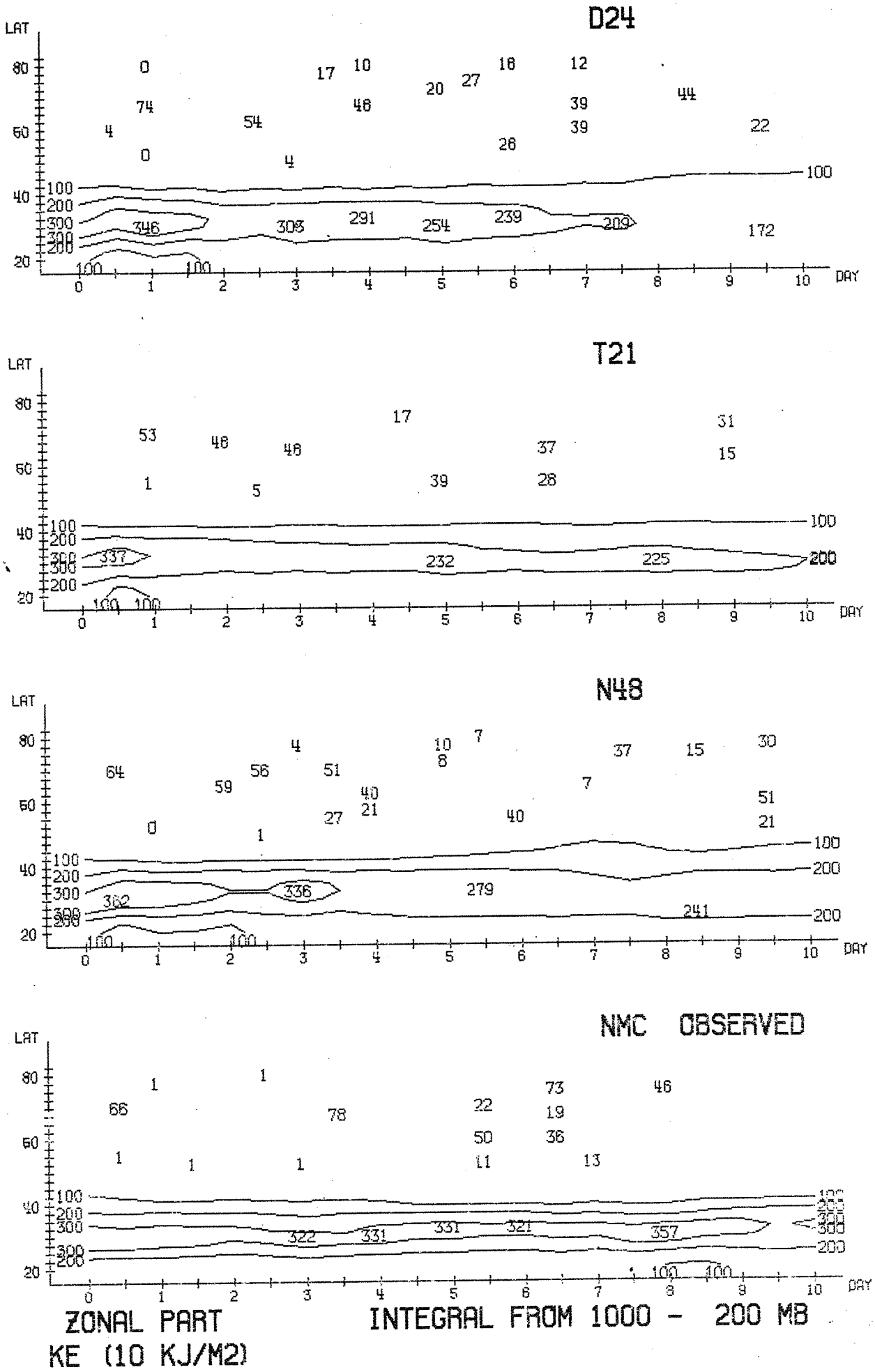
D24
LAT
80
60
40
20
0
74
4
0
17
10
54
4
48
20
27
18
26
12
39
39
44
22
100
100
200
300
346
308
291
254
239
209
172
100
100
0
1
2
3
4
5
6
7
8
9
10
DAY
T21
LAT
80
60
40
20
53
1
48
5
48
17
39
37
28
31
15
100
100
200
300
337
232
225
200
100
100
0
1
2
3
4
5
6
7
8
9
10
DAY
N48
LAT
80
60
40
20
64
0
59
56
1
4
51
27
40
21
10
8
7
40
37
7
15
30
51
21
100
100
200
300
362
336
279
241
200
100
100
0
1
2
3
4
5
6
7
8
9
10
DAY
NMC OBSERVED
LAT
80
60
40
20
66
1
1
1
78
1
1
22
50
11
73
19
36
13
46
100
200
300
322
331
331
321
357
300
200
100
100
0
1
2
3
4
5
6
7
8
9
10
DAY
ZONAL PART
KE (10 KJ/M2)
INTEGRAL FROM 1000 - 200 MB

Fig:III.13.

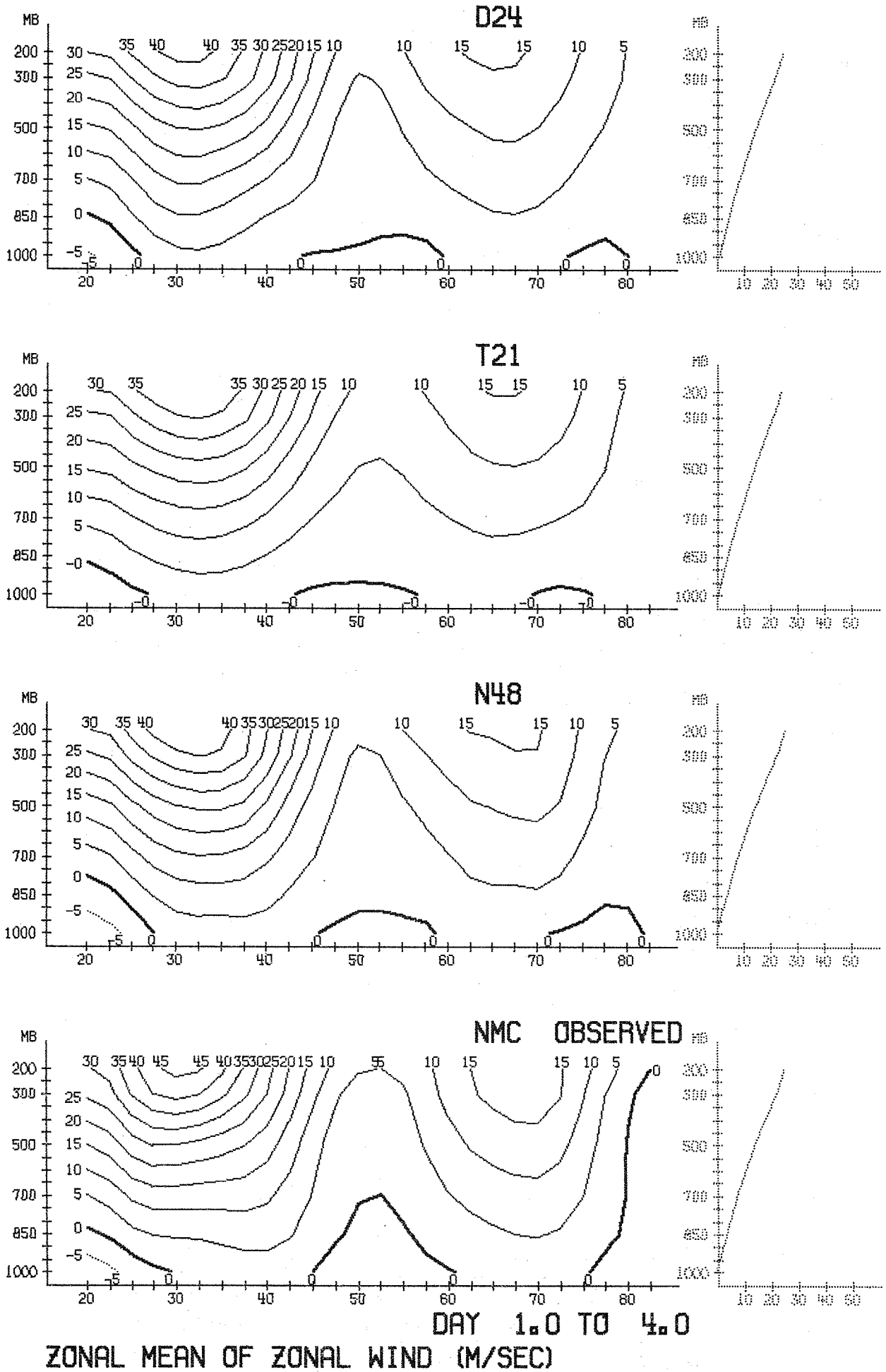
D24
T21
N48
NMC OBSERVED
MB
200
300
500
700
850
1000
20
30
40
50
60
70
80
DAY 1.0 TO 4.0
ZONAL MEAN OF ZONAL WIND (M/SEC)

Fig.III.14.

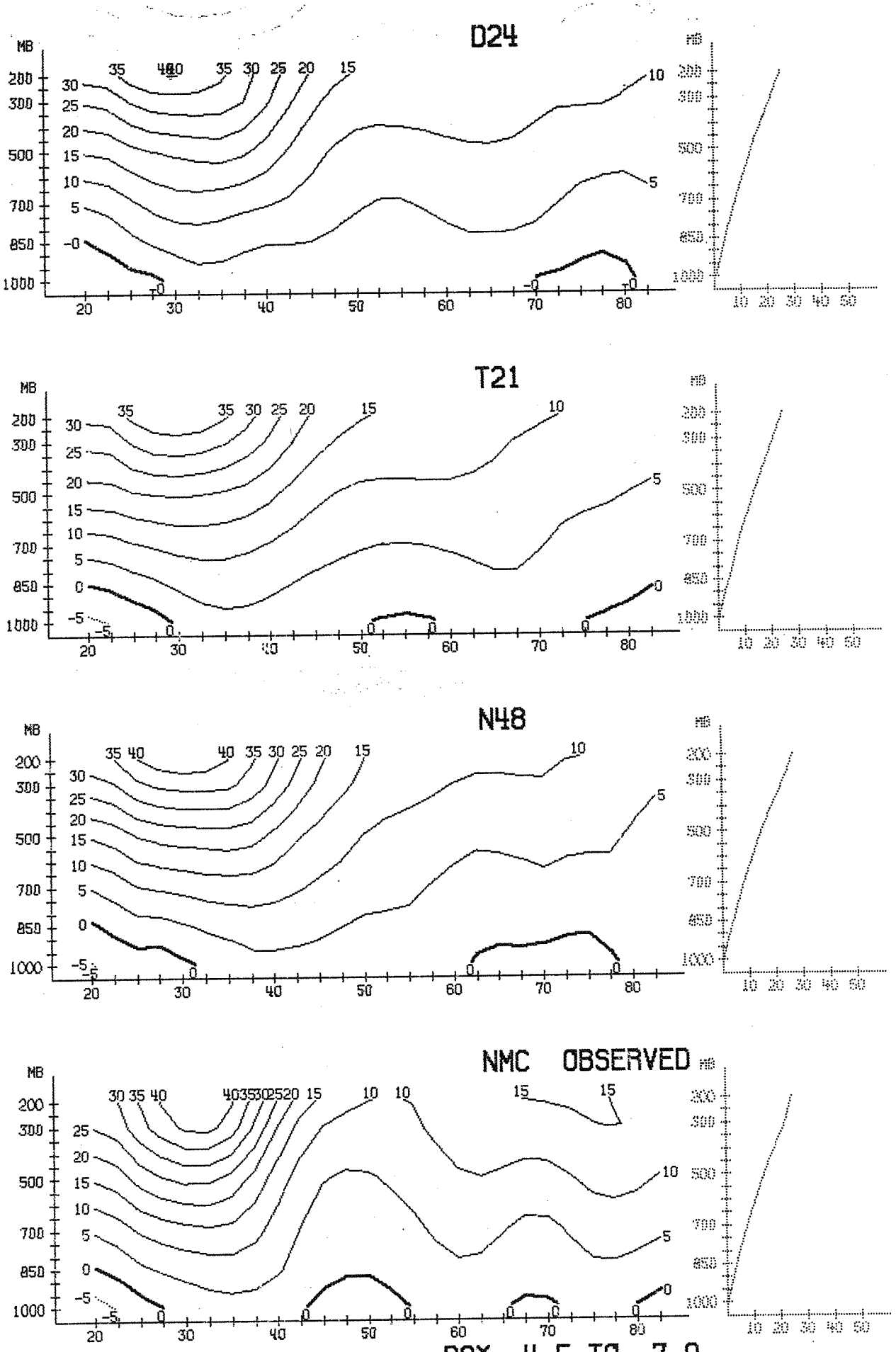
D24
T21
N48
NMC OBSERVED
MB
200
300
500
700
850
1000
20
30
40
50
60
70
80
10
20
30
40
50
DAY 4.5 TO 7.0
ZONAL MEAN OF ZONAL WIND (M/SEC)

Fig.III.15.

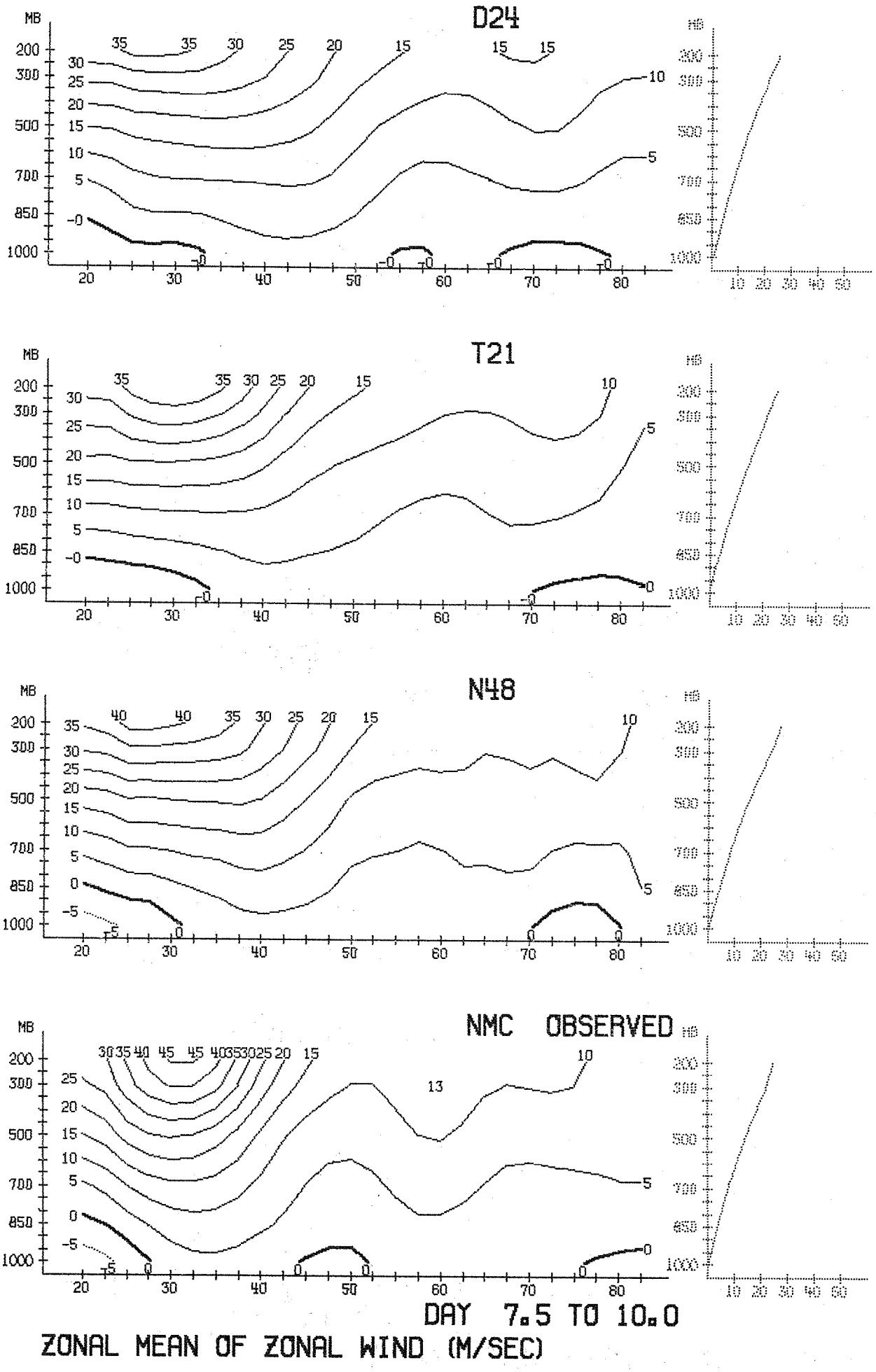
D24
T21
N48
NMC OBSERVED
MB
200
300
500
700
850
1000
20
30
40
50
60
70
80
10
DAY 7.5 TO 10.0
ZONAL MEAN OF ZONAL WIND (M/SEC)

Fig.III.16.

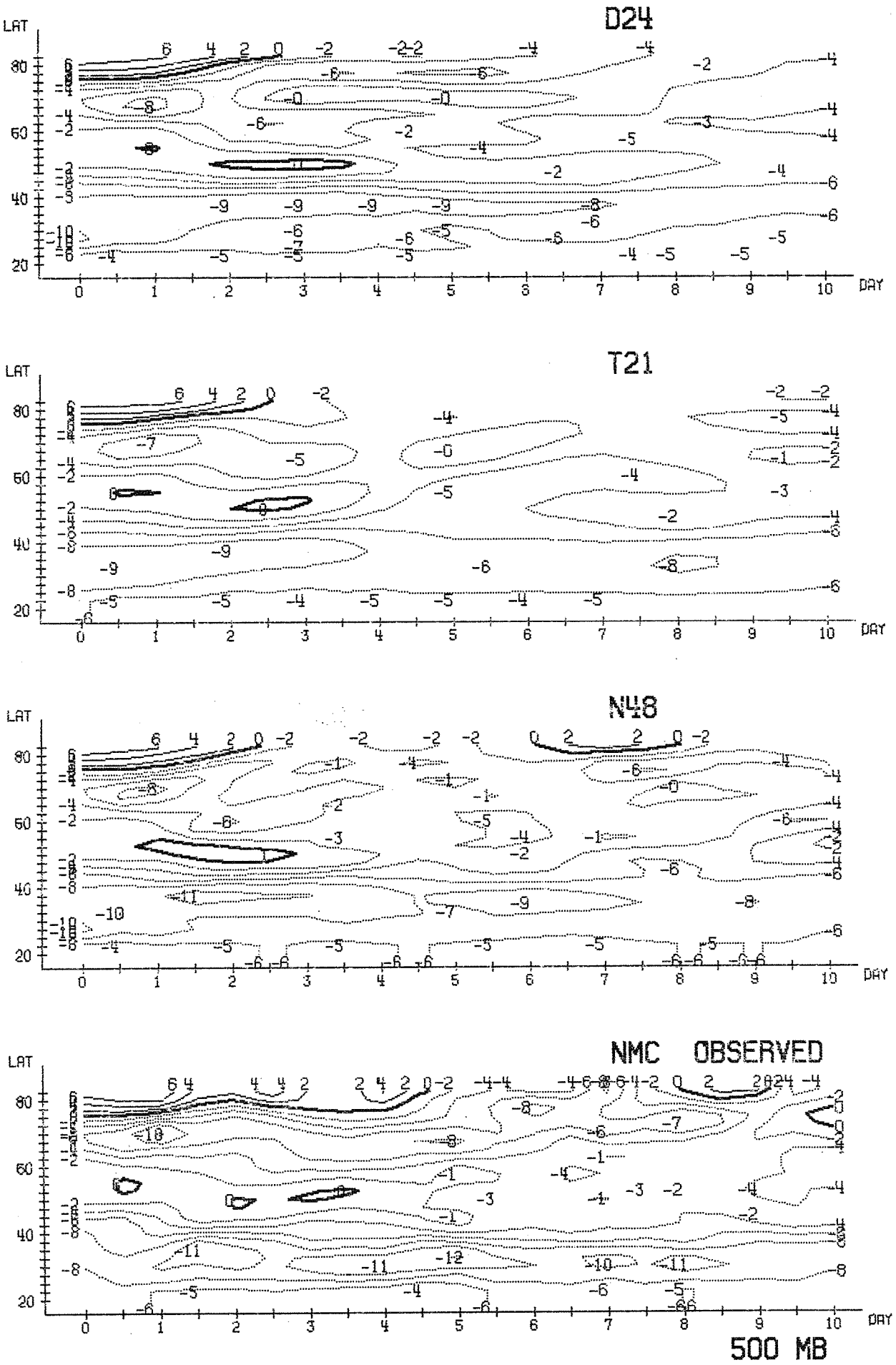

Fig.III.17.

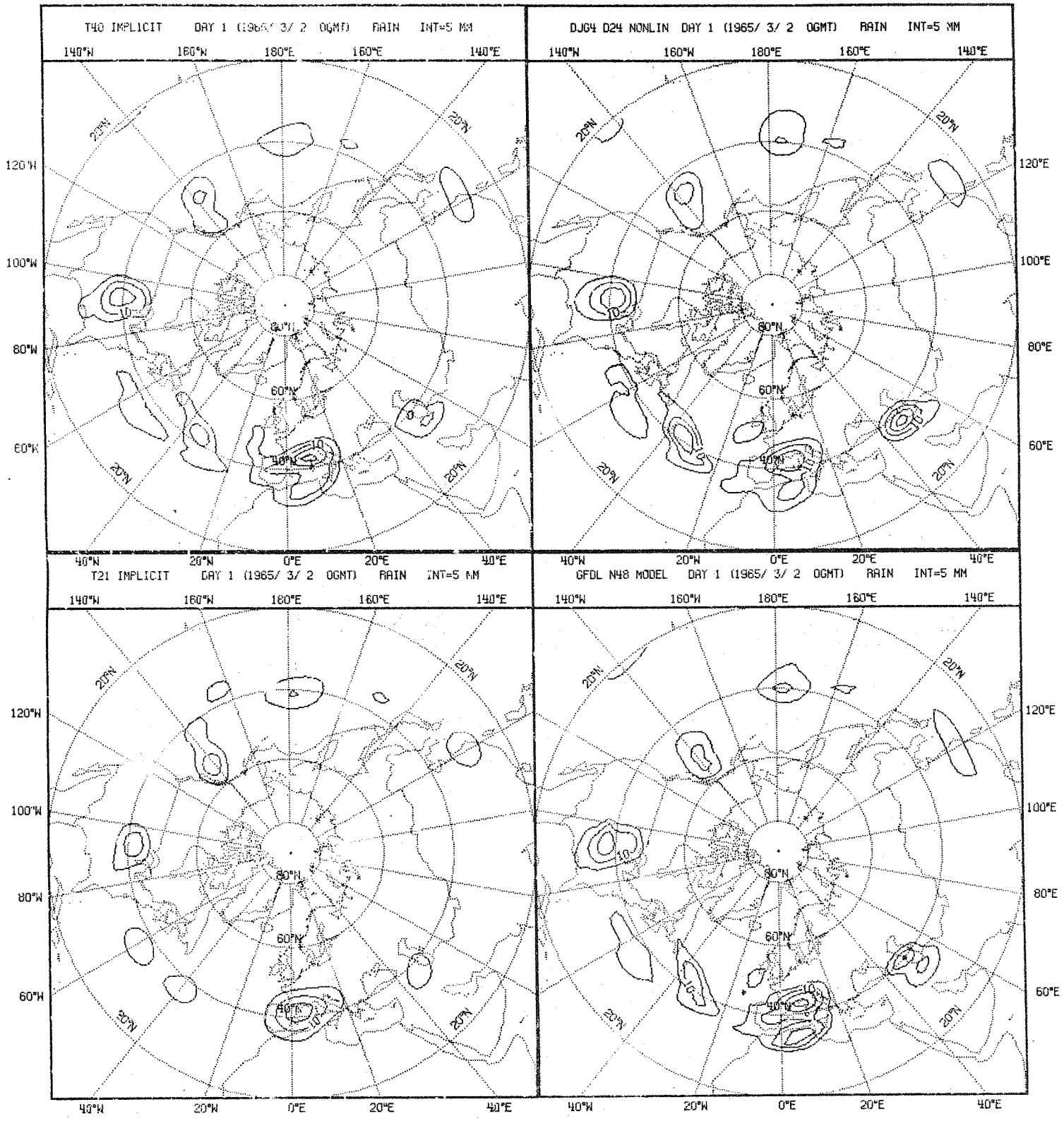
T40 IMPLICIT DAY 1 (1965/ 3/ 2 0GMT) RAIN INT=5 MM
DJG4 D24 NONLIN DAY 1 (1965/ 3/ 2 0GMT) RAIN INT=5 MM
T21 IMPLICIT DAY 1 (1965/ 3/ 2 0GMT) RAIN INT=5 MM
GFDL N48 MODEL DAY 1 (1965/ 3/ 2 0GMT) RAIN INT=5 MM
140°W
160°W
180°E
160°E
140°E
120°W
100°W
80°W
60°W
120°E
100°E
80°E
60°E
20°N
40°N
60°N
80°N
40°W
20°W
0°E
20°E
40°E

Fig. III.18a.

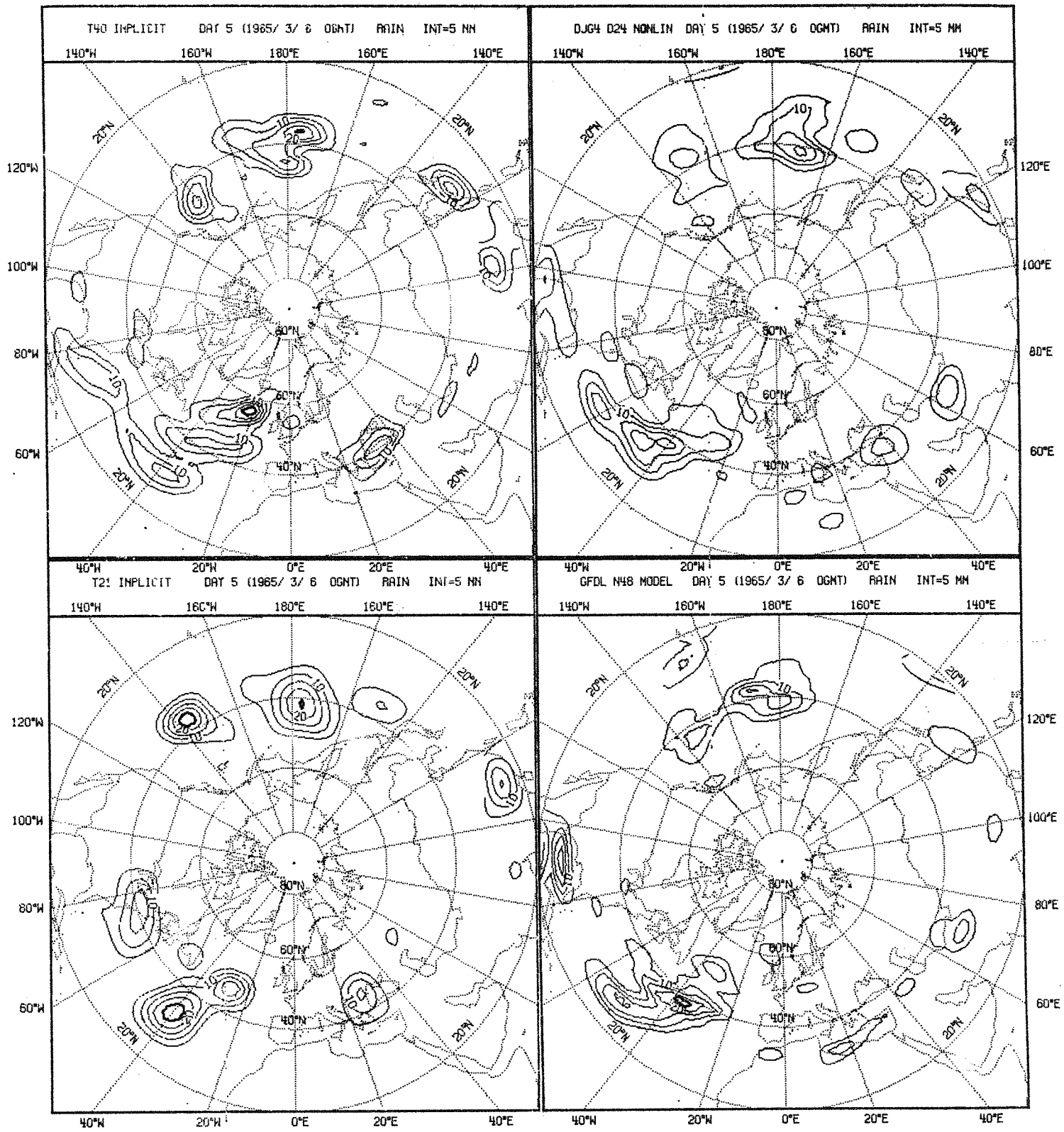

Fig. III.18b.

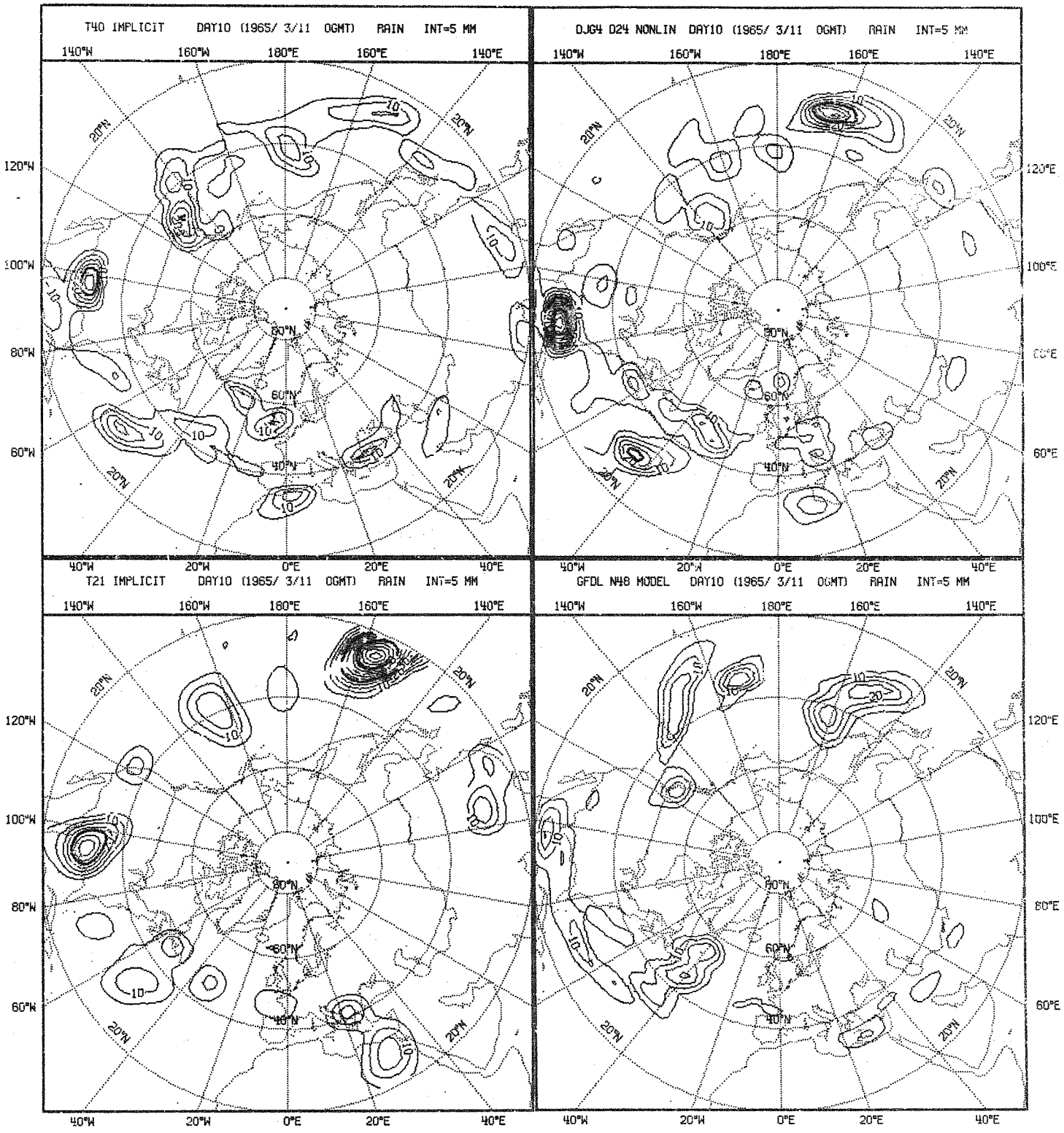
T40 IMPLICIT DAY10 (1965/ 3/11 0GMT) RAIN INT=5 MM
DJG4 D24 NONLIN DAY10 (1965/ 3/11 0GMT) RAIN INT=5 MM
T21 IMPLICIT DAY10 (1965/ 3/11 0GMT) RAIN INT=5 MM
GFDL N48 MODEL DAY10 (1965/ 3/11 0GMT) RAIN INT=5 MM
140°W
160°W
180°E
160°E
140°E
120°W
100°W
80°W
60°W
120°E
100°E
80°E
60°E
20°N
30°N
40°N
60°N
40°W
20°W
0°E
20°E
40°E

Fig. III.18c.

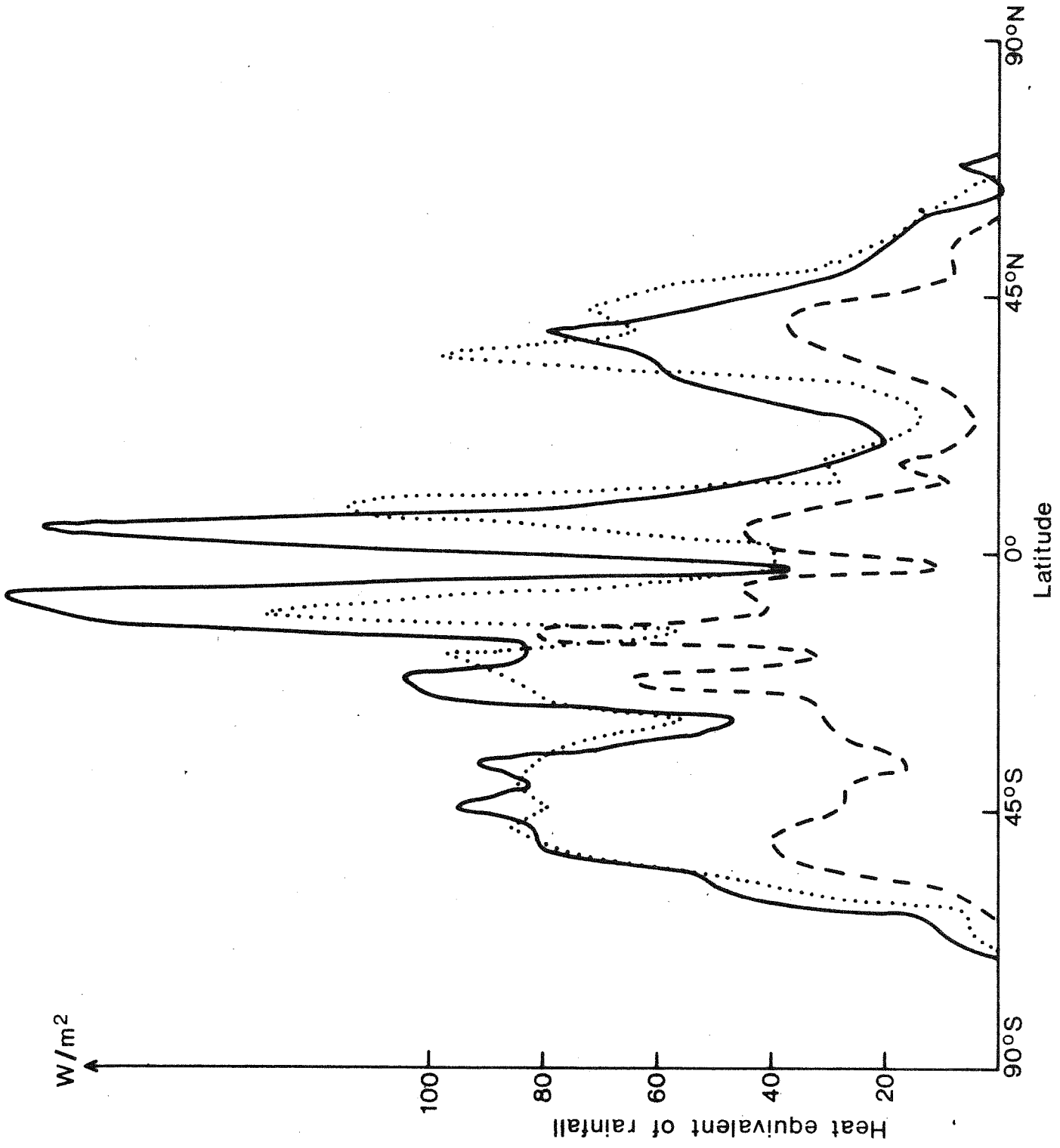

Fig. III.19. Latitudinal dependence of zonally averaged rainfall.
- - - - accumulated rain over 0 - 12 h
. . . . idem over 24 - 36 h
_____ idem over 48 - 60 h

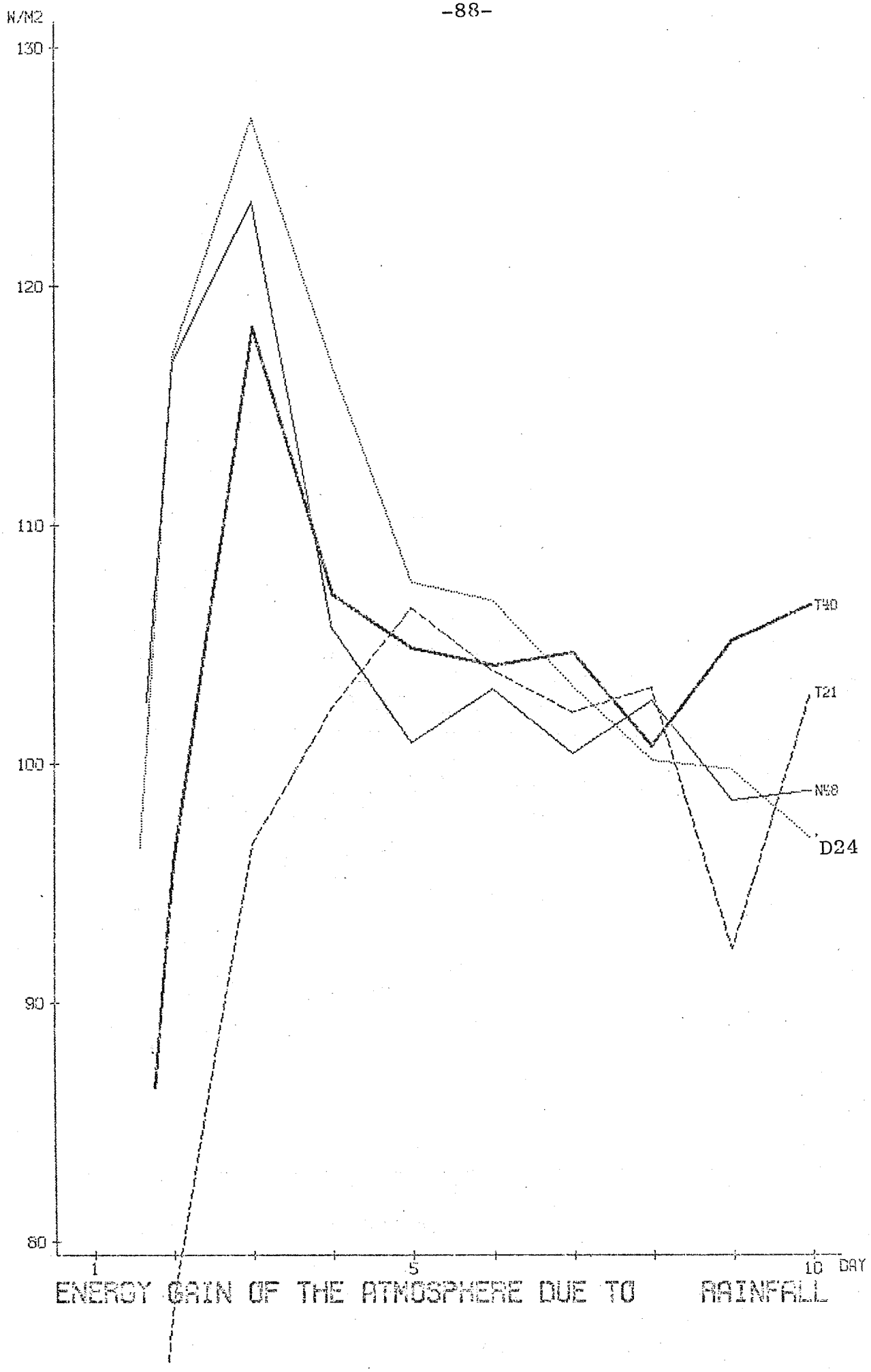
W/M2
130
120
110
100
90
80
1
5
10
DAY
T40
T21
N50
D24
ENERGY GAIN OF THE ATMOSPHERE DUE TO RAINFALL

Fig.III.20.

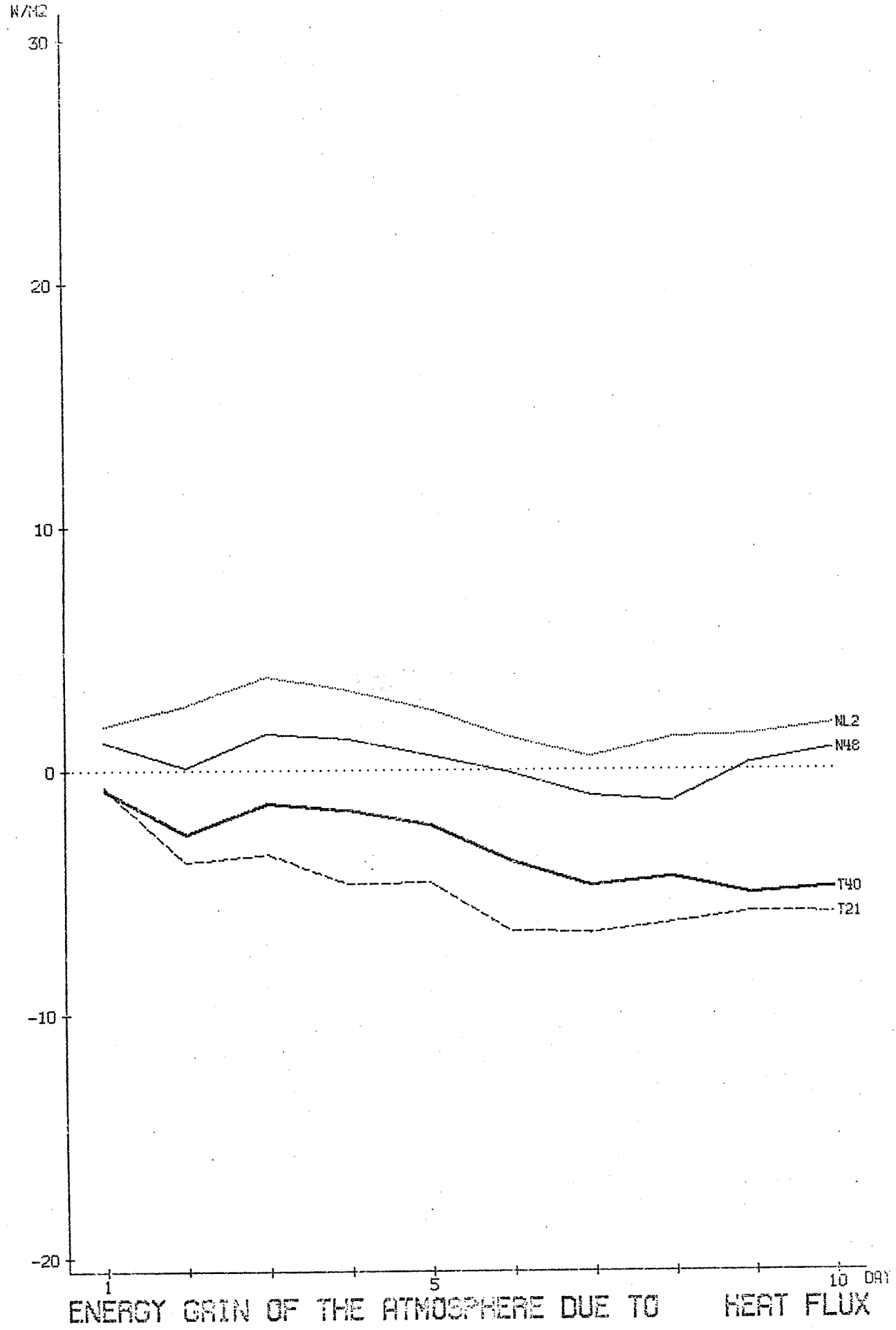
W/M2
30
20
10
0
-10
-20
NL2
N48
T40
T21
1
5
10
DAY
ENERGY GAIN OF THE ATMOSPHERE DUE TO HEAT FLUX

Fig.III.21.

EUROPEAN CENTRE FOR MEDIUM RANGE WEATHER FORECASTS

Research Department (RD)

Internal Report No. 17

No. 1 Users Guide for the GFDL Model (November 1976)

No. 2 The effect of Replacing Southern Hemispheric Analyses by Climatology on Medium Range Weather Forecasts (January 1977)

No. 3 Test of a Lateral Boundary Relaxation Scheme in a Barotropic Model (February 1977)

No. 4 Parameterization of the Surface Fluxes (February 1977)

No. 5 An Improved Algorithm for the Direct Solution of Poisson's Equation over Irregular Regions (February 1977)

No. 6 Comparative Extended Range Numerical Integrations with the ECMWF Global Forecasting Model 1 : The N24,Non-Adiabatic Experiment (March 1977)

No. 7 The ECMWF Limited Area Model (March 1977)

No. 8 A Comprehensive Radiation Scheme designed for Fast Computation (May 1977)

No. 9 Documentation for the ECMWF Grid-Point Model (May 1977)

No. 10 Numerical Tests of Parameterization Schemes at an Actual Case of Transformation of Arctic Air (June 1977)

No. 11 Analysis Error Calculations for the FGGE (June 1977)

No. 12 Normal Modes of a Barotropic Version of the ECMWF Grid-Point Model (July 1977)

No. 13 Direct Methods for the Solution of the Discrete Poisson Equation : Some Comparisons (July 1977)

EUROPEAN CENTRE FOR MEDIUM RANGE WEATHER FORECASTS

Research Department (RD)

Internal Report No. 17

No. 14 On the FACR (ℓ) Algorithm for the Discrete Poisson Equation (September 1977)

No. 15 A Routine for Normal Mode Initialisation with Non-Linear Correction for a Multi-Level Spectral Model with Triangular Truncation (August 1977)

No. 16 A Channel Version of the ECMWF Grid-Point Model (December 1977)

No. 17 A Comparative Study of Some Low Resolution Explicit and Semi-Implicit Spectral Integrations (August 1978)